Age and Paleomagnetic studies on Precambrian dyke swarms in Dharwar craton, India

Thesis submitted in partial fulfillment for the award of the Degree of

Doctor of Philosophy
in
Earth and Space Sciences

By
E. NAGARAJU
(Regd. No. 11ESPE02)

Centre for Earth and Space Sciences
(School of Physics)
University of Hyderabad
(P.O) Central University, Gachibowli
Hyderabad – 500046
India

Thesis Submitted for Review: 28-02-2017
Thesis Jury Defense and Presentation Date: 28-07-2017
Jury member: Prof. S.J. Sangode, Department of Geology, Savitribai Phule Pune University, Pune, 411007, India.

ACKNOWLEDGEMENTS

I wish to express deep sense of gratitude to my supervisor **Dr. Anil Kumar,** Chief Scientist, National Geophysical Research Institute (CSIR-NGRI) who gave me an opportunity to work in Paleomagnetism and Geochronology Laboratories. He has been a constant source of inspiration for me. I appreciate the independence, responsibilities and good advises he has given me during the course of my research work. I wholeheartedly thank him for all his valuable guidance, support and constant encouragement.

I am thankful to my Joint Supervisor **Prof. A.C. Narayana,** Centre for Earth and Space Sciences, University of Hyderabad for his valuable guidance and suggestions.

I am thankful to my doctoral committee member **Dr. Y.J. Bhasker Rao**, Chief Scientist, CSIR-NGRI for his valuable suggestions and constructive comments which helped me a lot to improve the quality of this work. I specially thank **Dr. M. Venkateshwarlu**, Senior Scientist, CSIR-NGRI for his encouragement and help during the beginning days of my research work.

My colleagues at the CSIR-NGRI, especially **N. Ramesh Babu, V. Parasharamulu, Ravi Shanker** and **G. Papanna** are thanked for their helpful cooperation during the course. I feel I have really been lucky to be working with them. I acknowledge the financial support rendered by **D.J.Patil**, CSIR-NGRI, during the final year of my tenure in NGRI.

I would like to extend my sincere thanks to **Prof. Jean Besse**, Head, Paleomagnetism Division, IPGP, France and **J.P. Vallet** for the scientific discussions and assisting in field work which have helped me a lot to gain a better understanding on several aspects and enhanced my scientific thoughts.

I sincerely acknowledge the support extended by the Director, and other scientists of NGRI for the facilities provided for my research work.

I sincerely thank the Head, UCESS, and faculty for all their support and facilities extended during my doctoral work. I am indebted to all of them.

Finally, I place on record my heartfelt gratitude to my parents who have supported me throughout my education with love and affection.

E. NAGARAJU

ABSTRACT

Title: ***Age and Paleomagnetic studies on Precambrian dyke swarms in Dharwar craton, India.***

Mafic dykes have been regarded as promising targets for paleomagnetic and geochronological studies because they cool rapidly and therefore provide an accurate, albeit instantaneous record of the Earth's magnetic field. Further the accessory minerals (Zircon and baddeleyite) present in dykes are used to establish the precise crystallization ages for the thermal event with a reasonable degree of precision. A single precise age match along with well defined paleomagnetic poles in two continents suggests a quick and tentative paleocontinental reconstruction. Determining precise emplacement ages and high quality paleomagnetism for multiple dyke swarms in the Dharwar craton is particularly important because this craton is central to many Precambrian paleogeographic reconstructions including the supercontinents of Columbia and Rodinia.

The Dharwar craton of south India is a large Archean cratonic fragment intruded by several generations of dykes, and numerous dykes of different trends are well exposed throughout the craton. They represent a significant phase of basic magmatism in the Dharwar craton. Radiometric age data suggest that these dykes are predominantly of Paleoproterozoic age apart from those of Cretaceous age. Recent paleomagnetic and geochronological work on the Dharwar craton indicates at least three major dyke emplacements during the Paleoproterozoic i.e. at 2369-2365, 2221-2209 and 2181-2177 Ma. Among the three age groupings, 2369-2365 Ma Dharwar giant dyke swarm covering the eastern Dharwar craton was well established and gives a paleopole position for the Dharwar craton. However, only a limited paleomagnetic and geochronological data are available for the other two dyke swarms. Hence an attempt has been made to carry out the integrated paleomagnetic and geochronological work to strengthen the paleomagnetic data as well as for establishing the geochronological data for 2221-2209 Ma dyke swarm.

In order to ease the method of precise geochronology, a new method is developed to obtain highly precise Pb age determinations on baddeleyite (ZrO_2), a common accessory mineral in mafic rocks using thermal extraction – thermal ionization mass spectrometer (TE-TIMS). Using the zircon TE-TIMS approach recently presented by Davis (2008), this new method was developed. TE-TIMS method produces strong ion beams that allow $^{207}Pb/^{206}Pb$ isotope ratios to be measured by a thermal ionization mass spectrometer to high precision ($\pm 10^{-4}$) with almost negligible contamination from common Pb. Pb/U ratios cannot be determined by this method. However, the presence of two geochronometers allows ages to be determined without Uranium information, purely from the ratio of the radiogenic Pb daughter isotopes. Results obtained using this new method are comparable to the conventional U-Pb ages in both accuracy and precision. This procedure completely avoids the need for sample dissolution and isotope dilution required for conventional U–Pb dating technique and hence the requirement of an ultra-clean laboratory.

Using the new developed method, precise geochronology on few samples at different localities reveals that all N-S dykes in Dharwar Craton are not of same age. Precise Pb-Pb TE-TIMS baddeleyite ages of 3 dykes along with recently reported U-Pb ID-TIMS baddeleyite ages of six dykes of varying trends reveal two dyke swarms are observed in N-S trending (2253 Ma and 2215 Ma) and one radiating dyke swarm (2207 Ma). Baddeleyite fractions from N-S striking mafic dyke (AKLD) in the Dharwar Craton yielded a ^{207}Pb-^{206}Pb weighted mean age of 2216.0±0.9 Ma (a weighted mean age of 4 determinations). Another dyke swarm in the same trend (N-S) yielded a U-Pb/Pb-Pb, baddeleyite weighted mean age (five determinations including 4 earlier reported and our new age determination) of 2253.2±1.4 Ma. Besides these two swarms, a newly recognised 2082 Ma radiating dyke swarm in recent studies include two precise dates on N-S dykes from north of Cuddapah basin.

The overall mean paleomagnetic directions obtained for different dyke swarms is as follows. (a) 2.21-2.22 Ga AKLD dyke swarm yielded a paleomagnetic pole position at P_{lat} = 36°S, P_{long} = 312°E (A_{95}=8°) (b) ~2.18 Ga dyke swarm yielded a mean pole at 60°N and 108°E (A_{95}=10°) (c) 2.25 Ga N-S dyke swarm yields a mean magnetic direction at 16°S and 299°E (A95=14°). Based on the available poles (already published and preset poles) from Dharwar craton tentative apparent polar wander path for India is proposed. Further, the 2215 Ma pole of

N-S dyke swarm is compared with other similar age poles from Superior, Slave and Rae cratons and an attempt is made to reconstruct them. Of the several possible Paleoreconstructions at ~2215 Ma, one shows that the four cratons Dharwar, Slave, Superior and Rae could have been juxtaposed at intermediate to shallow latitudes (20 to 45°) at this time. However, lack of reliable Neoarchean paleomagnetic data from the Dharwar craton inhibits tracing its ancestry to either of the Neoarchean Supercratons: Sclavia or Superia. The refined APWP for the Dharwar craton for the Paleoproterozoic period resembles the segment of APWP obtained for the superior craton and kaapaval craton.

Table of Contents

List of Tables:

List of Figures:

Chapter 1: Introduction

1.1. Introduction:

Earth's history records numerous periods of accentuated mafic magmatism. Those magmas genetically unrelated to seafloor spreading and subductions are the Large Igneous Provinces (LIPs) and include continental flood basalts. Proterozoic LIPs are generally deeply eroded to expose giant dyke swarms, several of them being of continental scale. Recognition of coeval giant dyke swarms on different continents could be extremely useful for continental reconstructions, for deciphering the frequency of mantle perturbation events and also for understanding the chemical evolution of the mantle through Proterozoic.

Like in most Archean cratons, the Dharwar craton was also invaded by a large number of mafic dyke swarms, which are predominantly of Paleoproterozoic age (for recent summaries: Halls et al., 2007; French and Heaman, 2010; Kumar et al., 2012a, 2012b; Radhakrishna et al., 2013; Belica et al., 2013), apart from those of Cretaceous age (Kumar et al., 1988, 2001; Radhakrishna et al., 1994). Of these, the recently discovered E-W to ENE-WSW trending giant radiating dyke swarm emplaced at 2367 Ma with an areal extent of nearly the entire eastern Dharwar craton appears to be the most dominant (Kumar et al., 2012a). Other dyke swarms that have been dated recently using U–Pb baddeleyite geochronology from the eastern Dharwar craton include a N-S to NNW-SSE striking swarm at 2221–2209 Ma and a radial WNW-ESE to NW-SE swarm at 2181–2177 Ma (French and Heaman, 2010). The N-S striking dyke swarm appears to extend for over 450 km and straddle nearly the entire length of the Dharwar craton. In order to establish the spatial extent of this dyke swarm, lateral variation in composition and study their paleomagnetic signature, a concerted paleomagnetic and geochronological study was undertaken.

This chapter briefly outlines the ideas of mafic dykes and their connection to tectonics and the present knowledge on the role of mafic dykes within the tectonic framework of Dharwar craton. Objectives of the present investigation are also presented.

1.2. Basic Magmatism and Mafic dykes:

Mafic magmatism is an important manifestation of geological processes both in ocean related and continental conditions. Plate boundary magmatism is connected with subduction zones and mid ocean ridges, while the within-plate magmatism is commonly related to hotspots or mantle plumes. Petrological, heat flow and earthquake related data designate that basaltic and ultramafic magmas were produced in the upper mantle. The composition of the magma produced in the mantle is reliant on the composition of the source rock and the degree of melting.

Mafic magma provides information on the mineralogy and chemistry of mantle source rocks. Significant difference in the incompatible elemental dispersion and isotope ratios in basic rocks in homogeneous tectonic setting has showed that the upper mantle is chemically heterogeneous. The distinct chemical features in different mantle areas have helped the identification of geochemical mantle reservoirs. Primordial mantle (PM), Depleted mantle (DM), High U/Pb mantle (HIMU), Enriched mantle (I, II) are some possible mantle remnant members identified (Zindler and Hart, 1986).

Dyke is a vertical or steeply inclined tabular igneous intrusion (mantle-derived magma) that cuts across strata of the pre-existing country rock. Dykes form as a result of the injection of melting magma into the pre-existing fractures of lithosphere. Melting in the mantle source region needs thermal energy. This energy might be provided directly from local concentrations of radioactive elements in the mantle. In the low speed zone, magma can be engendered by the addition of heat at constant pressure, lowering the pressure at steady temperature or by bringing down the underlying liquefying temperature of the mantle rock by hydration (Gallagher and Hawkesworth, 1992). If the hydrostatic pressure of magma developed in the mantle is greater than that of lithostatic pressure of the crust, the magma exerts strong pressure on its walls producing fractures by tensional stresses. The direction of fracture spread is decided by the preference of stress at the fracture tip and is thought to be perpendicular to the least compressive principal stress (Rubin, 1995; Baer, 1995). Dykes can vary in texture and their composition can range from diabase or basaltic to granitic or rhyolitic. Usually dykes display chilled margin (adjacent to the country rocks) with fine grained and becoming coarser towards the

centre. Chilled margin generally cools relatively faster than the dyke centre. Thickness of dykes can range from few centimetres to many meters and the lateral dimensions can spread over many kilometres. Sometimes dykes appear as systems of sets of en echelon, parallel, or collinear segments rather than as one continuous linear dyke.

Mafic dykes evolve in episodes of crustal extension during which enormous quantities of mafic material from the mantle were transferred to the crust. Mafic dykes profoundly occur in all continents, which reflects processes of crustal extension in both oceanic and continental areas and their evolution is related to global geodynamic processes (Halls, 1982). Several to hundreds of dykes emplaced as clusters following similar trends more or less contemporaneously during a single intrusive event within continental crust are known as dyke swarms. Trends of these dyke swarms can be either linear or radial. Giant dyke swarms are preserved in many Archean cratons and are often interpreted to represent the erosional remnants of continental large igneous provinces (LIPs).

In general, it is believed that dykes with same trends possibly have the same emplacement ages. However, there are few exceptions that mafic dykes with similar trends also have different emplacement ages. It is usually done that radiometric ages obtained for few dykes of a particular swarm are assigned to all the dykes of that swarm. However, it fails in many cases; many times mafic dykes having similar compositions and trends may have been emplaced at different ages.

1.3. Mafic dykes in the Dharwar craton:

Dykes and dyke swarms of different orientations emplaced in different periods and of various compositions are very easily seen in the entire Dharwar craton, but are more abundant in the eastern Dharwar craton. Based on the reported geochronology, paleomagnetism, dyke trend and cross-cutting field relationships these dykes ages range from Paleoproterozoic (Kumar et al., 2012a, b, 2014; Srivastava et al., 2011; French and Heaman, 2010; Halls et al., 2007) to Late Cretaceous (Kumar et al., 2001) and have been described in detail earlier (e.g. French and Heaman, 2010; Halls et al., 2007; Murthy et al., 1987; Halls, 1982). These dykes are intruded into Archean granites and gneisses and exposed in a wide variety of orientations (E-W, NE-SW, N-S, NW-SE; Halls, 1982; Bhaskar Rao et al., 1995; Halls et al., 2007; French et al., 2008; French and Heaman,

2010; Pradhan et al., 2010). Individual dykes range in thickness varies from tens to hundreds of meters and extended laterally for distance tens to several hundred kilometers. Composition of these dykes ranges from alkali-olivine basalts or tholeiites to metadolerites/metanorites (e.g. Srivastava et al., 2014; Rao and Pupper, 1996). In general, all mafic dikes are fresh, medium to coarse-grained and composed of subhedral grains of plagioclase and pyroxenes that show an ophitic or subophitic texture. They also contain accessory minerals like ilmenite, apatite, hornblende, zircon, and baddeleyite.

With the presently available U–Pb and Pb-Pb geochronological data on the mafic dykes of the Dharwar craton, several discrete large igneous provinces (LIPs) have been recognized in this region. This includes the ~2.37 Ga Dharwar giant dyke swarm consisting of ENE–WSW to NE–SW trending giant radiating dyke swarm (Kumar et al., 2012a; French and Heaman, 2010; Halls et al., 2007), the ~2.2 Ga and ~2.18 Ga radial Dharwar dyke swarms (Kumar et al., 2012b; Srivastava et al., 2011; French and Heaman, 2010), ~2.08 Ga radial dyke swarm (Kumar et al., 2015) and the ~1.89 Ga Dharwar LIP consisting of the dykes and mafic sills intruded in the Cuddapah basin (French et al., 2008).

1.4. Why this Study?:

Mafic dykes and sills are believed to be an important part of continental drifting and when they occur as spatially extensive swarms of adequate size can be of great utility in paleocontinental reconstructions (e.g. Goldberg, 2010; Ernst and Srivastava, 2008; Bryan and Ernst, 2008; Hou et al., 2008; Rogers and Santosh, 2002). Mafic dykes are ideal for paleomagnetic studies because they cool rapidly and therefore provide an accurate, albeit instantaneous record of the Earth's magnetic field. Primary nature of the remanent magnetization in dykes can be verified by baked contact test. In addition to that dykes contain accessory Uranium-bearing minerals (e.g. zircon and baddeleyite) and are used to establish the precise crystallization ages for the thermal event with a reasonable degree of precision

An early paleomagnetic study on dykes of Dharwar craton led before they were geochronologically distinguished and concluded that they were part of the same magmatic event based on remanence directions. Until recently, no paleomagnetic poles of Paleoproterozoic period from precisely dated events were available from the Dharwar

craton of Indian shield. Although paleomagnetism of the Paleoproterozoic rocks in south India has been studied by several workers, the data have been far from adequate to define a realistic Apparent Polar Wander Path (APWP) for the Indian shield. The main difficulty has been the lack of robust paleomagnetic results accompanied by detailed step-wise AF and thermal demagnetizations and a lack of precise age dating. Recently, Kumar et al. (2012a) and Halls et al. (2007) reported paleomagnetism along with high precision U–Pb baddeleyite ages. As a result, key paleopole of precisely dated event has been reported for the 2.365 Ga Giant radiating dyke swarm of the Dharwar craton. In spite of the fact that high quality paleomagnetic data are being generated more rapidly in recent years, there is no reliable age support. Despite the advancements in high precision U–Pb Isotope Dilution Thermal Ionization Mass Spectrometry (ID TIMS) studies of zircon and baddeleyite from mafic dykes, there still remains a paucity of geochronological constraints on the timing of mafic dyke emplacement from Dharwar craton. To address this deficiency, geochronological and paleomagnetic studies have been carried out on various dykes in the Dharwar craton. A new method of precise geochronology is also developed to obtain highly precise Pb age determinations on baddeleyite (ZrO_2), a typical trace mineral in mafic rocks utilizing thermal extraction – thermal ionization mass spectrometer (TE-TIMS).

Present study significantly augments the Paleoproterozoic dataset and permits a review and comparison of the Paleoproterozoic data across the Dharwar craton of south Indian shield to classify the magnetizations into distinct groups. A key paleomagnetic pole from each of three swarms is reported with a precise Pb-Pb TE-TIMS (Thermal Extraction - Thermal Ionization Mass Spectrometry) baddeleyite age obtained at a paleomagnetic sampling site. Furthermore, the present study has been able to take advantage of the high precision U–Pb and Pb-Pb baddeleyite ages to define a sequence of well-dated paleomagnetic poles of Paleoproterozoic age. APWP of the Dharwar craton between 2.365 Ga and 1.885 Ga is refined by combining the present paleopoles with other published poles from precisely dated dykes. Present study also discusses the significance of paleoreconstruction at 2.22-2.21 Ga involving Dharwar, Superior and Slave cratons.

1.5. Goals of this study

To accomplish this study, following goals were set

- Precise age determination of dyke swarms using Pb-Pb (TE-TIMS baddeleyite) method.
- Detailed rock magnetic studies of the samples to identify the major magnetic minerals contributing to the remnant magnetism in these rocks.
- Detailed paleomagnetic studies of the oriented samples collected for determining the pole position during the Precambrian period.
- To understand the drift history of Dharwar craton during the Precambrian period.
- Integration of all these data and previous geological information will be made to better constrain the existing apparent polar wander path for the Dharwar craton during the Paleoproterozoic.

Chapter 2: Geological setting and Sampling

2.1. Introduction:

The study of petrogenetic and geotectonic aspects of dyke intrusion requires a comprehensive understanding of the regional geological setting of the terrain and the geology of host rocks. Therefore, the regional geology of the southern Indian terrain under three broad tectono-thermal units namely Granite-Greenstone Terrain, Eastern Ghat Mobile Belt and Southern Granulite Terrain has been discussed. Eastern Dharwar host rock geology including the metamorphic and deformation history are also discussed. In the later part, the field characteristics of the dykes and their petrographic details are described. These descriptions guided the sample selection for paleomagnetic and geochronological studies, and further to evaluate the data more meaningfully in the subsequent chapters.

The geology of the peninsular India has been recently summarised in a comprehensive account by Meert et al., 2010. Only a brief account of Dharwar geology, with emphasis on parts of direct relevance to this thesis will be given here.

2.2. Regional geology:

The Indian sub-continent has a unique history of rifting, multiple plume interactions and continental breakups. It covers an area of about 5,000,000 sq km and contains several Archean-Proterozoic cratons. The Indian sub-continent comprises (i) Peninsular Shield, (ii) Indo-Gangetic Basin (IGB) and (iii) The Himalayas (Bhattacharyya et al., 2000).

Each unit differs in crustal composition, thickness and seismic structure due to time-bound integrated evolution.

The Peninsular Shield, one of the oldest in the world, is marked by early Archaean cratonization and associated mobile belts.

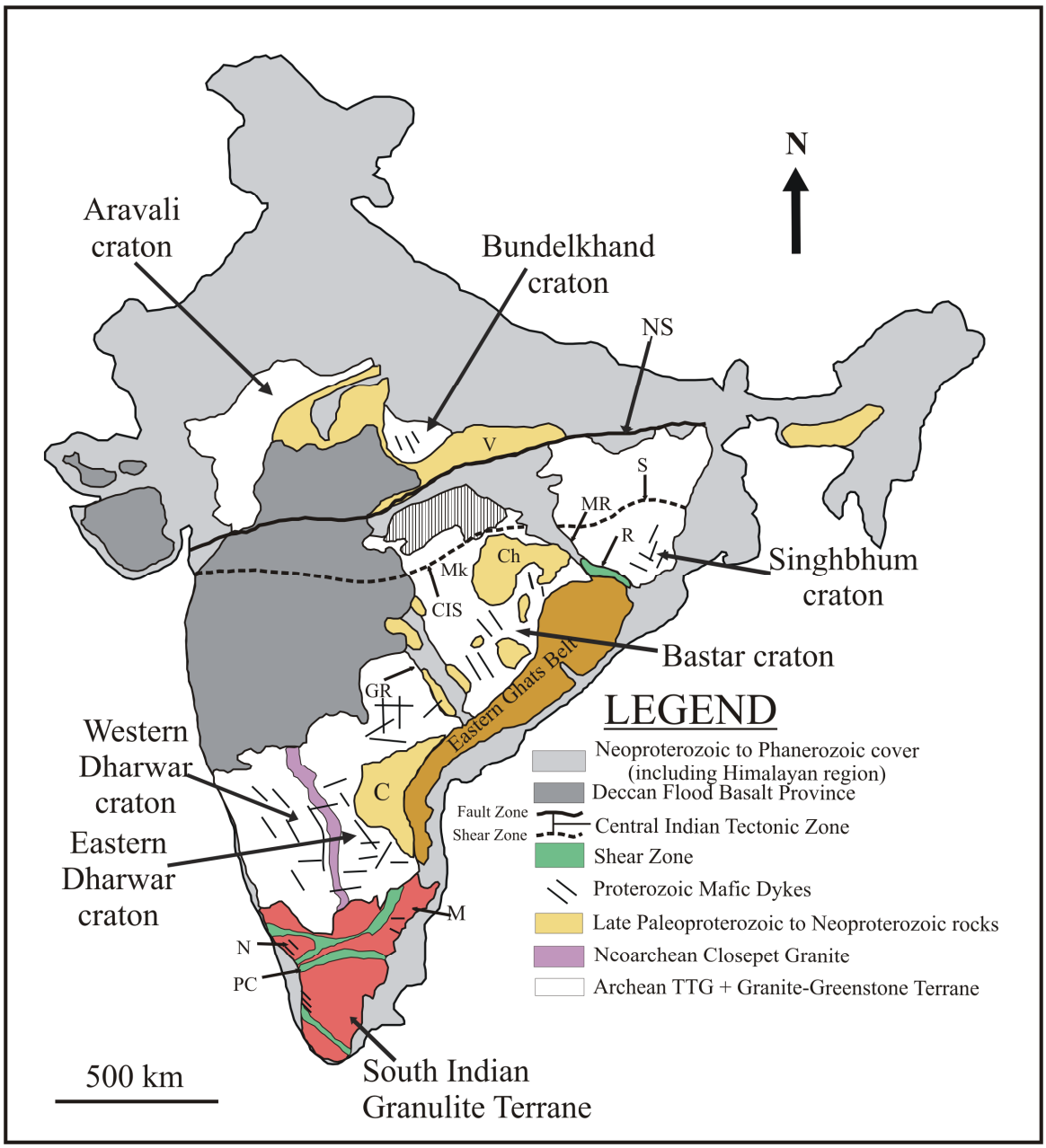

Figure 2.1. *Generalized geological map of the Indian shield (adapted and modified from Srivastava et al., 2014). Ch – Chattisgarth Basin; CIS – Central Indian Shear Zone; GR – Godavari Rift; M – Madras Block; Mk – Malanjkhand; MR – Mahanadi Rift; N – Nilgiri Block; NS – Narmada-Son Fault Zone; PC – Palghat-Cauvery Shear Zone; R – Rengali Province and Kerajang Shear Zone; S – Singhbhum Shear Zone; v – Vindyan Basin; c - Cuddapah basin.*

About two-thirds of the Indian Peninsula comprises Precambrian formations. The Peninsular shield constitutes Precambrian metamorphic terrains of low to high-grade crystalline rocks ranging in age 3.6–2.6 Ga. The cratons flanked by fold belts suggest that the cratons have moved, collided and generated the fold belts (Naqvi, 2005). These cratons might have resulted from fragmentation of a larger cratons.

Peninsular India consists of four major Cratonic nuclei: the Banded Gneiss Complex-Bundelkhand craton (northwest and central regions), the Bastar Craton (in the south-central region), the Singhbhum craton (eastern region), and the Dharwar craton (in the south) (Fig2.1; Naqvi et al., 1974; Naganjaneyulu and Santosh, 2010; Bhandari et al., 2010; Meert et al., 2010). The three Archaean domains of the BGC, Berach and Bundelkhand granites (the Banded Gneiss Complex-Bundelkhand craton) are considered a single Protocontinent to the north of the Son-Narmada lineament (SONA Zone), while , there are three other cratonic regions, to the south of this E-W trending lineament, namely the Bastar, the Dharwar, and the Singhbhum cratons which collectively constitute the southern Proto-continent of the Indian shield (Radhakrishna and Naqvi, 1986).

2.3. Geology of the study area:

Dharwar craton encompasses ~ 400,000 sq km area and lies between 12 to 18 degree latitudes and 74 to 80 degree longitudes. The Dharwar Craton is a classical greenstone granite terrain, consisting of Proterozoic mafic-ultramafic rocks and intra-cratonic sedimentary basins. The northern margin of the craton is concealed by Proterozoic sedimentary rocks and the Deccan lavas, the Eastern Ghats and the Godavari Rift in the east, the Arabian Sea in the west, and the Southern Granulite Terrane in the south (Rogers 1986; Naqvi and Rogers 1987). The Dharwar craton of the Southern Indian shield occupies northern part of the Southern Granulite terrain, separated by Palghat-Kavery shear zone. Dharwar craton displays a tilted section through an Archean continental crust (Rollinson et al., 1981; Raase et al., 1986). In the Dharwar craton, both volcanic and sediments were laid upon the basement of Peninsular gneiss (>3.0 Ga) as supracrustal rocks. Multiple phases of Proterozoic dolerite intrusive swarms, dated at 2.45–1.0 Ga with a peak at 1.8–1.4 Ga (Srivastava and Ahmad, 2009), indicate a shallow level brittleness to the Dharwar cratonic crust. The whole Archean continental crust in the Dharwar craton experienced geological activity for more than 900 m.y., between 3.4

and 2.5 Ga (Radhakrishna and Naqvi, 1986) and is further classified into Western and Eastern Dharwar cratons on the basis of divergent geological and tectonic characteristics (Swami Nath and Ramakrishnan, 1981; Jayananda et al., 2006; Naqvi and Rogers, 1987; Chardon et al., 2008). The N-S trending 400 km long 'Closepet Granite' (Viswanatha and Ramakrishnan, 1981; Allen et al., 1986) is thought to be boundary between these two cratons. Later, an arcuate N-S trending shear zone, that forms the eastern boundary of the Chitradurga greenstone belt, separates western and eastern parts of the Dharwar cratons which have distinct characteristics (Chadwick et al., 1992, 2000). Amalgamation of the western and eastern Dharwar cratonic blocks is considered to have taken place at ~2.5 Ga (Chadwick et al., 1997).

The Western Block is characterized by the presence of 3000 Ma old TTG (tonalite-trondhjemite-granodiorite) gneisses—the Peninsular Gneiss Complex. The Peninsular Gneisses contain 3400–3580 Ma old basement tonalitic gneiss enclaves (Nutman et al., 1992). Swami Nath and Ramakrishnan (1981) suggest that the peninsular gneisses enclose relics of older supracrustals as narrow belts and enclaves or synclinal keels, which exhibit amphibolite facies mineral assemblages. They were called Ancient Supracrustals by Ramakrishnan (1990) and later Swami Nath and Ramakrishnan (1990) designated them as Sargur Group (3000–3200 Ma old). The metamorphic fabric of these Ancient Supracrustals (the Sargur Group rocks) and the surrounding gneiss complex is truncated by the low-grade Dharwar Schists (Bababudan Group) and both are unconformably overlain by the main schist belts of the Dharwar Supergroup (2600–2800 Ma). Because of this, Swami Nath and Ramakrishnan (1990) proposed an orogeny (Sargur orogeny) that has taken place before the deposition of the Dharwar supracrustals. The type Sargur Group, developed around Hole Narsipura, is represented by high-grade pelitic schists (kyanite-staurolite-garnet-mica schists), fuchsite quartzite, marble and calc-silicate rocks, besides mafic and ultramafic bodies. The mafic rocks (amphibolites) show typical tholeiitic trend and are essentially low K-tholeiites with normative olivine and hypersthene. Detrital zircons from metapelites yielded ~3.3 Ga and 3.1-3.3 Ga (SHRIMP U-Pb age), and ultramafic rocks yielded Sm-Nd model age of ~3.1 Ga (Nutman et al., 1992, Peucat et al., 1995).

The Eastern Dharwar craton is dominated by late Archean gneissic rocks, calc-alkaline granites interleaved with 2.7 Ga narrow greenstone belts, intrusive volcanics and

middle proterozoic to more recent sedimentary formations (Naqvi and Rogers, 1987; Chadwik et al., 2000; Jayananda et al., 2000; Ramakrishnan and Vaidyanadhan, 2010). The craton is interspersed with several schist belts such as the Kolar, Ramagiri and Hutti schist belts. These schist belts of Eastern Dharwar craton (EDC) are made up of basaltic rocks and there is no recognizable basement to these schist belts because these belts are engulfed on all sides by 2500–2600 Ma old granites and gneisses. Majority of the intrusive events in this craton are represented by mafic dykes, kimberlites and lamporites. Three main trends of mafic dyke swarms (viz. NW-SE, NE-SW to E-W and N-S) related to Large Igneous province are observed in this craton (French and Heaman, 2010; Kumar et al., 2012a; Kumar et al., 2012b, Radhakrishna et al., 2013). Among these NE-SW to E-W dyke swarm is extensively studied and dated at 2365-2367 Ma (Halls et al., 2007; Kumar et al., 2012a). Kimberlites and lamporites (1124 Ma to 1085 Ma) are found in relative abundance within the craton (Kumar et al., 2007). The Eastern Block consists mainly of volcanic (greenstone) belts of Dharwar group (2600–2800 Ma old). The greenstone belts in the EDC do not preserve unconformable relations with their surrounding granite–gneiss terrains. Margins of most of these belts have sheared intrusive contacts with the late Archean neighboring syn-tectonic plutons. EDC greenstone sequences are dominated by volcanic rocks (minor komatiite, high- Mgbasalt, andesite, adakite and rhyolite) and banded iron formations (BIFs) (Viswanatha and Ramakrishnan, 1981; Balakrishnan et al., 1990, 1999; Kazmi and Kumar, 1991; Srinivasan, 1990; Srinivasan and Krishnappa, 1991; Srikantia, 1995; Manikyamba et al., 2004, 2009; Naqvi et al., 2002; Anand and Balakrishnan, 2010). The prominent meridional Closepet Granite occurring close to the boundary between the Eastern and Western blocks is one such younger granite, running parallel to the trend of the schist belts. According to Narayanaswami (1970), there are numerous elongated granites running parallel to the schist belts of the Eastern Block, that occur as a series of parallel plutonic belts which have been designated as Dharwar Batholith (Chadwick et al., 2000) in order to distinguish them from the widely used term Peninsular gneiss, scarcely exposed in the EDC. The gneisses span the age from 2.7 to 2.8 Ga (SHRIMP U–Pb and Rb–Sr methods). The protolith ages are >2.9 Ga, corresponding to the main thermal event of WDC. Amongst the younger granites, the Closepet Granite is an elongated (600×15 km) body intruding the Bababudan schist belts as well as the basement gneiss. It is a biotite granite or granodiorite to quartz monzonite composition. The granite yielded well-defined Pb–Pb

and Rb–Sr isochron of age ~2.6 Ga which is also the U–Pb zircon age of the granite (Chadwick et al., 2007). The involvement of gneissic basement in the generation of the Closepet Granite and other late to post-tectonic granites (Arsikere, Banovara, Hosdurga) of Dharwar craton is evident from Sm–Nd model ages (TDM) of the granite at ~3.0 Ga. Deformation of Dharwar Schist Belts show N-S trending folds superposed on older E-trending recumbent folds, giving rise to the prevalent NNW to NNE Dharwar trend with convexity toward the east. But this view became untenable because the older E-W folds superposed by N-S folds could not be found on a regional scale. Structural studies of Dharwar craton by Naha et al. (1986) showed that the Sargur, Dharwar and Peninsular gneiss (and Dharwar Batholith) have similar style, sequence, and orientation of folding (named Structural Unity). In areas of intense deformation, the Dharwar folds and fabric are superposed on Sargur folds and fabric, resulting in apparent parallelism as a result of rotation of earlier Sargur fabric during the younger Dharwar deformation (Ramakrishnan and Vaidyanadhan, 2008).

Geothermobarometry along with fluid inclusion studies demonstrated that the P-T conditions in the low grade rocks in the north are 500°C/4 kb which increases to 600°C/5–7 kb in middle grade and 700–750°C/7–8 kb in the granulite grade rocks of the Dharwar craton (Peucat et al., 1993). The regional metamorphism of EDC also occurred in a similar way, but is of low-pressure facies series. P-T conditions of EDC range from 670°C/3 kb in the Sandur belt in the north through 710°C/4–5 kb in the middle to 750°C/6–7 kb in the Krishnagiri-Dharmapuram area in the south (Jayananda et al., 2000). The low pressure metamorphism of EDC is caused by the abundance of younger granites that seem to have supplied advective heat. Based on regional geology, metamorphic conditions and P-T calculations from granulite-facies in the southern part to greenschist-facies in the northern part, Dharwar Craton provides a cross section of the Late Archean crust (e.g. Rollinson et al., 1981; Harris and Jayaram, 1982; Moyen et al., 2003). The dip of the present erosion surface relative to the Archean paleo-depth is about 2° (equivalent to a vertical distance of 10-13 km). Crustal thickness varies from 35 Km to 45 km in the Eastern Dharwar Craton as estimated from teleseismic and deep seismic sounding studies (Gupta et al., 2003; Reddy et al., 2003). This crustal cross section of about 10 km from north to south is due to the northward tilting and subsequent erosion of crust in the Dharwar Craton.

2.4. Proterozoic Dyke swarms in Dharwar Craton:

The Indian cratons are cross-cut by numerous Precambrian mafic dyke swarms as well as sills and mafic-ultramafic intrusions (Ernst and Srivastava, 2008). The dykes and dykes swarms of different generations cross cut Archean granites and gneisses and have a wide variety of orientations (E-W, WNW-NW, NE-ENE, and N-S; Halls, 1982; Bhaskar Rao et al., 1995; Halls et al., 2007; French et al., 2008; French and Heaman, 2010; Pradhan et al., 2010; Kumar et al., 2012a, 2012b; Belica et al., 2013, Radhakrishna et al., 2013). These dykes are widespread in the eastern Dharwar craton and are well exposed in the vicinity of Cuddapah basin (Figure 2.2).

2.4.1. 2.37 Ga dykes

It was recognized very early through geological mapping (Smeeth, 1915) and remote sensing studies (Drury and Holt, 1980; Halls, 1982; Drury, 1984), that the most prominent mafic dyke swarm in the Dharwar craton is a predominantly E–W trending swarm that extends across a large tract of the craton (referred to as the Dharwar giant dyke swarm or Bangalore dyke swarm; French et al., 2004; French, 2007; Halls et al., 2007; Kumar et al., 2012a). The age of Dharwar giant dyke swarm (Bangalore swarm) is constrained by several precise U-Pb ages of 2367 ± 1 Ma (Yeragumballi diabasedyke, baddeleyite; Halls et al., 2007), 2365.4 ± 1.0, 2365.9 ± 1.5and 2368.6 ± 1.3 Ma (Harohalli, Penukonda, and Chennekotta-palle dykes, baddeleyite; French and Heaman, 2010), as well as2368.5 ± 2.6 Ma and 2367.1 ± 3.1 Ma (Karimnagar dykes, badde-leyite; Kumar et al., 2012a). The highest density of dykes from this swarm is in Tirupathi-Rayachoti area at the southwest margin of the Cuddapah basin, and can be traced along strike in a westerly direction from the southern tip of the basin (near Tirupati) for about 500 km across the southern Indian shield (Halls 1982; Drury, 1984; Murty et al., 1987; Halls et al., 2007). This predominately E-W trending swarm consists of iron-rich tholeiites, and was emplaced fairly rapidly (~5 Myr; Kumar et al., 2012a; Ernst and Srivastava, 2008). It has been suggested that the dykes associated with this magmatic event are part of a radiating swarm, with a focal point west of the present day craton boundary (Kumar et al., 2012a).

2.4.2. 2.22-2.21 Ga dykes

The N-S to NNW-SSE trending dyke swarm is one of the major dyke swarms recognized all over the eastern Dharwar craton (Murthy 1987; Ernst and Srivastava 2008; French and Heaman 2010; Srivastava et al., 2011; Kumar et al., 2012b). A prominent N-S trending dyke in this swarm runs ~450 km along the western margin of the Closepet granite. ID-TIMS (Isotope Dilution – Thermal Ionization Mass Spectrometry) and TE-TIMS (Thermal Extraction – Thermal Ionization Mass Spectrometry) baddeleyite ages for this long dyke is recently presented by Srivastava et al., (2011), which yields 2215.2±2.0 Ma (U-Pb), and by Kumar et al. (2014), yields an age of 2215.9±0.3 Ma (Pb-Pb). Another dyke of this swarm also yields similar age 2211.7±0.9 Ma (Srivastava et al., 2011). A number of similar N-S trending mafic dykes are also encountered from south and north of the Cuddapah basin. Additional ages on two more dykes in this swarm, located south of the Cuddapah basin yield U-Pb baddeleyite ages of 2220.5±4.9 Ma(N-S trend; Kandlamadugu) and 2209.3 ± 2.8 Ma (NNW-SSE trend; Somala dyke) confirming the existence of a major 2.2 Ga dyke swarm (French and Heaman 2010).

2.4.3. 2.18 Ga dykes

Northwest trending dykes of the 2180 Ma Mahabubnagar swarm are mainly gabbro, dolerite, and metapyroxenite, and geochem-ically tholeiitic or sub-alkalic and quartz or olivine normative (Ernst and Srivastava, 2008; Pandey et al., 1997). It has been suggested that the dykes are fairly widespread throughout the Dharwar craton, and recent U-Pb ages indicate the presence of 2.18 Ga dyke swarm (NW-SE and E-W), with a possible convergence point west of the Deccan Flood basalt province (French and Heaman, 2010). The E-W trending Bandapalem dyke and NW-SE trending Dandeli dyke have ages of 2176.5 ± 3.7 Ma (baddeleyite and zircon) and 2180.8 ± 0.9 Ma (baddeleyite). Ernst and Srivastava (2008) proposed that dykes from mahabubnagar dyke swarm trend NW-SE to E-W with a fanning angle of ~60°.

2.4.4. 2.08 Ga dykes

Recent work on dykes in the Dharwar craton recognises a set of 2082 Ma radiating dykes intruding the basement rocks on the northern, north-western and western periphery of the Cuddapah basin. Kumar et al. (2015) obtained high precision Pb-Pb

baddeleyite age 2081.8±1.1 Ma for NW dyke, 2082.8±0.9 Ma for NNE dyke, 2081.8±0.7 Ma for NS dyke and 2081.1±0.7 Ma for another NS dyke in this swarm. Similar ages are reported by Demirer, 2012 on these dykes. A weighted mean of three U-Pb ID-TIMS determinations is 2081.0±1.6 Ma.

2.4.5. 1.88 Ga dykes

Recent work within the Dharwar craton hints at the presence of a Large Igneous Province (LIP) at1.88 Ga. French et al. (2008) obtained high precision U–Pb date1885 ± 3.1 Ma for the Pulivendula mafic sill within the Cuddapah basin. Preliminary U-Pb age on E-W trending dyke near humpi region (west of Cuddapah basin) gives a primary crystallization age of approximately 1894 Ma, indicating this dyke swarm could be feeder to Cuddapah sills (Halls et al., 2007). Similar ages are also observed in Bastar craton. U-Pb baddeleyite and zircon ages on NW-SE trending mafic dykes (BD2 dyke swarm) from Southern Bastar craton include 1891.1 ± 0.9 Ma and 1883.0 ± 1.4 Ma (French et al., 2008). Ernst and Srivastava (2008) linked 1.88 Ga NW-SE trending dykes in the Bastar craton (French et al., 2008) with an E-W trending dyke west of the Cuddapah basin (Halls et al., 2007) and speculated that a major radiating dyke swarm could be present within the Dharwar craton, with a convergence point located east of the craton boundary.

2.5. Description of mafic dykes:

The dykes are generally medium to coarse grained dolerites without metamorphism or tectonically-induced foliation. Dyke thicknesses are mostly of the order of 25-30m; however, dykes of larger thicknesses (>50m) are also common and such dyke centers may be gabbroic in nature. Fine-grained chilled margins are sometimes observed when contacts are exposed. The dykes have near uniform mineral assemblages containing plagioclase and clinopyroxene and opaque oxides. Textures are typically ophitic and interstitial, frequently with plagioclase phenocrysts. Deuteric alteration is quite common and in some cases hydrothermal alteration is characterised by the formation of chlorite/actinolite. Opaque minerals are distributed as euhedral disseminations or have skeletal shapes. There are no prominent petrographic or chemical criteria to distinguish dykes of different strike directions and furthermore, the dykes of similar strike directions have yielded variable ages.

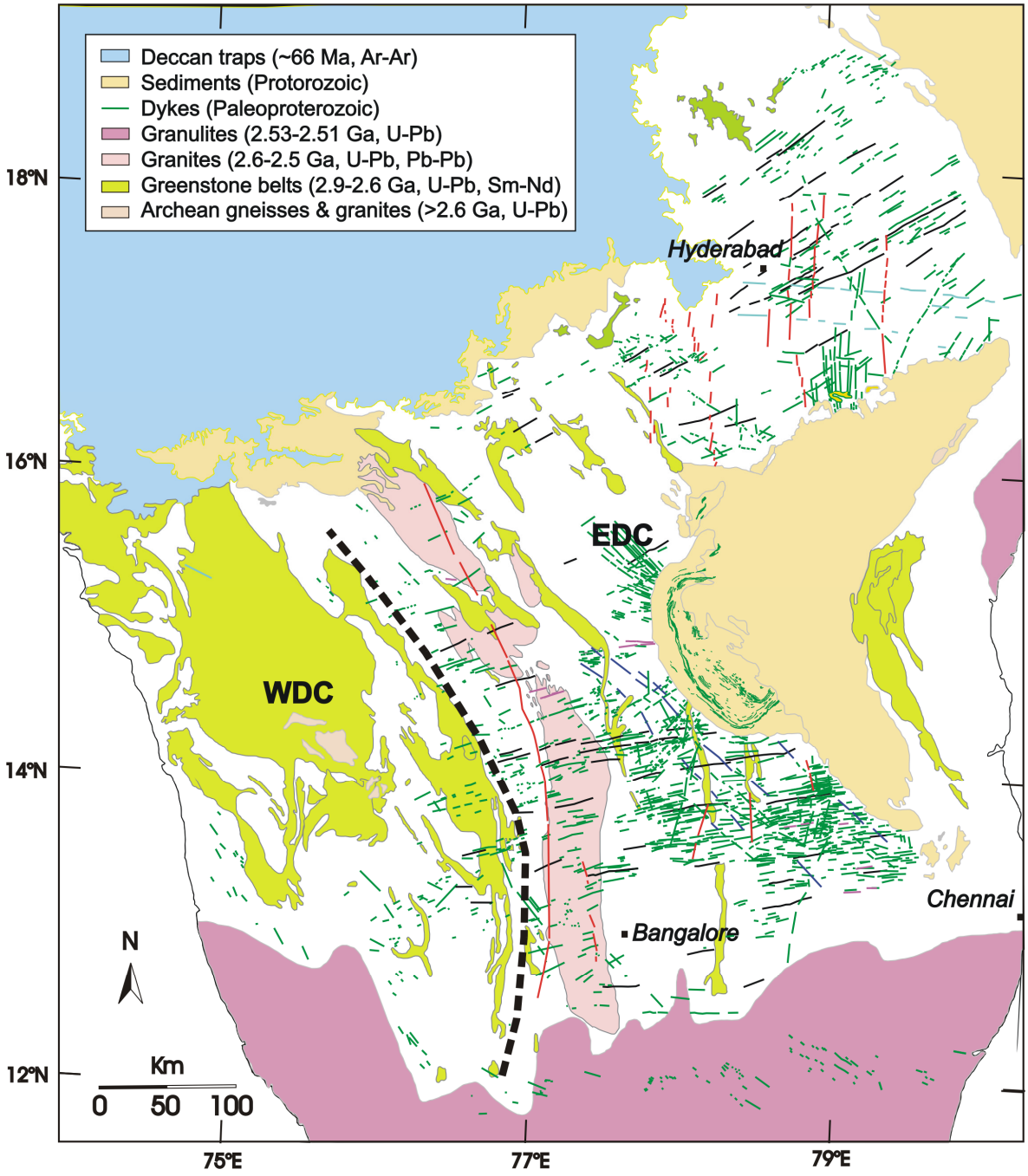

Figure 2.2. *Simplified geology of south India (modified after Geological Survey of India (1998) and Naqvi and Rogers (1987)), showing the distribution of Paleoproterzoic dykes (dyke distribution after French and Heaman (2010), Halls et al. (2007) and Google Earth maps). Dykes in black coloured are part of 2.37 Ga, red colour are part of 2.21 Ga, blue colour are part of 2.18 Ga and pink colour are part of 1.88 ga dyke swarm. EDC and WDC are Eastern Dharwar Craton and Western Dharwar Craton respectively. Black dashed line demarcates the boundary between the two blocks EDC and WDC.*

2.6. Sampling:

Samples for this study have been taken from Precambrian mafic dykes from eastern Dharwar craton. Extensive independent field works have been conducted to identify suitable dykes and to collect samples on many of these dykes. The details of the sample locations are shown in the Figure 2.3 and given in Table 2.1. The majority of the samples were taken as hand samples and a few were taken with the help of portable field drills. Collection of oriented dyke samples was done in a systematic manner. The first step in this study is to locate/trace the dykes on the toposheets available in NGRI using Google Earth program. Toposheets depict the dykes as dotted contours. Most dykes are made up of several linear segments that lie on a straight line, but in some cases dykes do not form as continuous segments. Locating the dykes on toposheets was followed by field work to examine and sample the dykes at fresh exposures like quarries, road cuts and canal cuts. Field photographs of well exposed and insitu outcrops and hand sample collection for paleomagnetic studies are shown in figure 2.4. The dykes are all typical dolerites, quite fresh and un-metamorphosed. Host rock samples are also collected in few sites to examine the stability of the remanent magnetization. Determining the right sampling location within a feature is important and it mainly includes identifying in-situ outcrop to sample. The samples were oriented with Brunton compass (Magnetic compass) and spirit level. Brunton compass measures only the angle in horizontal plane (with respect to the magnetic north; called as azimuth). Brunton compass is also used to detect the presence of anomalously strong magnetization induced by lightning strike, so as to avoid such lightning-struck regions, areas were marked for sampling collection where the compass needle deflection was minimum. Common technique of orienting a block sample is to draw a horizontal line with an arrow parallel to the North direction on the sampled rock surface and a horizontal line on any two perpendicular faces. A common practice is to collect 5 to 8 separately oriented samples at an outcrop (site). Each of these Samples is labled in a sequential order. The strike of each individual site and sample information (thickness, Lat. and Long.) were noted in the field and strike direction is confirmed with traced dykes on toposheets or locating the site on google earth. Care was taken to collect samples from large, structurally simple blocks that were part of the main mountain ranges. Also, the samples collected per site were spaced over large enough exposures to avoid difficulties from small block rotations. Precautions are necessary because the

paleomagnetic directions obtained from a site should be applicable to the entire dyke. These samples are then transported to NGRI laboratory for further studies.

The block samples were cored in the laboratory after orienting the samples in to the field position with the help of markings on the sample. Multiple cores were drilled from each sample using coring machine. Sample numbers and north orientation mark are transferred to drilled cores. Drilled in cores were cut in to uniform cylindrical specimens of standard cylindrical size (2.5 cm in diameter and 2.2 cm in length).

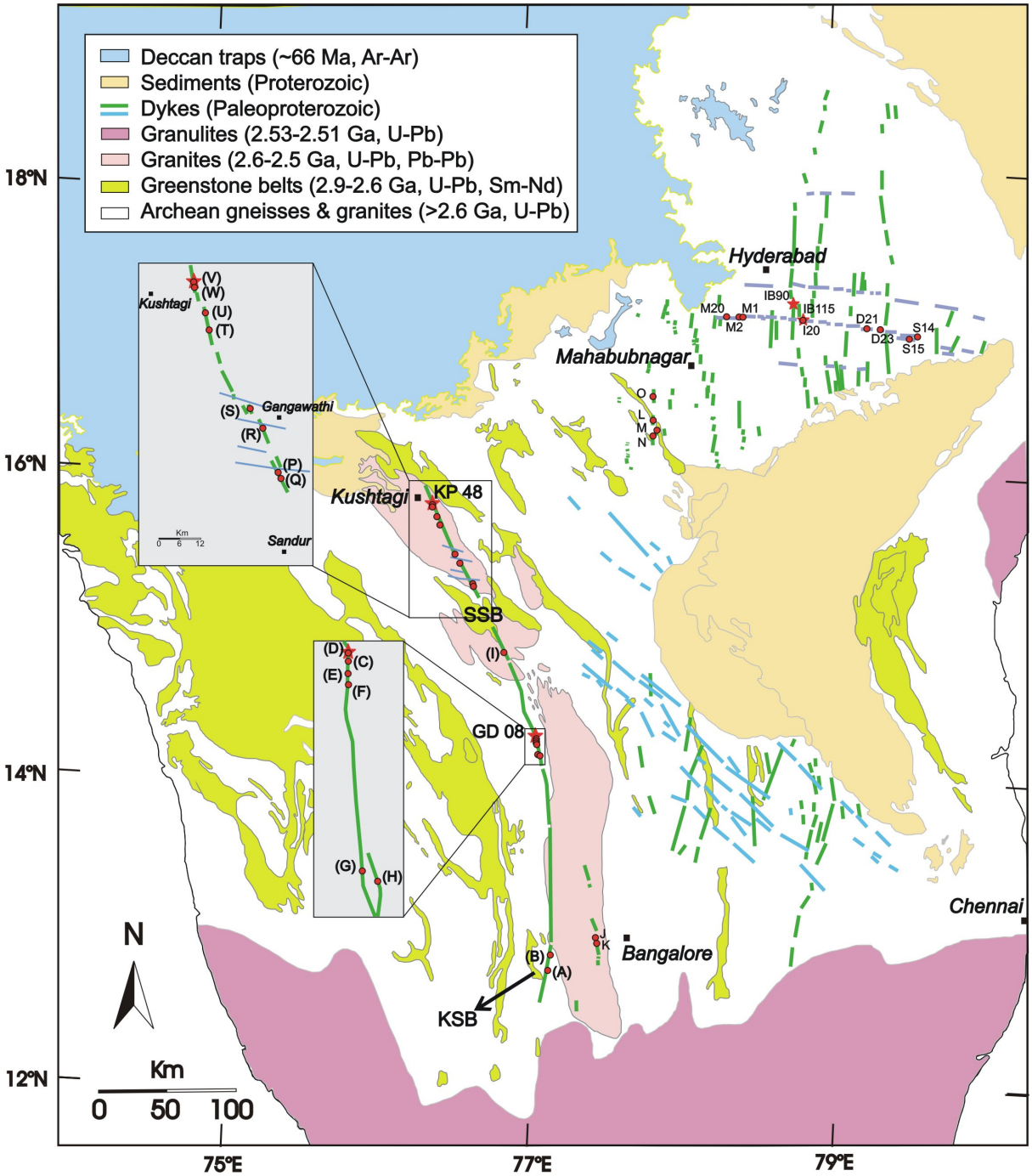

Figure 2.3. *Simplified geology map of the Dharwar craton showing N-S, NW-SE and E-W striking mafic dykes distribution (modified after Naqvi and Rogers, 1987, dykes traced from Google earth and French and Heaman, 2010). Red coloured circles indicate the sampling locations for paleomagnetism and red stars indicate the samples chosen for geochronology. SSB: Sandur schist belt, CSB: Chitradurga schist belt, KSB: Kunigal schist belt. Black dashed-line demarcates the boundary between the Eastern and Western Dharwar craton.*

Figure 2.4. *Field photographs of well exposed and insitu outcrops and hand sample collection for paleomagnetic studies using Brunton compass.*

Table 2.1. *Paleomagnetic sampling details including the location wise description of dyke trend along with nearest village names.*

Site	Sample No	Latitude (°N)	Longitude (°E)	Trend	Location
A	HD 10 & HD 12	12.767	77.056	N14E	Hunugana Halli
B	HD 16 & HD 17	12.851	77.069	N357E	Hasige Hobli
C	GD 3-GD6	14.216	76.977	N1E	Kolapala
D	GD 7-GD10	14.218	76.977	N359E	Kolapala
E	GD 11-GD13	14.209	76.977	N357E	Kolapala
F	GD 14-GD17	14.204	76.977	N358E	Kyadigunte
G	GD 18-GD21	14.117	76.985	N350E	Amarapuram
H	GD 23-GD25	14.112	76.993	N343E	Udagur
I	GD 26-GD31	14.778	76.786	N335E	Mecchiri
P	KP 2-KP8	15.292	76.529	N341E	Kamalapur
Q	KP 10-KP15	15.303	76.521	N344E	Kamalapur
R	KP 24-KP29	15.404	76.487	N338E	Mallapur
S	KP31-KP37	15.456	76.452	N337E	Dasanalla
T	KP 38-KP42	15.662	76.342	N350E	Homminhal
U	KP 44-KP48	15.705	76.331	N338E	Gudadhanamsagar
V	KP 49-KP54	15.777	76.301	N358E	Hiremannapur
W	KP 55-KP58	15.773	76.301	N350E	Hiremannapur
J	HDT1-HDT6	12.974	77.353	N354E	Marenahalli
K	HDT7-HDT11	12.950	77.378	N350E	Puradapalya
L	MB70-MB75	16.361	77.721	N357E	Nandimalla
M	MB76-MB80	16.287	77.741	N4E	Peddapad
N	MB83-MB86	16.266	77.720	N5E	Pacherla
O	MB87-MB91	16.512	77.717	N13E	Undekode
M20	MB95-MB99	17.086	78.070	N0°E	Chetanpally
M1	MB1-MB6	17.076	78.314	N102°E	Kudacharla Thanda
M2	MB7-MB11	17.055	78.319	N102°E	Kudacharla Thanda
I20	IB110-IB117	17.047	78.723	N67°E	Dedpally
D21	DK114-DK119	16.957	79.206	N82°E	Parvathagiri
D23	DK125-DK129	16.958	79.282	N98°E	Botthugudem
S14	MS62-MS66	16.932	79.487	N93°E	Peddadevulapally
S15	MS67-MS71	16.918	79.433	N98°E	Kampalapally
IB90	IB90	17.132	78.684	N356E	Aghapally

Chapter 3: Principles of Geochronology

3.1. Introduction:

Geochronology alludes to the utilization of radioactive decay in closed systems to acquire the time of particular geologic event, which is known as an age. This has made great technical advances facilitating precise dating, particularly with enhancements in the recovery of small mineral grains (Söderlund and Johansson, 2002). Felsic and mafic rocks are best considered for precise radiometric dating of geological events because they possess common accessory minerals (like baddeleyite and zircon) which generally contain high concentrations of radioactive uranium (500 ppm to several thousand ppm). Age determination is mainly predicted on the decay of long lived radioactive isotope (ex: ^{40}K, ^{87}Rb, ^{147}Sm, ^{235}U, ^{232}Th etc.) to stable daughters. A particular mineral that contains a radioactive isotope is carefully studied to figure out the number of parent and daughter isotopes present. With this information the time since the mineral is formed can be calculated. This chapter presents common principles of Pb-Pb geochronology and description of methods that were utilized as a part of thermal-extraction thermal ionization mass spectrometer (TE-TIMS).

3.2. Principles of radioactive decay:

In nature, many elements contain different isotopes. Atoms with different mass numbers (different number of neutrons) and same atomic number are known as isotopes. A few of these isotopes are natural radioactive elements, whose nuclei are unstable and spontaneously decay to stable isotopes of various elements. If the newly formed isotope is stable, this process will be stopped. Rate of decay of each individual isotope is different and is termed as decay constant (λ). This decay constant is independent of temperature, pressure and chemical state. According to the theory of Rutherford and Soddy, the rate of decay of a radioactive isotope is proportional to the number of atoms (N) remained at any time (t).

$$-dN/dt \propto N$$

$$-dN/dt = \lambda N$$

Here, λ is disintegration constant or decay constant and dN/dt is negative because out of original nuclei, a few have decayed.

$$-\int dN/N = \lambda \int dt$$

Which yields $- ln\, N = \lambda t + C$

Where '*ln N*' is the logarithum to the base e of *N* and C is the constant of integration.

This constant can be evaluated from the condition that $N=N_0$ when t = 0. Therefore,

$$C = - ln\, N_0$$

$$- ln\, N = \lambda t - ln N_0$$

$$ln\, N - ln\, N_0 = - \lambda t$$

$$ln(N/N_0) = - \lambda t$$

$$\frac{N}{N_0} = e^{-\lambda t}$$

$$N = N_0\, e^{-\lambda t}$$

The above basic equation gives the number of radioactive parent atoms (*N*) that ant time (t) of an original number of atoms (N_0) that were present when t = 0.

The above equation is utilized to decide the age of the mineral based on the radioactive decay of unstable parent isotope to stable daughter isotope.

3.2.1. Half -life time ($T_{1/2}$) and mean life time (τ)

The half-life is the time in which radioactive parent isotope has been reduced to one half of its initial amount. It follows therefore that, when $t=T_{1/2}$, $N=N_0/2$. Substituting these values into basic equation yields

$$\frac{N_0}{2} = N_0 e^{-\lambda T_{1/2}}$$

$$\ln\left(\frac{1}{2}\right) = -\lambda T_{1/2}$$

$$\ln 2 = \lambda T_{1/2}$$

$$\boxed{T_{1/2} = \frac{\ln 2}{\lambda} = \frac{0.693}{\lambda}}$$

Above equation provides a convenient relation between the half-life of a radioactive isotope and its decay constant.

Mean life (τ) of a radioactive isotope is the time at which radioactive parent isotope has been reduced to 1/e of its initial amount. It can be expressed as:

$$\tau = \frac{-1}{N_0} \int_{t=0}^{t=\infty} t \; dN$$

Substituting the equations $-dN/dt = \lambda N$ and $N = N_0 e^{-\lambda t}$ in above equation, we will get,

$$\tau = \frac{1}{\lambda}$$

$$\tau = \frac{T_{1/2}}{0.693}$$

3.3. Application of radioactivity to Pb-Pb method:

Lead (Pb) is a carbon group chemical element with atomic number 82. Lead is the fourth heaviest element which occurs naturally in the form of isotopes. Observationally, Pb has four stable isotopes, ^{204}Pb, ^{206}Pb, ^{207}Pb, and ^{208}Pb. Of these, ^{204}Pb is the only non-radiogenic Pb isotope, consequently is not a daughter isotope. The remaining three are stable daughter isotopes of Pb and derive from the radioactive decay of U (uranium) and Th (Thorium) (^{208}Pb, ^{207}Pb and ^{206}Pb). These daughter isotopes are the final products of ^{238}U, ^{235}U and ^{232}Th radioactive series respectively. This can be represented by the decay equations given below:

$$^{238}_{92}U \rightarrow {}^{206}_{82}Pb + 8\,{}^{4}_{2}He + 6\beta^{-} + Q$$ (Where Q=47.4 MeV/atom or 0.71 cal/g y)

$$^{235}_{92}U \rightarrow {}^{207}_{82}Pb + 7\,{}^{4}_{2}He + 4\beta^{-} + Q$$ (Where Q=45.2 MeV/atom or 4.30 cal/g y)

$$^{232}_{90}Th \rightarrow {}^{208}_{82}Pb + 6\,{}^{4}_{2}He + 4\beta^{-} + Q$$ (Where Q=39.8 MeV/atom or 0.20 cal/g y)

As time progresses, due to the decay of parent isotope, daughter isotope accumulates at a constant rate. With this the ratio of radiogenic Pb and non radiogenic ^{204}Pb (^{206}Pb/^{204}Pb or ^{207}Pb/^{204}Pb) shifts in favour of radiogenic ^{206}Pb or ^{207}Pb. The accumulation of the radiogenic isotopes of Pb by decay of their respective parents, is written in terms of the

atomic $^{208}Pb/^{204}Pb$, $^{207}Pb/^{204}Pb$ and $^{206}Pb/^{204}Pb$ ratios because ^{204}Pb is the only stable non radiogenic isotope of Pb. The ratios can be written as

$$\frac{^{206}Pb}{^{204}Pb} = \left(\frac{^{206}Pb}{^{204}Pb}\right)_i + \frac{^{238}U}{^{204}Pb}\left(e^{\lambda_1 t} - 1\right) \quad \ldots\ldots. \ (1)$$

$$\frac{^{207}Pb}{^{204}Pb} = \left(\frac{^{207}Pb}{^{204}Pb}\right)_i + \frac{^{235}U}{^{204}Pb}\left(e^{\lambda_2 t} - 1\right) \quad \ldots\ldots. \ (2)$$

$$\frac{^{208}Pb}{^{204}Pb} = \left(\frac{^{208}Pb}{^{204}Pb}\right)_i + \frac{^{232}Th}{^{204}Pb}\left(e^{\lambda_3 t} - 1\right) \quad \ldots\ldots. \ (3)$$

` Where λ_1, λ_2, λ_3 are decay constants of ^{238}U, ^{235}U and ^{232}Th (λ_1=1.55125 X 10^{-10} /yr, λ_2=9.8485X 10^{-10} /yr and λ_3=14.010 X 10^{-11} /yr) respectively. The subscript '*i*' refers to the initial values.

Age can be calculated based on the slope of Pb-Pb isochron which is derived by combining equations 1 & 2 to yield following equation.

$$\left(\frac{^{207}Pb}{^{206}Pb}\right)^* = \frac{^{207}Pb/^{204}Pb - \left(^{207}Pb/^{204}Pb\right)_i}{^{206}Pb/^{204}Pb - \left(^{206}Pb/^{204}Pb\right)_i}$$

Chapter 4: Methods and Results of Geochronology

4.1. Introduction:

Baddeleyite (ZrO_2) mineral is commonly occurred mineral in mafic rocks. Precise age determination of mafic magmatism can be attained by the analysis of baddeleyite mineral. Baddeleyite mineral typically contains adequately high Uranium concentrations (five hundred to several thousand ppm, Heaman and LeCheminant, 1993) with nearly concordant or concordant (commonly < 1% discordant) U–Pb data even without any of the pre-treatments typically required for zircon preparation, as it appears to be much less susceptible to Pb loss than zircon (Bayanova, 2006; Li et al., 2005; Wingate et al., 1998; Heaman and LeCheminant, 1993; Heaman and Tarney, 1989). It also rarely occurs as xenocrysts in mafic rocks. Because of such good chemical and physical properties, baddeleyite mineral is treated as perfect geochronometer for Pb-Pb and U-Pb dating of ultramafic and mafic rocks.

Regardless of its potential as a perfect geochronometer for qualitative analysis of for silica under-saturated igneous rocks (where number of zircons are very much less), there are relatively few baddeleyite age determinations reported. This can be partially as a result of standard U–Pb dating using isotope dilution thermal ionization mass spectrometry (ID-TIMS). This technique is limited to just a couple of research laboratories with the essential ultra clean lab environment, with less than 1 pg Pb blanks for precise determination of the concentrations of U and Pb by isotope dilution and Pb isotopic composition using thermal ionization mass spectrometry. Moreover, in contrast to the case of zircon and different uranium rich minerals, high precision U-Pb age estimation of baddeleyite mineral using high resolution secondary ion mass spectrometry (SIMS) was not significantly made till recently (Li et al., 2010), attributable to crystal orientation or twinning effects that bias the measured $^{206}Pb/^{238}U$ ratio, resulting in lower age precisions (Wingate and Compston, 2000).

A new approach was recently presented by Davis (2008), wherein it was demonstrated that 'Pb' thermally extracted from zircon into a silica melt ionization activator (TE-TIMS method) produces strong ion beams that allow $^{207}Pb/^{206}Pb$ isotope ratios to be measured by a thermal ionization mass spectrometer to high precision ($\pm 10^{-4}$)

with almost negligible contamination from common Pb. Pb/U ratios cannot be determined using this process. However, ages can be determined without U information, purely from the radiogenic daughter isotope ratios. U–Pb error systematics are such that ages based on $^{207}Pb/^{206}Pb$ measurements are more precise than those based on the measurements of Pb/U ratios for rocks that are Mesoproterozoic or older. Therefore, the lack of U measurement does not degrade age information for most Precambrian samples where a single age population can be isolated. Closed system behaviour can be confirmed by reproducibility of ages for different fractions. Age reproducibility is a necessary test even for concordant U–Pb data to confirm the absence of inheritance. This study presents replicate $^{207}Pb/^{206}Pb$ age determinations using the TE-TIMS approach on several fractions of Phalaborwa baddeleyite standard and on a Paleoproterozoic dyke (GD-08) from the Dharwar craton (Fig. 4.1). Both were earlier dated by the conventional U–Pb technique.

4.2. Baddeleyite

Baddeleyite is a prevalent zirconium oxide mineral (ZrO_2), that crystallizes under marginally saturated or undersaturated conditions in a variety of rock types such as cabonatites, kimberlites, syenites, anorthosites, alkaline rocks, layered mafic intrusions, gabbro/dolerite dykes and sills (e.g. Lumpkin, 1999; Heaman and LeCheminant, 1993 and references there in). Conventionally it occurs in minute crystal size (generally less than 30 mm in width) with a very low abundance. This mineral has a 6.5 hardness and density 5.5-6 g/cm^3 with a melting point of 2700°C. During metamorphism baddeleyite mineral recrystallizes to zircon (ZrSiO4) (e.g. Heaman and LeCheminant, 1993; Davidson and van Breemen, 1988). Though the mineral is chemically homogeneous, it may contain impurities such as Fe (iron), Ti (Titanium) and Hf (hafnium). Higher concentrations of Fe and Ti are generally observed in mafic and ultramafic rocks. Hafnium may be present in quantity ranges from 0.1 to several percent.

Baddeleyite has long been considered as the most prominent uranium bearing mineral for reliably dating the crystallization of mafic-ultramafic or other silica undersaturated intrusive rocks (where zircons are extremely rare) by U–Pb / Pb-Pb method (e.g. Bayanova, 2006; Heaman and LeCheminant, 1993; Krogh et al., 1987). This is because of some unique characteristics:

- It crystallizes in the late-stage, chemically fractionated portions of mafic magmas.

- It contains invariably high U concentrations (500–1000 ppm) and negligible initial common Pb content allow for precise age (to ~0.1% precision) determinations with statistical errors of a few million years or less.
- Baddeleyite as a xenocryst has not been reported in mafic-ultramafic intrusions.
- It appears to be much less susceptible to Pb loss than zircon (Heaman and Tarney, 1989; Heaman and LeCheminant, 1993; Wingate et al., 1998; Li et al., 2005; Bayanova, 2006).

4.3. Background:

Early attempts at Pb isotopic analysis using TIMS were carried out by loading zircon ($ZrSiO_4$) grains directly on a single filament and using available silica in the mineral as a Pb+ emitter (Zykov and Stupnikova, 1957 and Kosztolanyi, 1965). Subsequent analytical modifications (Chukhonin, 1978; Gentry et al., 1982; Sunin and Malyshev, 1983) led to improved results. Later, it was demonstrated that stable Pb ion beams could be more successfully generated with a double filament arrangement (Kober, 1986, 1987). Though this method did not require any preliminary clean chemical preparation and advanced instrumentation, its application has been limited because extraction, deposition of primary Pb and emission from the condensation filament produced diminished ion beams and hence lower age precision.

In the Kober method heating of the zircon grain in a TIMS source promotes the breakdown of $ZrSiO_4$ to ZrO_2 (Chapman and Roddick, 1994) releasing SiO_2 along with Pb, which deposit on the condensation filament. The condensed silica enhances the ionization of Pb, imparting an effect similar to that seen in silica gel fused sample loads (Cameron et al., 1969; Gerstenberger and Haase, 1997). This method therefore cannot be applied to non-silicate minerals like baddeleyite for Pb isotopic analysis and age determination. However, Davis (2008) has developed an alternative method, the thermal extraction-TIMS procedure that could overcome the main deficiency in the 'Kober' method, namely the insufficient amount of silica activator derived from the sample grain, by embedding pre-treated mineral grains in silica glass by fusion with silica gel on an out-gassed Re filament. Heating the embedded sample to >1500°C in the mass spectrometer source results in extraction of Pb into the silica melt. With enough sample, sufficiently strong ion beams are produced that allow $^{207}Pb/^{206}Pb$ isotope ratios to be measured to a

high precision ($\pm 10^{-4}$) on a multicollector TIMS. There is almost negligible common Pb contamination due to the simplicity of the procedure (resulting in low blank) and the fact that loading blank Pb diffuses out faster than radiogenic Pb released from progressive breakdown of the mineral. This new approach (TE-TIMS) was used by Davis (2008) to achieve sub-million year precisions on Pb ages using embedded zircon. The potential of this procedure motivated us to apply it (with modifications) to baddeleyite Pb geochronology.

4.4. Analytical procedures

4.4.1. Thermal Ionization Mass Spectrometer

Relative abundance of different isotopes is determined, based on the charge to mass ratios obtained using mass spectrometer. Thermal ionization mass spectrometer (TIMS; Figure 4.2) uses highly sensitive isotope mass spectrometry characterization technique which is equipped for making estimations of isotope proportions of elements that can be ionized thermally, more often by passing a current through a thin metal strip or strips under vacuum. The ions made on the metal strip(s) are accelerated over an electrical potential (up to 10 KV) and then focused into a beam through a series of openings (slits) and electro statically charged plates. This particle beam then goes through a uniform field and is separated into isolated beams according to the mass to charge ratio. These mass related particle beams are then directed into collectors where the particle beam is converted into a voltage. Correlations of voltages comparing to individual particle beams yield exact isotope proportions.

Thermal ionization mass spectrometer comprises of three essential segments:

(i) **Ion source** is the place where ions are generated, accelerated and focused

(ii) **Analyzer** is the locale where the beam is isolated according to mass to charge ratio

(iii) **Collector** is the region where the ion beams are measured either by using single collector (with different beams measured one after another, known as dynamic mode) or multi collector (at the same time, known as static mode).

The ion source contains halogen lamp heaters for the system bake out. An optional cool trap (cryo pump) can be used to improve the vacuum in the source housing during measurement. The sample is loaded into the inlet system using sample wheel. Sample

wheel is equipped with filament holder with single or double filaments, which carry samples, and is then inserted in to the ion source. It is held at a potential of 10 kV. A large door provides easy access to the sample wheel and the ion source. The temperature of the filaments is monitored by a low temperature pyrometer. The entrance slit with a width of 0.2 mm is located in the ion source, just behind the sample.

The ion beam is focussed on to the slit by the ion source and then enters the analyzer region. Next to the entrance slit, an analyzer gate valve is located. If the analyzer gate valve is closed, the vacuum in this region is isolated from the ion source and can be maintained by two ion getter pumps. The ions are then directed through the focus quad, which is used to optimize the peak shape with the help of lenses of dynamic zoom optics. The dynamic zoom optics allows changing the dispersion of the ion beam by using quadrupole lenses in the ion beam path before and after the magnet. The radius of the magnetic sector field is 23 cm and the deflection angle is 90°. This gives a mass dispersion equal to that of an 81 cm range area using standard (a 60 degree Nier-type design) geometry. Inside the magnetic sector field, ions of different mass travel on different tracks depending on their mass to charge ratio.

After passing through the uniform magnetic field, the ions are finally detected in the detectors of the variable multi collector. Eight movable collector supports and one fixed centre channel are installed on the optical bench of the multi-collector module. Faraday cup is attached to the center module. Each movable support can carry an ion counter and faraday cup. A fully equipped system is therefore loaded with a maximum of 17 channels: nine Faraday cups and eight ion counters. The multi-collector simultaneously measures a maximum of nine different isotopes, variable detector types can detect up to 17 ion beams. Every Faraday cup is associated with a current amplifier. The amplifiers are mounted in an evacuated, doubly shielded and thermally stabilized housing. The extended dynamic range of 50 V in positive mode and 15 V in the negative mode supports the measurement of large isotope ratios, as it measures signal to noise ratio for the minor isotopes.

4.4.2. Sample preparation and analysis

Fresh and coarse-grained (preferably from central portion of the dyke) dolerite dyke samples were chosen for baddeleyite mineral separation and isotope analysis. Samples were processed at NGRI, Hyderabad. The main principle during mineral separation is to avoid cross contamination and to make the separation efficient. In the first step, each sample (500 grams) was chipped to gravel size (2-3 cm) thick slices using sledge hammer. Weathered portion was removed and taken care to avoid contamination of other minerals. An appropriate amount (about 300 grams) of the sample is careful crushed (<1cm) by jaw crusher. 200grams sample was powdered using harzog ring grinder and sized through a 125 μm mesh disposable nylon sieve. Part of 100gram powder sample (~20 grams) was loaded onto a Wilfley water- shaking table, followed procedures of Söderlund and Johansson, 2002. After ~100seconds, the finest material was washed off successively from the table deck using a squit bottle and collected in plastic beakers. After 3-5 loadings the collected heavy mineral concentrate was transferred to a petri dish. Fe-mg minerals (Oxides and silicates) were removed using a strong pencil-magnet and fraction was cleaned by acetone. For each sample, ~100-120 baddeleyite grains were handpicked under a binocular microscope (Figure 4.3).

Baddeleyite used for Phalaborwa carbonatite, South Africa (weighing 360 mg) was donated by Neal McNaughton, from his Curtin University collection. The Phalaborwa carbonatite was crushed in an agate mortar and sized through a 125 μm mesh disposable nylon sieve to match the size of grains separated from the mafic dyke.

The best quality (mineral inclusions, fractures and alteration free) baddeleyite crystals from both carbonatite standard and mafic dyke were carefully selected based on visible inspection using a binocular microscope and backscatter electron imaging using a Hitachi S-3400N scanning electron microscope. The selected fractions, which varied from 15 to 30 grains corresponding to between 4 and 12 μg (depending on the grain size), were cleaned in 4 N HNO_3 at room temperature for 2 h with intermittent ultrasonication in a Teflon beaker. Following this step the grains were rinsed several times in MQ H_2O and dried.

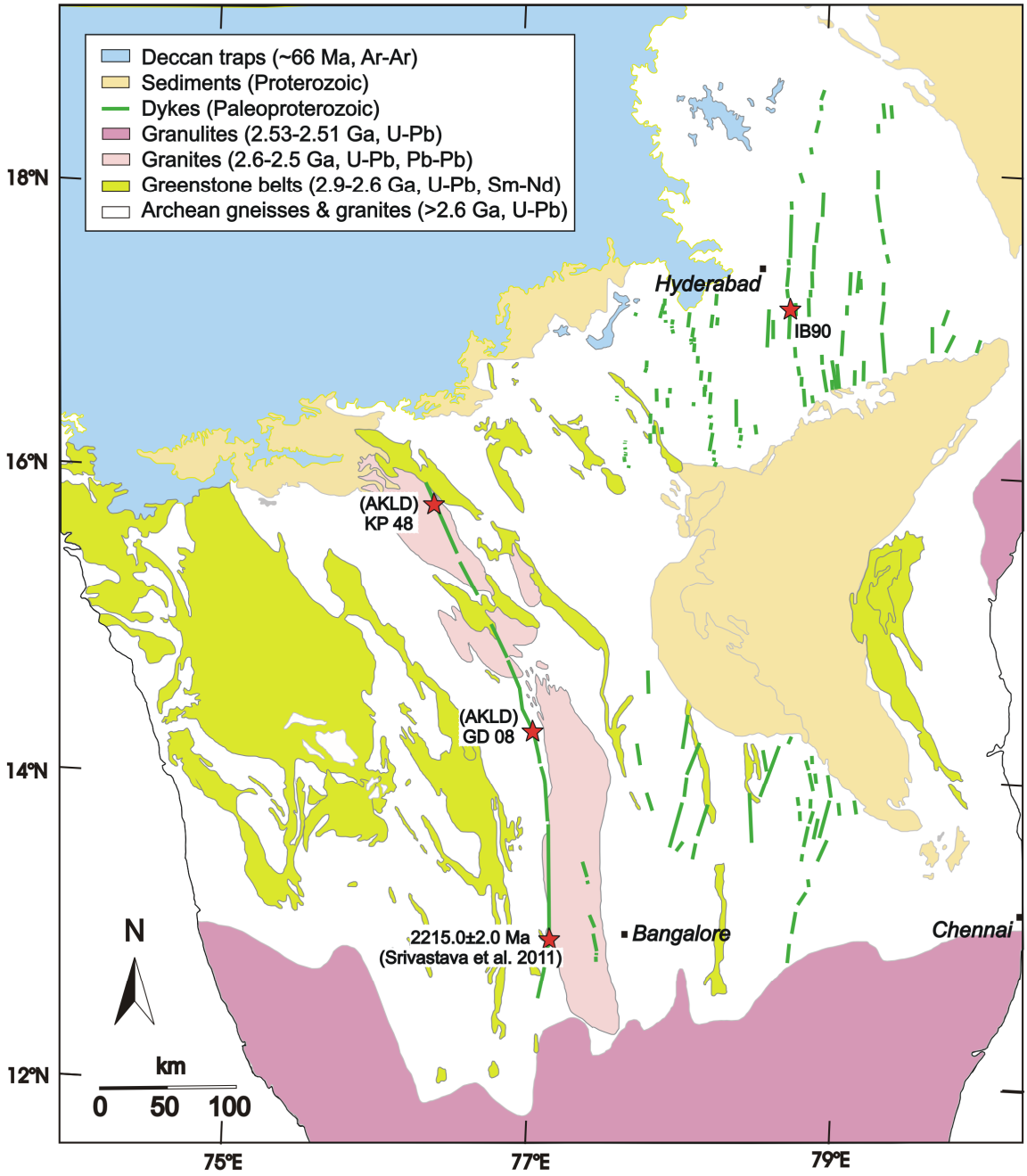

Figure 4.1. *Simplified geologic map of a part of the Dharwar craton showing the extension of the N-S dyke swarm (after French and Heaman, 2010) in the region. Stars in the map indicate site locations of samples used for Pb-Pb and U-Pb age determinations in the present and in earlier studies. Sites on AKLD include GD-08, KP-48 (this study) and the one dated by Srivastava et al. (2011), the location of which is only approximate.*

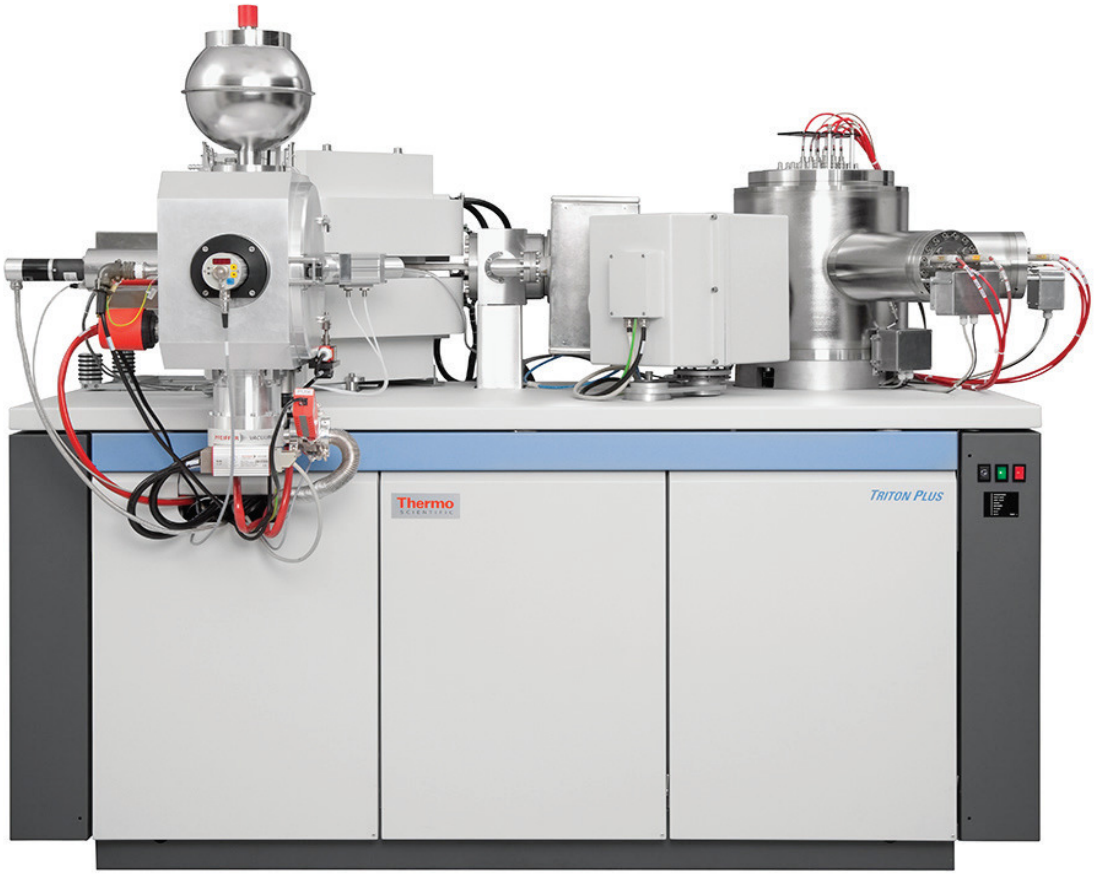

Figure 4.2. *Thermo Scientific TRITON Plus Thermal Ionization Mass Spectrometer (TIMS) installed at NGRI, Hyderabad was used for obtaining all the data presented in this thesis.*

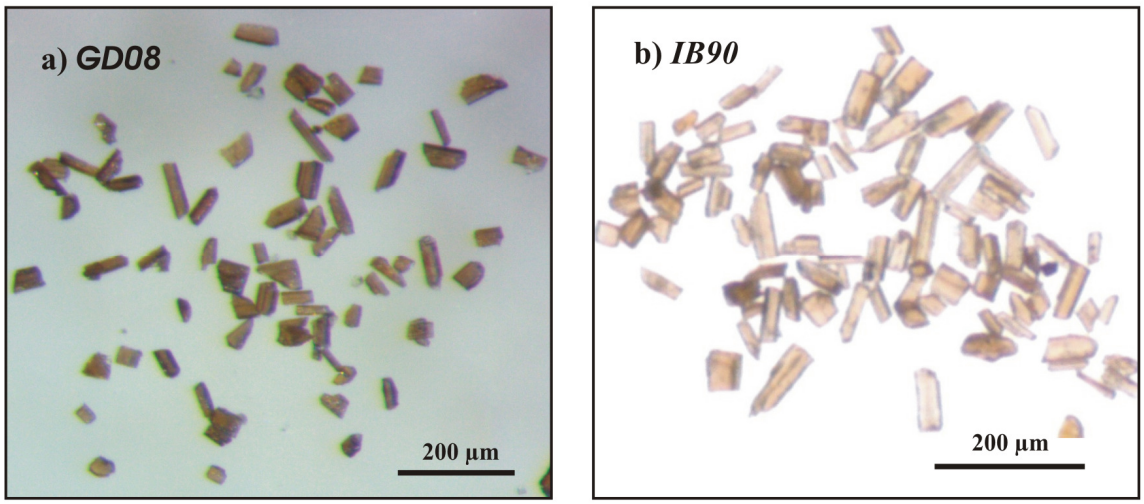

Figure 4.3. *Photographs of handpicked baddeleyite grains under binocular microscope from samples (a) GD08 and (b) IB90.*

Zone refined rhenium filaments (0.030 in. wide by 0.001 in. thick) used for loading the baddeleyite were welded on the posts and bent using a jig to form a transverse 0.5 mm broad and 0.5 mm deep 'U' shaped valley in the centre. These were outgassed and cleaned at alternating high (4.0 A) and low (2.0 A) temperature steps with the complete sequence lasting for 90 min, and left for at least a week before loading. The grains were loaded onto the bottom of the valley and kept in place with a minute droplet of silica gel for annealing at 1250°C in a vacuum chamber at ~1 * 10^{-7} mbar for 30 min to expel disturbed Pb from altered domains. The grains were subsequently embedded in silica glass on the same Re filament by fusing the sample with silica gel and phosphoric acid mixture at 1200°C for ~10 min in a vacuum chamber (Fig. 4.4). The silica gel–phosphoric acid mixture used was either that recommended by Gerstenberger and Haase (1997) of 0.2 g silicic acid: 19.6 g 0.035 M H_3PO_4 or that used by Davis (2008) of 2:1 of concentrated silicic acid and 9 N phosphoric acid. The maximum amount of silica gel mixture used was restricted to less than 2 µl in the case of the former recipe and less than 1 µl in the latter, to keep the blank to a minimum (~2 pg) and also to minimise condensed silica on the focussing plates. Results obtained using both recipes are presented. All these operations were performed under a stereomicroscope in a clean air station fitted with a HEPA filter.

4.4.3. Data acquisition

Analyses were performed on a TRITONPLUS Thermal Ionization Mass Spectrometer at the CSIR—National Geophysical Research Institute, Hyderabad (described in detail in earlier chapter). The three high mass Faraday detectors (H1 to H3) connected to 10^{11} Ω resistors were used to measure ^{206}Pb, ^{207}Pb and ^{208}Pb, in static multi-collector mode with virtual amplifier rotation. The ^{204}Pb signal was very small and therefore was collected simultaneously by a secondary electron multiplier–ion counting system on the axial channel. Each cycle consisted of three 1.049 s integrations and each block of two cycles (resulting in six ratios each). A 10 s instrument baseline was performed at the start of the analysis and after every 10 blocks with the beam deflected out of the Faraday cups using the x-symmetry lens. ^{206}Pb beam intensities varied between 60 and 400 mV (and depended on the size of the sample loaded) where the ^{207}Pb beam was always greater than 5mV. Data acquisition was made when the temperature of the

ionization filament was generally between 1530 and 1580°C and was monitored using a Keller pyrometer (Model — PZ409x/D).

4.4.4. Data reduction

Amplifier gains and Faraday/SEM-ion counter calibration were performed at least once every day and corrections were applied to the data. During this period count gains were in the range of 97.0±0.3% relative to the axial Faraday cup. The dead time correction for the ion counting system is 20 ns. It was determined during installation and verified after the measurements. It is not significant for measurements of ^{204}Pb where the signal was on the order of several hundred counts per second but an incorrect value would affect the relative gain correction for the ion counter.

Isotopic ratios were corrected for instrumental mass fractionation of 0.18% / amu. This value is marginally higher than the average of 0.1% generally observed with Pb emission for dissolved silica gel loads (Huyskens et al., 2012) and is based on a comparison of TE-TIMS and ID-TIMS age determinations on zircon from several Precambrian rocks (Davis, 2008). Part of the purpose of this study was to test the absolute value and stability of Pb fractionation during TE-TIMS analysis of baddeleyite. The zircon value was used as a baseline but was found to produce ages within error of ID-TIMS measurements on the same rock units. All baddeleyite fraction data acquired with ^{206}Pb intensities between 80 to 220 mV.

Correction of ^{207}Pb/^{206}Pb and ^{208}Pb/^{206}Pb ratios for measured common Pb, based on ^{206}Pb/^{204}Pb, was done on a block-by-block basis following Davis (2008). This was required as the ^{206}Pb/^{204}Pb ratio was observed to constantly change during the run, as the source of the non-radiogenic ^{204}Pb is different from that of the radiogenic ^{207}Pb and ^{206}Pb isotopes. The ages for each block were evaluated from the determined ^{207}Pb/^{206}Pb and ^{204}Pb/^{206}Pb ratios with common Pb corrections according to the model proposed by Stacey and Kramers (1975). Although zircon is considered to form with negligible common Pb, it is unclear whether this is true of baddeleyite and at least some of the common Pb will have been from the loading blank with a modern isotopic composition. In any case, the corrections for common Pb are so low that the use of either a modern or Precambrian isotopic composition has a negligible effect on the ^{207}Pb/^{206}Pb age (e.g. sample BD 1-6, Table 4.1, with the lowest ^{206}Pb/^{204}Pb will have a difference in age of

0.17 Ma, were as for sample BD 1-7 with a higher $^{206}Pb/^{204}Pb$ ratio the difference is only 0.06 Ma).

Ages are determined from weighted means of fraction averages using accepted decay constants (Jaffey et al., 1971). Since the decay constants reported by Jaffey et al., 1971 have been used by most of the labs, we preferred these constants. However, on calculating the age of IB 90, AKLD sites and Phalaborwa baddeleyite standard we get a age difference of 1.75 Ma younger which is of 0.08%. It is assumed that all excess scatter between runs is due to fractionation uncertainty and an additional error of ±0.055%, as calculated using the external error function in Isoplot (Ludwig, 2003), was added to the weighted averages. This corresponds to a fractionation uncertainty of ±0.03%. All age errors are quoted at either 2σ or 95% confidence. The corrected $^{208}Pb/^{206}Pb$ ratio is converted into a Th/U ratio, based on the $^{207}Pb/^{206}Pb$ age.

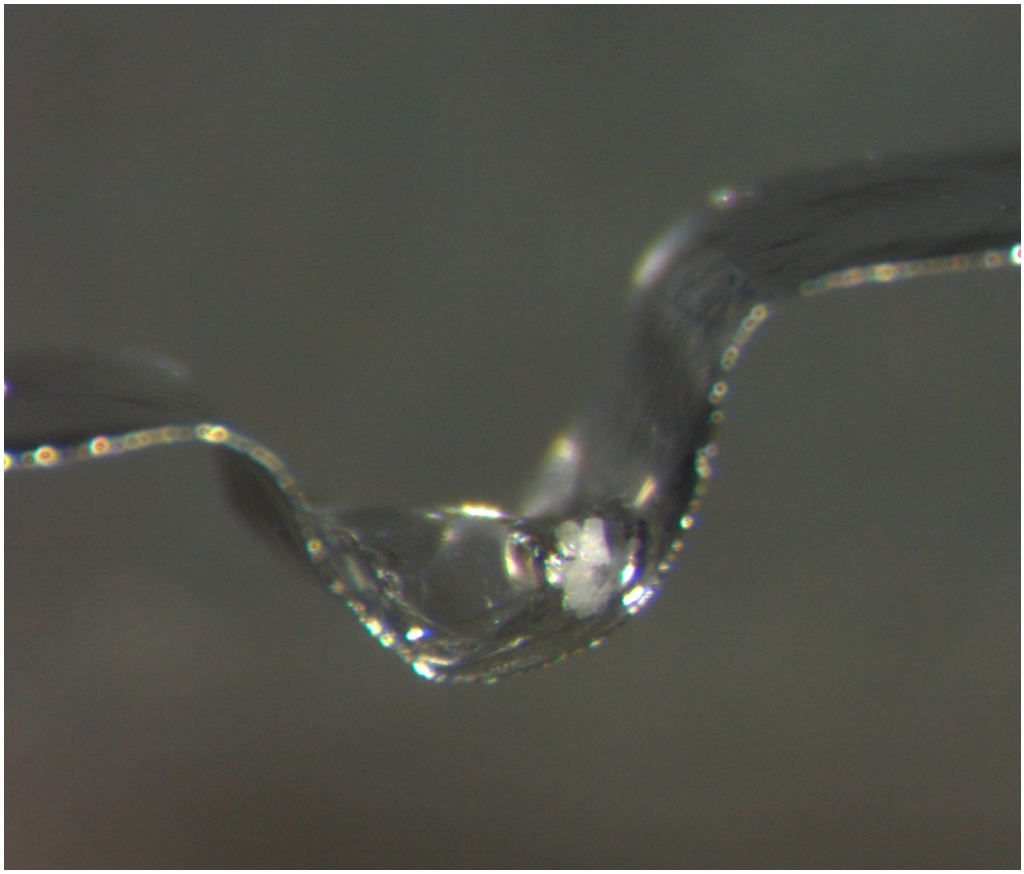

Figure 4.4. *U' shaped Re filament showing annealed Phalaborwa carbonatite baddeleyite grains (~75 µm) embedded in a silica glass bead at the bottom of the valley. A minimal amount of silica gel (< 1µl) was used for making the bead to minimise loading blank and avoid source contamination.*

4.4.5. Imaging of baddeleyite grains

To investigate the effects of heating on baddeleyite, grains from both Phalaborwa carbonatite and the mafic dyke were heated at different temperatures ranging from 1250 to 1586°C in vacuum, their chemical composition, structure and morphology were studied using Hitachi, S-3400N SEM and their BSE images are shown in Figs. 4.5–4.8. Spot analyses were also performed using energy dispersive X-ray spectroscopy (EDS) to estimate the composition of the different phases observed (Figs. 4.6 and 4.8).

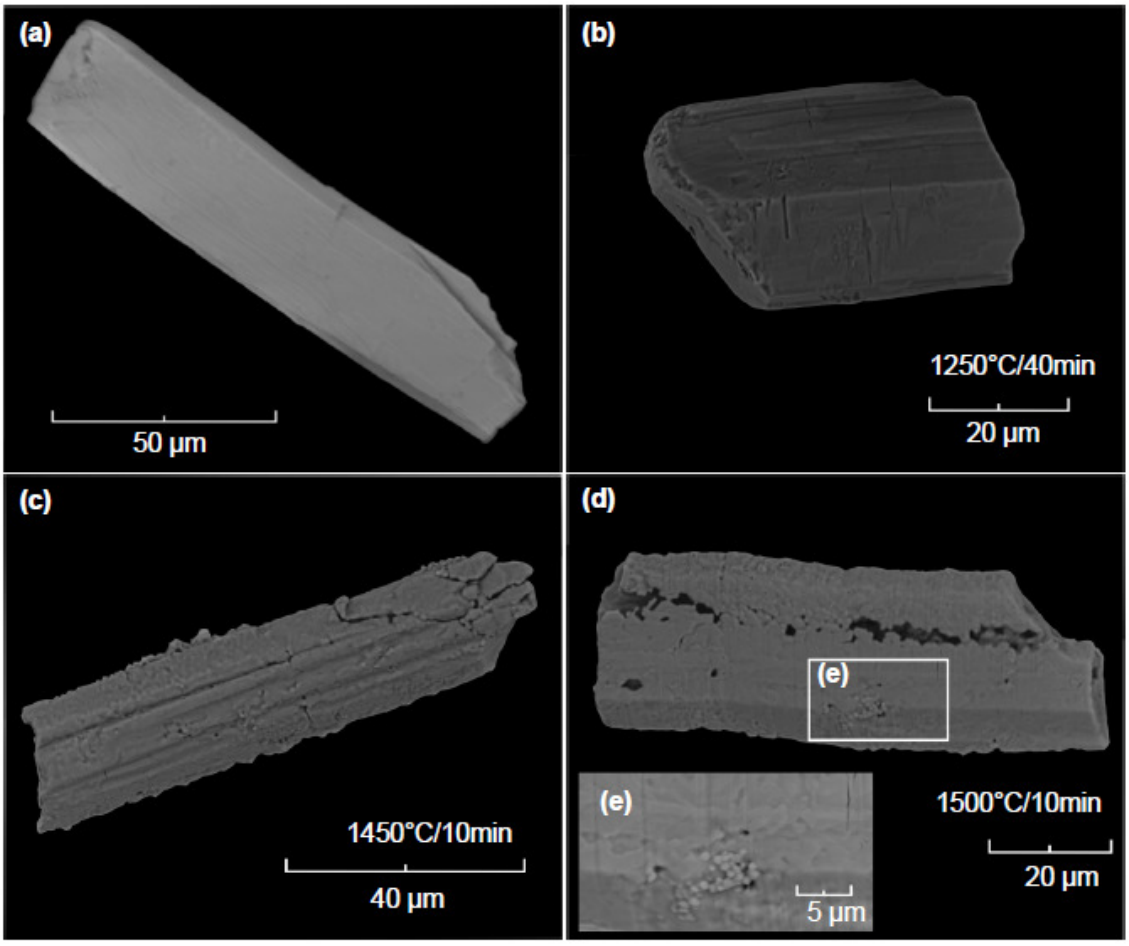

Figure 4.5. *BSE images of baddeleyite grains from GD-08 sample (a) unheated grain, (b, c, d and e) grains heated at successively higher temperatures to observe progression in disintegration with temperature. Images c, d and e show recrystallization of baddeleyite at 1450°C and 1500°C. No compositional change was observed across grains on recrystallization, as shown in Figs. 4.6 and 4.7. Image (e) was taken at a higher magnification to show typical recrystallization of baddeleyite at 1500 °C.*

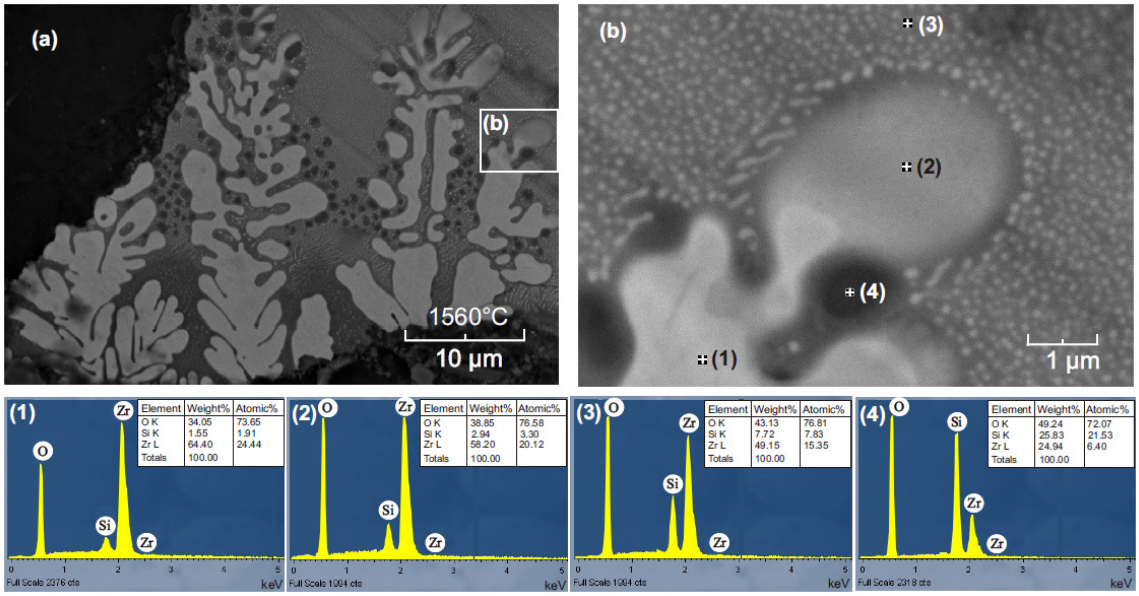

Figure 4.6. *BSE images of dentritic baddeleyite (light grey) in cross section embedded in silica glass from sample GD-08. Dendritic patterns displayed by the baddeleyite are inferred to reflect melting and partial immisicibility with silica during heating at 1560 °C. Fig a shows dentritic baddeleyite (light grey) set in darker grey silica glass, which is peppered with fine-grained exsolved baddeleyite. Black dots are voids in the silica glass, possibly created by vapourized silica. Compositional variation between these phases is shown in Fig. b, which is a magnified image of a small part of Fig. a.*

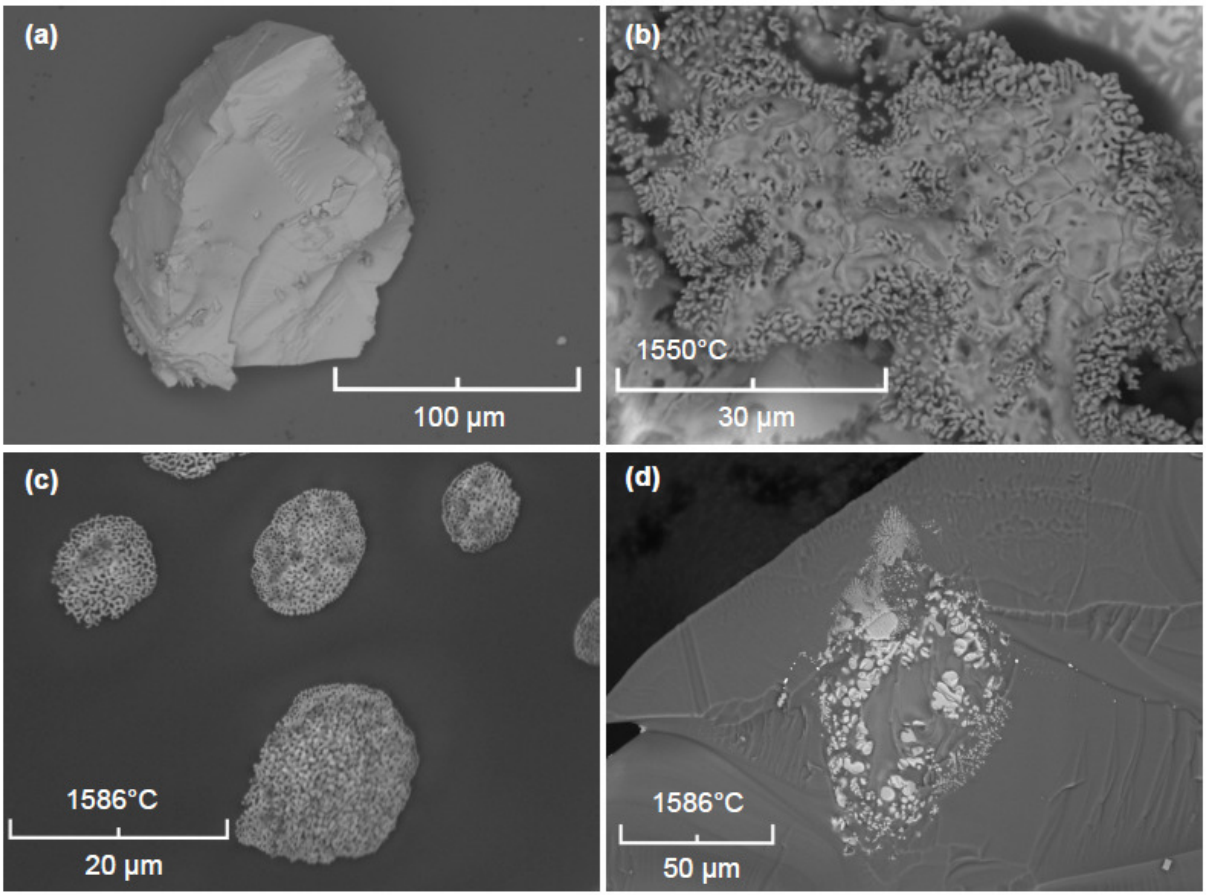

Figure 4.7. *BSE images of baddeleyite from the Phalaborwa carbonatite (a) unheated grain, (b, c and d) baddeleyite-silica immisicibility textures after heating at 1550°C and higher. Images (c) and (d) are of globular residual baddeleyite taken after Pb isotopic analysis by TIMS.*

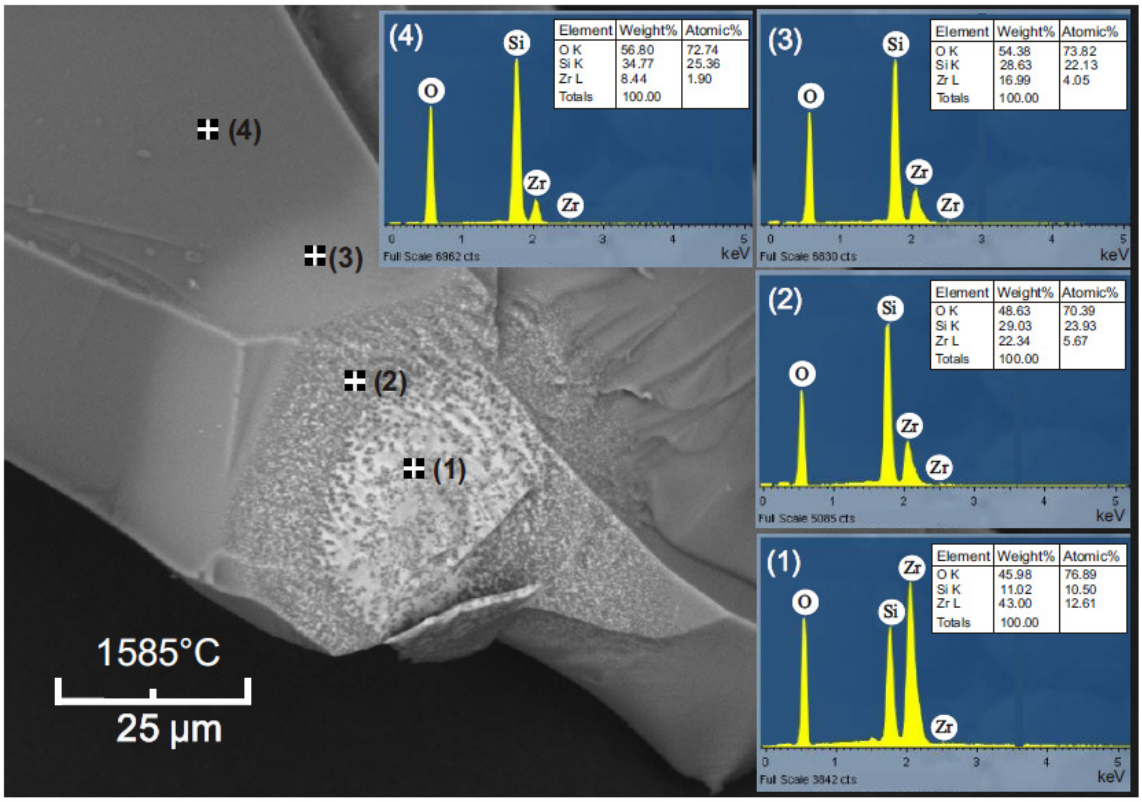

Figure 4.8. *A SEM-BSE image and spot EDS analysis across an embedded baddeleyite grain within silica glass, after heating to 1585°C (Pb isotopic analysis was successfully completed on this sample), depicting the breakdown of the grain and release of Zr into the silica-melt ionization activator.*

4.5. Results

Baddeleyite grains from the Phalaborwa carbonatite standard and an earlier dated (U–Pb method) dyke swarm intruding the Dharwar craton are reported here as a test case.

4.5.1. Phalaborwa carbonatite

Pb isotopic results for 12 baddeleyite fractions (crystal BD-1) separated from the Phalaborwa carbonatite are given in Table 4.1 and illustrated in Fig. 4.9. The fraction weighted mean ^{207}Pb–^{206}Pb ages scatter outside of measurement uncertainty, with a grand mean of 2060.3 ±0.4Ma (MSWD=4.2, n=12). The reason for a high MSWD is discussed below. The number of blocks used for calculating the ^{207}Pb–^{206}Pb ages of these fractions varied from 14 to 37 (Table 4.1). Block results are individually plotted in Appendix 1. Th/U ratios determined from $^{208}Pb/^{206}Pb$ for the 12 fractions give values varying from 0.014 to 0.019 and a mean of 0.016.

4.5.2. Paleoproterozoic mafic dyke (GD-08)

Fourteen baddeleyite fractions were analysed from sample GD-08, collected from a large 450 km long N–S striking dyke (Fig. 4.1) in the Dharwar craton. This is part of the Andhra–Karnataka long dyke, AKLD swarm (Kumar et al., 2012b). Results are given in Table 4.1 and plotted in Fig. 4.10. The 14 fractions again scatter outside of measurement error with a weighted mean ^{207}Pb–^{206}Pb age of 2215.9 ± 0.3 Ma (MSWD = 11.4, n = 14). Each fraction average contains at least 15 blocks (Table 4.1 and Appendix 2). The calculated Th/U ratios for all the baddeleyite fractions are consistent between 0.040 and 0.056 with a mean of 0.047.

As mentioned above, baddeleyite grains were embedded using two different silica gel recipes (of 0.2 g silicic acid: 19.6 g 0.035 M H_3PO_4, Gerstenberger and Haase, 1997 and 2:1 of concentrated silicic acid and 9 N phosphoric acid, Davis, 2008). Based on the sample runs, we infer that ionization efficiency does not depend on the silica gel used but on successfully embedding the grains in the gel, which is more easily done using the concentrated silica gel solution. However, to acquire a sufficiently large (about 150 to 200 mV) ^{206}Pb signal, a minimum of 5 μg is required (number of grains could vary between 15 and 30, depending on their size with U concentration of about 500 ppm).

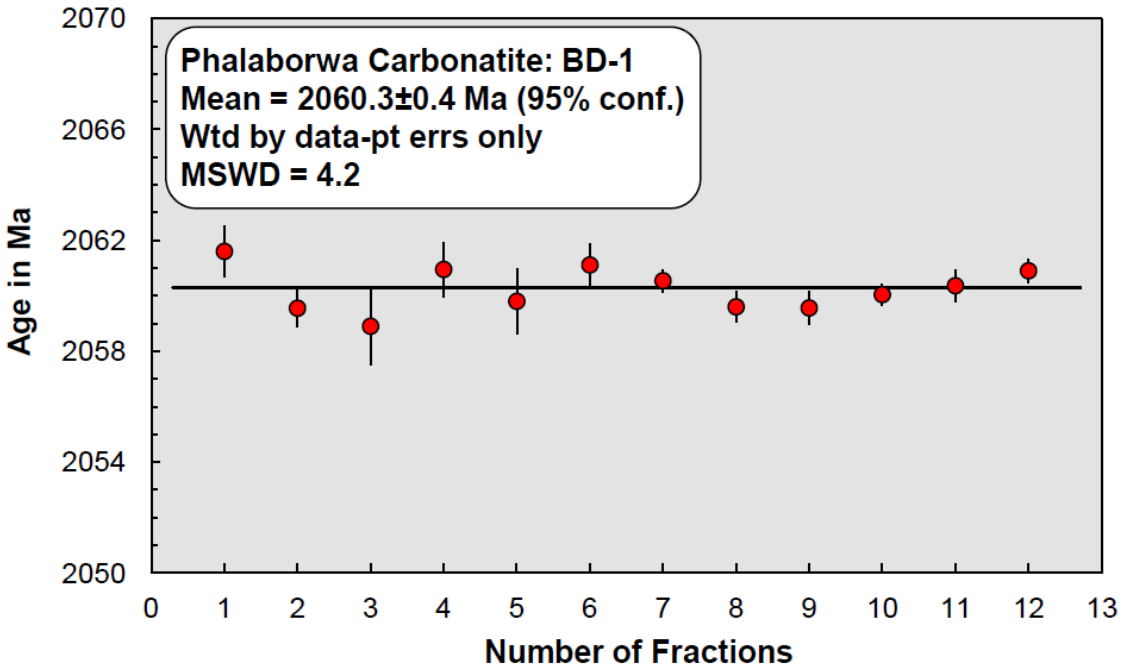

Figure 4.9. *TE-TIMS weighted mean $^{207}Pb/^{206}Pb$ age from the Phalaborwa carbonatite yielded from 12 baddeleyite fractions. Errors bars signifies 95% confidence limits of measurements. Common Pb corrected individual block ages for each of the 12 fractions are shown in Appendix-1.*

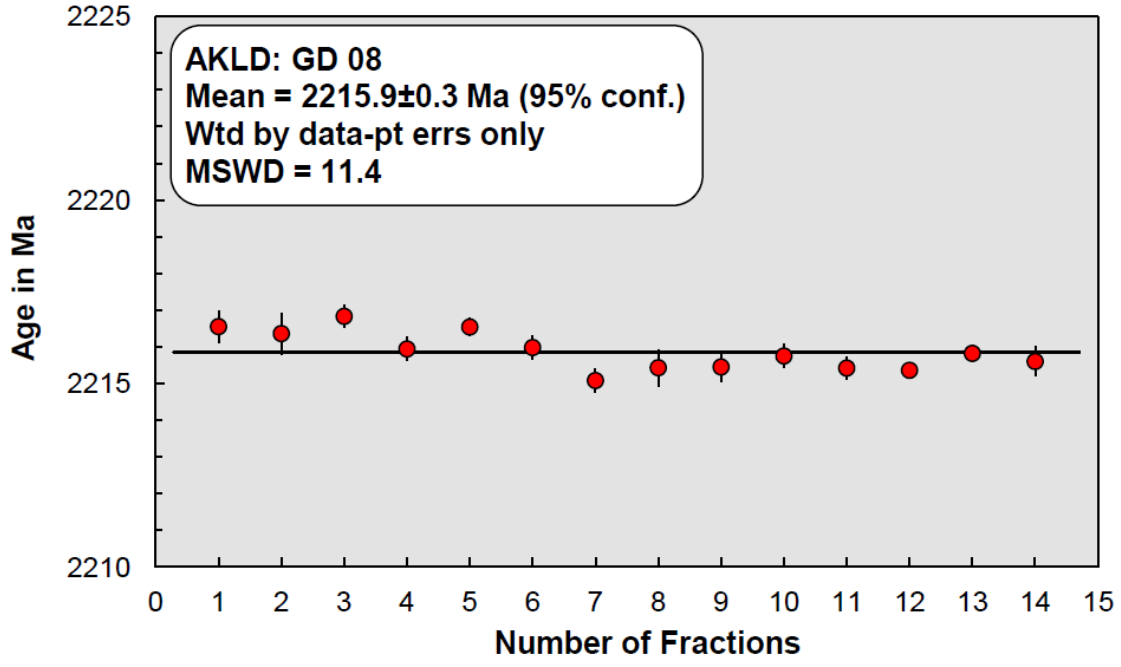

Figure 4.10. *TE-TIMS weighted mean $^{207}Pb/^{206}Pb$ ages on 14 baddeleyite fractions from GD 08 sample (AKLD mafic dyke swarm). Errors bars signifies 95% confidence limits of measurements. Individual block ages for each of the 14 fractions are plotted in Appendix-2*

4.5.3. KP-48

Four baddeleyite fractions were analysed from sample KP 48-2 (site P). Each fraction average contains at least 15 blocks. The grand weighted mean Pb-Pb TE-TIMS age for the four fractions from this sample is 2216.6±0.7 Ma (MSWD=0.57). Results are plotted in Fig. 4.11 and given in Table 4.2.

4.5.4. IB-90

Twelve baddeleyite fractions were analysed from sample IB 90, which is collected from N_S dyke in the northern part of Cuddapah basin. Results are plotted in Fig. 4.12 and given in Table 4.2. The 14 fractions yields a weighted mean $^{207}Pb–^{206}Pb$ age of 2252.66 ± 0.49 Ma (MSWD = 0.52, n = 12). The number of blocks used for calculating the $^{207}Pb–^{206}Pb$ ages of these fractions varied from 46 to 50 (Table 4.2).

4.6. Discussion

4.6.1. Pre-treatment of baddeleyite

In an attempt to reduce the impact of Pb loss in baddeleyite, Rioux et al. (2010) subjected Phalaborwa baddeleyite to multi-step digestion after annealing at 900°C, similar to the chemical abrasion (CA-TIMS) method of Mattinson (2005) developed for improving U–Pb zircon geochronology. However, this method was ineffective as the analysis of individual digestion steps generated complex results with both normal and reverse discordance, suspected to be due to differential leaching of U and Pb from the system. We used an alternative approach noted by Kober (1986, 1987) and successfully used for Pb zircon TE-TIMS geochronology by Davis (2008), wherein zircon grains were heated in vacuum to temperatures between 1400 and 1500°C prior to their analysis to remove Pb residing in altered crystal domains by evaporation. In the present approach, baddeleyite was heated at a relatively lower temperature (1250°C). This temperature was fixed based on the following considerations, i) monitoring common Pb evaporated from baddeleyite grains with increasing temperature on TIMS, ii) effect of progressive heating as seen in the SEM images (Figs. 4.5–4.8), and iii) report of reverse discordance in annealed (at 1300°C) baddeleyite grains (Niihara et al., 2012). Heating of baddeleyite grains at 1250°C before embedding appears to purge altered reservoirs with negligible loss of Pb from unaltered domains, resulting in remarkable consistency in $^{207}Pb–^{206}Pb$ baddeleyite ages between different fractions from both Phalaborwa carbonatite and the

mafic dyke (~0.1% of the mean values) compared to the reported ^{207}Pb–^{206}Pb ages obtained, without preheating, by conventional U–Pb analysis on these rocks (Phalaborwa baddeleyite vary by 0.66% , Heaman, 2009 and by 0.65% in the case of the Kandlamadugu mafic dyke (Fig. 4.13, French and Heaman, 2010).

Table 4.1. TE-TIMS Pb isotopic data on Baddeleyite fractions

Sample No.	Samp. wt.	No. bloc.	$^{206}Pb/^{204}$ Pb (m)	Abs. error	$^{207}Pb/^{206}Pb$ (m)	$^{207}Pb/^{206}Pb$ (c)	Pb-Pb Age (Ma)	Th/U
Phalaborwa carbonatite baddaleyite								
BD 1-1	6.6	23	3889	36	0.130688±051	0.127228±052	2061.6±0.9	0.019
BD 1-2	6.2	33	3983	140	0.130639±114	0.127193±049	2059.6±0.7	0.016
BD 1-3	6.2	22	10212	562	0.128539±083	0.127150±100	2058.9±1.4	0.015
BD 1-4	6.5	37	3463	28	0.131101±051	0.127295±071	2061.0±1.0	0.017
BD 1-5	6.5	28	3423	11	0.131126±043	0.127214±087	2059.8±1.2	0.016
BD 1-6	6.3	29	2999	9	0.131674±029	0.127306±055	2061.1±0.8	0.017
BD 1-7	12.4	27	9494	260	0.128678±041	0.127265±030	2060.5±0.4	0.017
BD 1-8	12.4	17	26661	1654	0.127734±032	0.127198±041	2059.6±0.6	0.017
BD 1-9	11.6	14	12855	543	0.128296±068	0.127195±044	2059.6±0.6	0.016
BD 1-10	12.0	16	10315	829	0.128566±091	0.127230±028	2060.0±0.4	0.015
BD 1-11	5.8	25	23056	392	0.127862±043	0.127252±042	2060.4±0.6	0.014
BD 1-12	5.8	22	26882	489	0.127799±043	0.127292±032	2060.9±0.4	0.014
Grand weighted mean age: 2060.3±0.4 Ma (MSWD=4.2)								
Inverse isochron age: 2060.7±0.4 Ma (MSDW=0.68)								
AKLD (GD 08)								
GD 08-1	3.8	27	8367	104	0.140711±022	0.139140±032	2216.6±0.4	0.050
GD 08-2	4.6	15	15181	232	0.139990±029	0.139123±043	2216.4±0.6	0.056
GD 08-3	4.6	24	16497	91	0.139963±012	0.139170±025	2216.8±0.3	0.055
GD 08-4	4.6	20	18227	97	0.139809±014	0.139095±025	2215.9±0.3	0.053
GD 08-5	4.6	20	23198	480	0.139704±015	0.139138±019	2216.5±0.2	0.037
GD 08-6	4.6	17	18794	398	0.139805±018	0.139095±024	2216.0±0.3	0.046
GD 08-7	4.4	27	14853	234	0.139915±014	0.139027±025	2215.1±0.3	0.046
GD 08-8	4.4	29	4936	16	0.141720±023	0.139051±040	2215.4±0.5	0.043
GD 08-9	4.4	29	5257	17	0.141529±020	0.139053±033	2215.5±0.4	0.043
GD 08-10	4.4	28	5404	10	0.141473±015	0.139080±026	2215.8±0.3	0.045
GD 08-11	4.4	28	6502	21	0.141060±015	0.139049±023	2215.4±0.3	0.044
GD 08-12	4.4	29	5920	11	0.141255±010	0.139047±018	2215.4±0.2	0.045
GD 08-13	4.4	30	8477	45	0.140630±014	0.139083±017	2215.8±0.2	0.046
GD 08-14	4.4	29	8270	29	0.140649±017	0.139059±021	2215.6±0.4	0.040
Grand weighted mean age: 2215.9±0.3 Ma (MSWD=11.4)								
Inverse isochron age: 2216.6±0.6 Ma (MSWD=17)								

Sample wt. is in micrograms. $^{206}Pb/^{204}Pb$ (m) and $^{207}Pb/^{206}Pb$ (m) are measured values (fraction means with standard error) and $^{207}Pb/^{206}Pb$ (c) is the corrected value (wtd. means and errors). Uncertainties are $2\sigma_m$ and refer to the least significant digits.

Table-4.2. TE-TIMS Pb isotopic data on baddeleyite fractions from KP 48 and IB 90 samples.

Sample No.	Samp. wt.	No. bloc.	$^{206}Pb/^{204}Pb$ (m)	Abs. error	$^{207}Pb/^{206}Pb$ (m)	$^{207}Pb/^{206}Pb$ (c)	Pb-Pb Age (Ma)
AKLD (KP 48)							
KP 48-2-1	6.1	23	23201	484	0.139704±015	0.139138±019	2216.5±1.4
KP 48-2-2	4.9	19	6755	281	0.141142±094	0.139164±012	2216.9±1.7
KP 48-2-3	5.1	19	3431	117	0.143061±135	0.139184±020	2217.1±1.5
KP 48-2-4	5.4	25	8477	145	0.140630±014	0.139083±017	2215.8±1.5
Grand weighted mean age: 2216.6±0.7 Ma (MSWD=0.57)							
IB 90							
IB 90-1	2.2	47	3842	113	0.145606±110	0.142083±031	2252.8±1.8
IB 90-2	2.3	50	6994	106	0.144021±045	0.142143±027	2253.5±1.7
IB 90-3	2.4	50	10677	85	0.143292±025	0.142072±022	2252.6±1.7
IB 90-4	2.2	45	8739	35	0.143578±034	0.142091±034	2252.8±1.8
IB 90-5	2.6	50	12185	91	0.143090±027	0.142021±025	2251.9±1.7
IB 90-6	2.0	49	2957	10	0.146511±033	0.142120±030	2253.2±1.8
IB 90-7	2.1	50	5026	25	0.144606±022	0.142021±017	2251.9±1.6
IB 90-8	2.1	50	4369	136	0.145139±113	0.142006±020	2251.8±1.6
IB 90-9	2.0	46	3608	109	0.145782±110	0.142050±028	2252.4±1.8
IB 90-10	1.8	46	2577	28	0.147241±061	0.142178±038	2253.9±1.9
IB 90-11	2.1	50	4035	11	0.145316±026	0.142099±026	2252.9±1.7
IB 90-12	2.2	50	4883	164	0.144873±102	0.142061±026	2252.5±1.7
Grand weighted mean age: 2252.7 ± 0.5 Ma (MSWD=0.52)							

Sample wt. is in micrograms. $^{206}Pb/^{204}Pb$ (m) and $^{207}Pb/^{206}Pb$ (m) are measured values (fraction means with standard error) and $^{207}Pb/^{206}Pb$ (c) is the corrected value (wtd. means and errors). Uncertainties are $2\sigma_m$ and refer to the least significant digits.

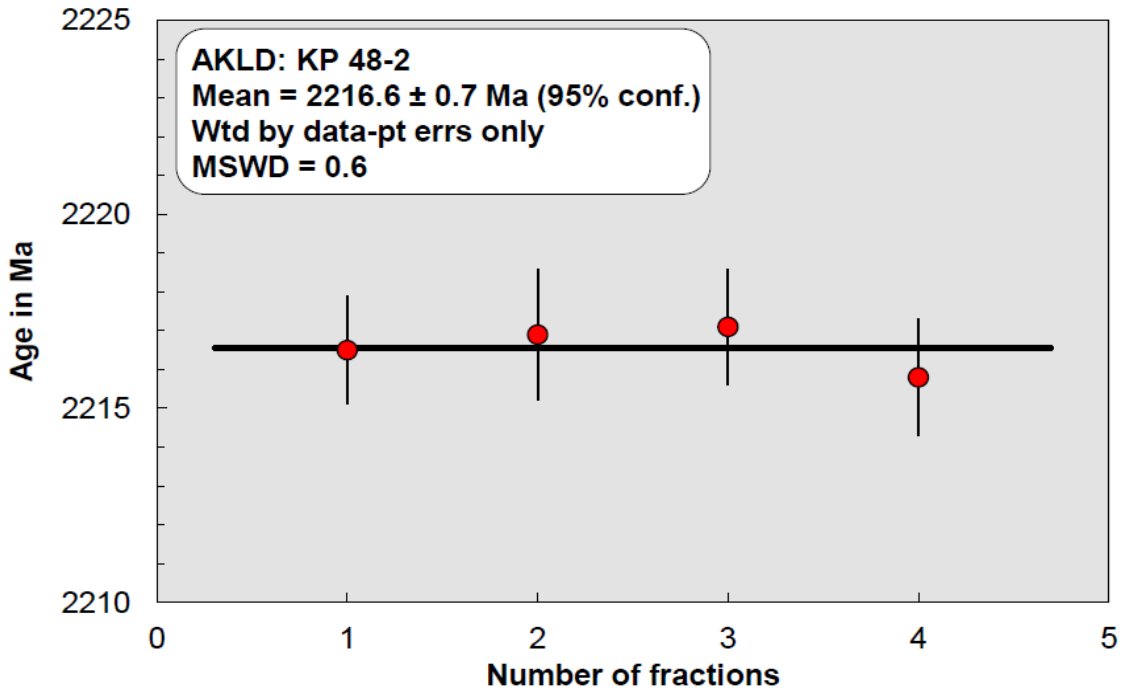

Figure 4.11. *TE-TIMS weighted mean $^{207}Pb/^{206}Pb$ ages on 4 baddeleyite fractions from KP 48-2 sample (AKLD mafic dyke swarm). Errors bars signify 95% confidence limits of measurements.*

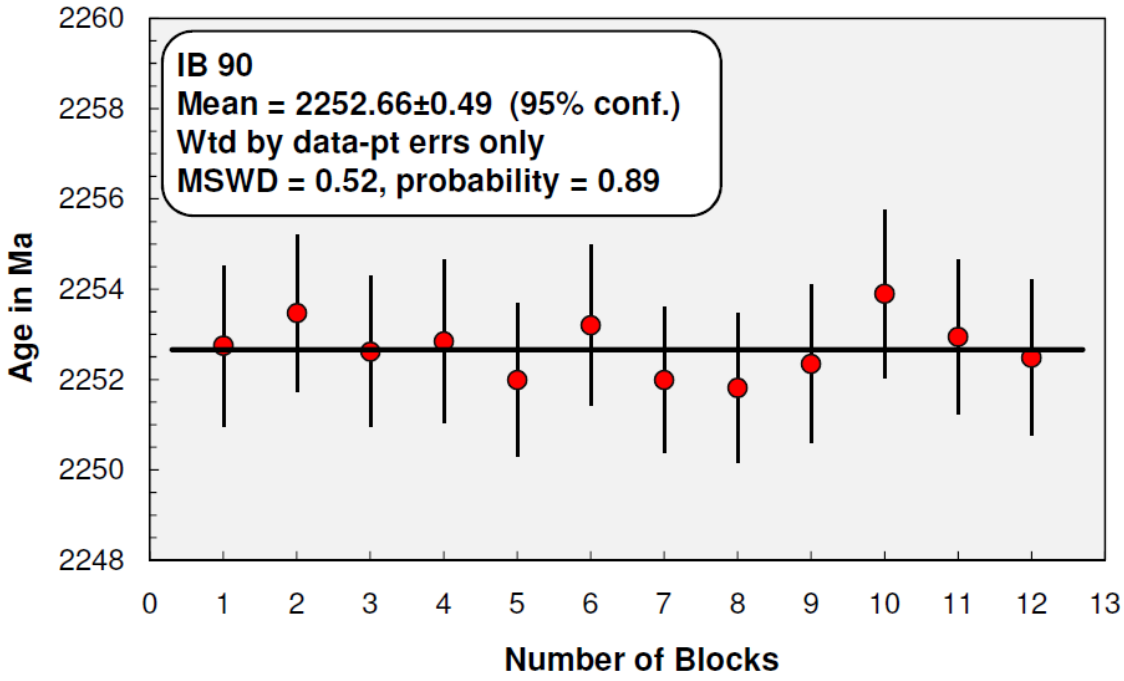

Figure 4.12. *TE-TIMS weighted mean $^{207}Pb/^{206}Pb$ ages on 12 baddeleyite fractions from IB 90 sample (N-S mafic dyke). Errors bars signify 95% confidence limits of measurements.*

4.6.2. Textural changes in baddeleyite following thermal extraction of Pb

Baddeleyite grains from both Phalaborwa carbonatite and AKLD mafic dyke (sample GD-08) heated at successively higher temperatures to observe progression in disintegration with temperature are shown in BSE-SEM images (Figs. 4.5–4.8). No compositional change was detected within the baddeleyite grains on heating (Figs. 4.6 and 4.8). Also, there was no change in physical appearance up to about 1250°C for 40 min (Fig. 4.5b). However, heating for even 10 min at temperatures of 1450°C and 1500°C (Fig. 4.5c and 4.5d) showed surface textures indicating alteration due to disintegration of the grains. Fig. 4.7b–4.7d shows silica glass embedded baddeleyite grains that were heated beyond 1550°C (data acquisition temperature). Clear signs of disintegration of grains occur close to 1450°C (Fig. 4.5c). This corresponds to small 206Pb emission (generally ~5 to 10 thousand counts on the secondary electron multiplier), suggesting preliminary release of Pb into the silica gel. Gradual increase in filament temperature promotes further breakdown, resulting in ^{206}Pb beams N 15 mV, by about 1500°C, indicating more radiogenic Pb release. Between 1530°C and 1590°C ionization increases spontaneously resulting in ^{206}Pb beam reaching its maximum(between 80 and 400 mV), depending on the amount of radiogenic Pb released from the sample. At this temperature baddeleyite disintegrates considerably as shown in Figs. 4.6–4.8. An SEM-BSE image and spot EDS analysis shown in Figs. 4.6 and 4.8, across embedded baddeleyite grains and silica glass, after heating to 1560 and 1585°C respectively, depicts the breakdown of the grains and release of ZrO_2 (along with Pb and other elements) into the silica-melt ionization activator. This accounts for peak Pb ionization from silica embedded baddeleyite grains, as from embedded zircon (Davis, 2008), occurring at a higher temperature (by about 100°C) compared to dissolved Pb-silica gel loads that yield sufficiently large Pb beams at filament temperatures of 1400°C or less.

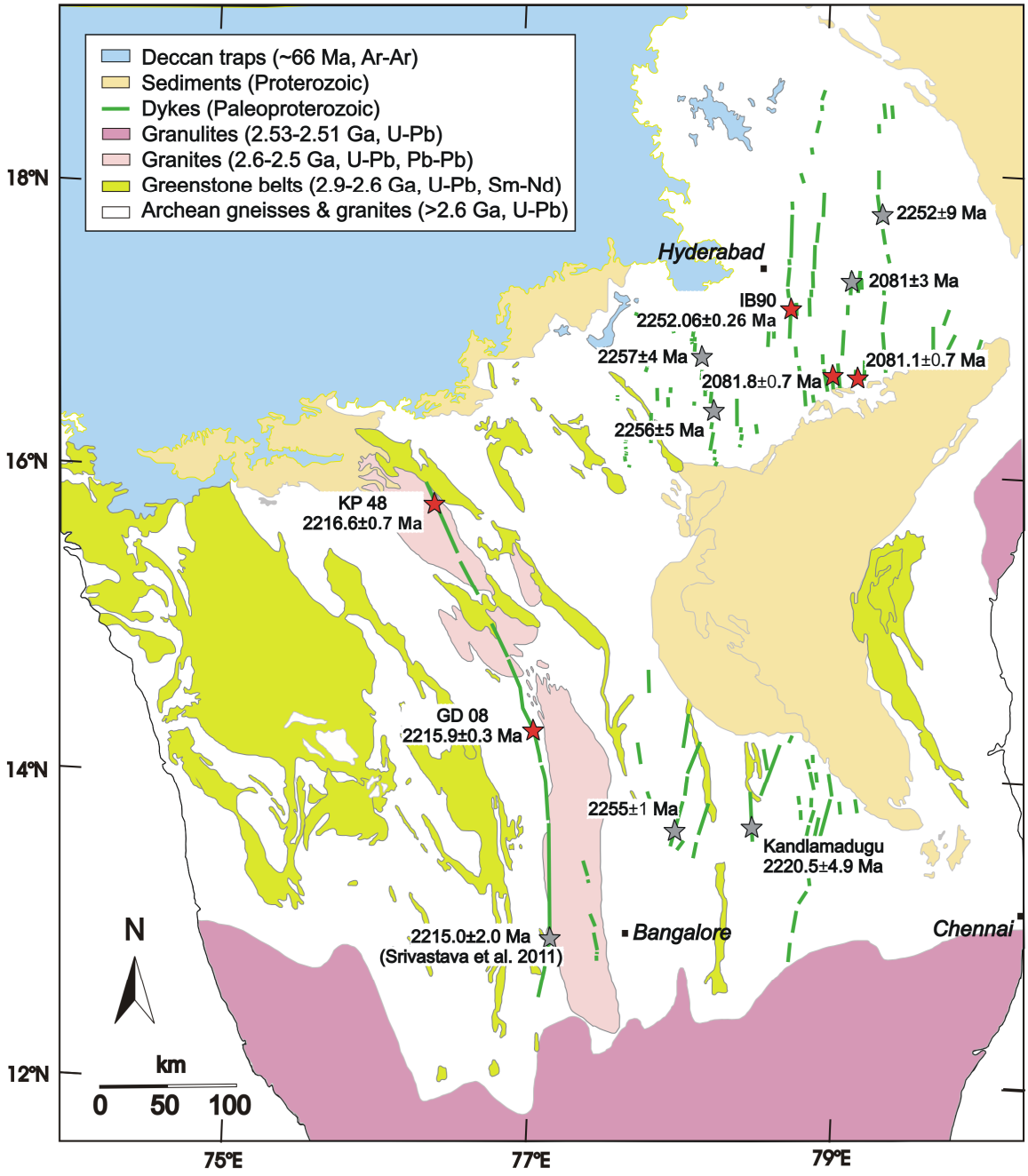

Figure 4.13. *Simplified geologic map of a part of the Dharwar craton showing the extension of the N-S dyke swarm (after French and Heaman, 2010) in the region. Stars in the map indicate site locations of samples used for Pb-Pb and U-Pb age determinations in the present and in earlier studies. Ages in the present study are shown in red colour and the other dated dykes (French and Heaman 2010; Srivastava et al., 2011; Demirer, 2012; Kumar et al., 2015) are presented with grey colour.*

4.6.3. Comparison with ID-TIMS results

The mean TE-TIMS age for Phalaborwa baddeleyite of 2060.3 ± 0.4 Ma (MSWD = 4.2) is similar within error to the reported (ID-TIMS) ^{207}Pb–^{206}Pb age of 2059.7 ± 0.4 Ma (MSWD = 7.7, n = 59) by Heaman (2009) and the 2060.6 ± 0.5 Ma age reported by Reischmann (1995) for a different baddeleyite crystal from the same carbonatite complex. Both the Heaman and TE-TIMS data sets scatter well outside of measurement error, which calls into question the accuracy of the averages. As discussed below, random variations in fractionation can account for the excess scatter in TE-TIMS data. In addition to this, small degrees of ancient Pb loss could account for the excess scatter and slightly younger mean age. This is more likely from the untreated baddeleyite analysed by ID-TIMS than from the TE-TIMS samples, which were thermally pretreated to remove any Pb from disturbed domains, a process that has been shown to be effective for zircon (Kober, 1987; Davis, 2008). The calculated average Th/U of 0.016 is consistent with other reported Th/U ratios for Phalaborwa carbonatite baddeleyite (Heaman, 2009), which vary from 0.007 to 0.031 with an average value of 0.014.

The weighted mean ^{207}Pb–^{206}Pb TE-TIMS age of 2215.9 ± 0.3 Ma with an MSWD of 11.4, for dyke sample GD-08 is consistent with the previously reported conventional dates of 2215.0 ± 2.0 Ma (Srivastava et al., 2011) on a dyke from the same swarm sampled about 100 km south of our site (Fig. 4.1), and 2220.5 ± 4.9 Ma (French and Heaman, 2010) from another N–S striking dyke located about 150 km east of GD-08. Again, the scatter of data is well outside of analytical error. The mean calculated Th/U value of 0.047 is considerably higher than that obtained for the carbonatite (0.016), but is typical of baddeleyite crystallized in mafic dolerite dykes (Heaman and LeCheminant, 1993).

4.6.4. Mass fractionation and limitations to age precision

The process of thermal extraction of Pb from the mineral into the silica melt was assumed to be a non-fractionating process in the case of zircon (Davis, 2008), as the time needed for Pb to diffuse across a zircon crystal at 1500°C is well in excess of the analysis time(Cherniak and Watson, 2003). Though there are no published experimental data about the rate of Pb diffusion in baddeleyite, inferences from geochronological studies of baddeleyite (Heaman and LeCheminant, 2000) are consistent with slow diffusion rates for

U and Pb in this mineral. However, mass fractionation occurs during evaporation of Pb from the silica melt due to the relatively high volatility of lighter isotopes. In normal dissolved sample loads, mass fractionation normally starts at about 0.13%/amu and decreases continuously leading to a systematic increase in $^{207}Pb/^{206}Pb$ ratio as the lighter isotope becomes more depleted. No systematic increase in ages is evident in the sequential block averages from the different fractions as shown in Appendix 1 and 2. Although some of the fractions show approximately random scatter consistent with measurement errors (MSWD around 1) seven out of twelve fractions from sample BD and thirteen out of fourteen fractions from sample GD-8 scatter outside of measurement errors. In some cases this excess scatter appears to be random while in others the data appear to exhibit oscillating trends (e.g. BD 1-1). A similar pattern was seen for TE-TIMS emission from zircon by Davis (2008). The average fractionation correction, which gives results most compatible with ID-TIMS ages, is found to be about 0.18%/amu for baddeleyite, the same as was found with zircon. The difference in ages will be less than 3.0 Ma for fractionation ranging from 0.1%/amu to 0.24%/amu. Fractionations this high are almost never observed with dissolved Pb loads. The relative volatility of isotopes is predicted from kinetic theory (Habfast, 1998) to be the square root of the ratio of the masses, which would result in a fractionation of 0.24%/amu for $^{207}Pb/^{206}Pb$. The reason that such high fractionation is not observed during evaporation from silica melt may be because the light isotope rapidly becomes depleted within a thin boundary at the surface of the melt. Volatile fractionation continues to be 0.24% at the surface but, after a short initial period of fractionation instability (noted by Doucelance and Manhes, 2001), the light isotope becomes depleted in the boundary layer to the point where the apparent fractionation relative to the starting composition is close to 0.13% for dissolved loads. The boundary layer tends to maintain its composition over a significant part of the run by slow exchange with the main reservoir of Pb inside the viscous melt droplet. In TE-TIMS, not only is unfractionated Pb being continuously introduced into the melt, but the temperature of baddeleyite and zircon breakdown is close to the temperature for significant silica evaporation. Hence, the fractionated boundary layer is continuously evaporated, causing a higher fractionation of measured Pb, which is closer to that from the unfractionated reservoir. However, it is unclear why fractionation under this condition generally does not exhibit a progressively decreasing trend since the reservoir becomes relatively depleted in the light isotope.

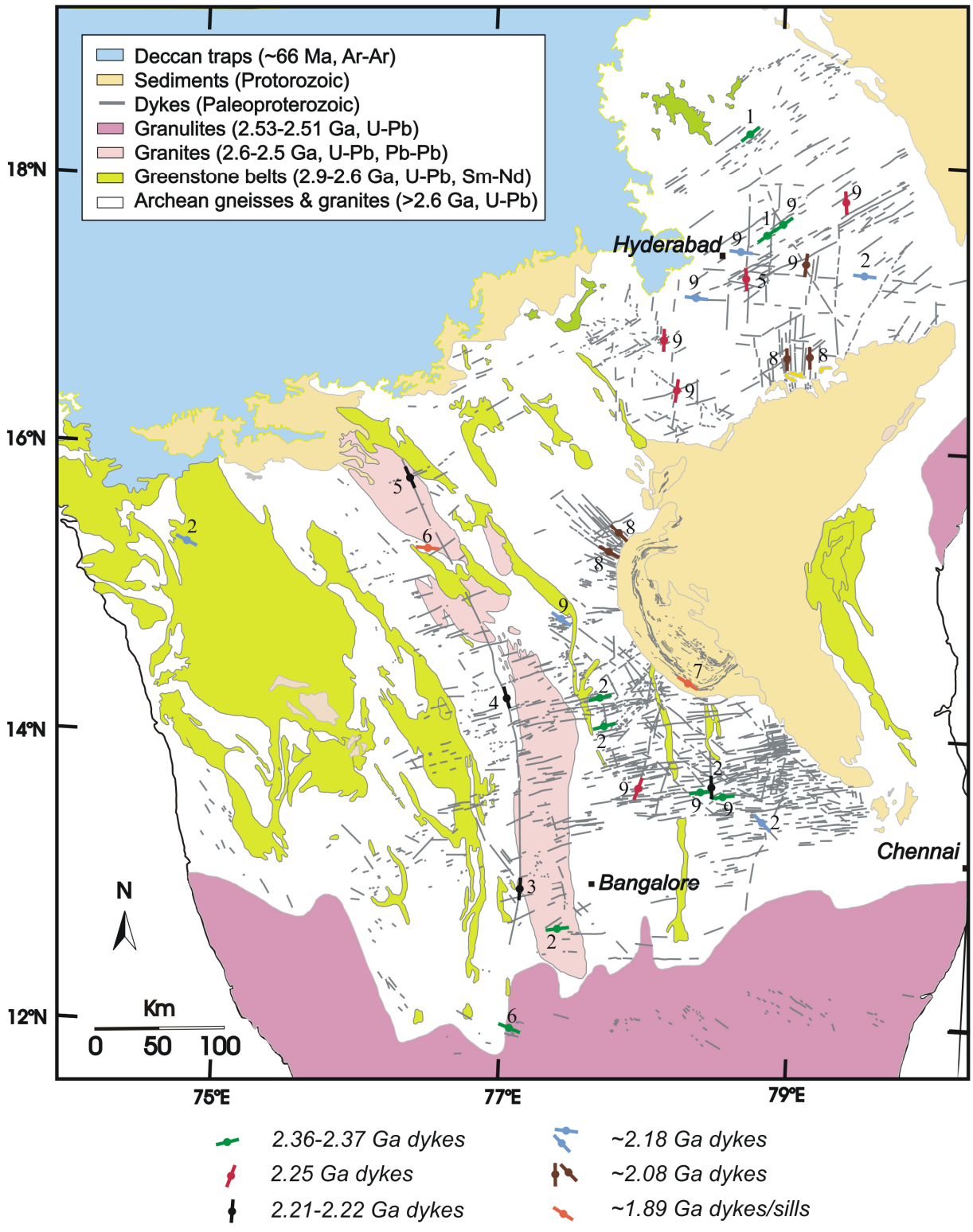

Figure 4.14. *Simplified geologic map of a part of the Dharwar craton showing mafic dyke occurrences and basement geoly (after French and Heaman, 2010) in the region. Coloured symbols and numbers indicate distinct dykes/sills that have been dated by U-Pb/Pb-Pb method and references respectively. 1-Kumar et al., 2012a; 2-French and Heaman 2010; 3-Srivastava et al., 2011; 4-Kumar et al., 2014; 5-Present data; 6-Halls et al., 2007; 7-French et al., 2008; 8-Kumar et al., 2015; 9-Demirer, 2012.*

During the zircon runs on TE-TIMS, boiling silica on heating results in large rapid spikes in emission, usually as the load is being fused. Sometimes it is possible to see bubbles bursting off the side of the load and even it goes away sometimes, resulting in failure of run. But such a problem rarely happened in the case of baddeleyite. During the baddeleyite runs, ionization of Pb usually stared at 1500°C when silica boiling is observed with spiky emission up to 1520°C and yields a smooth runs between 1540 to 1560°C generally.

Fractionation is a major source of uncertainty for precise Pb isotopic measurements. In solution loads, it can be controlled by using a ^{202}Pb–^{205}Pb spike although spike measurement uncertainty can be itself a significant source of error. If fractionation during TE-TIMS measurements can be sufficiently well understood and controlled it may provide a way to reduce this source of uncertainty without the use of a double spike. However, the present data demonstrate a limit to the reproducibility of fractionation from the scatter of age results among the different fractions. For both samples, scatter is in excess of measurement errors (Figs. 4.9 and 4.10). The excess scatter can be resolved by adding a constant external 2 sigma error to each of the fraction averages of ±1.1 Ma (0.055%) for BD and ±0.96 Ma (0.043%) for GD-08. This likely represents the fractionation uncertainty.

4.7. Summary

These results demonstrate that TE-TIMS on baddeleyite can easily furnish ^{207}Pb/^{206}Pb ages (~0.1%) that are as accurate as can be achieved by conventional methods. This procedure completely avoids the need for sample dissolution and isotope dilution required for conventional U–Pb dating technique and hence the requirement of an ultra-clean laboratory. The main limitation to precision is fractionation uncertainty, which is estimated to be about ±0.05% at 2 sigma. Baddeleyite is considered as a better suited mineral than zircon for Pb–Pb TE-TIMS geochronology due to exceptional qualities such as containing sufficiently high concentrations of U, being much less susceptible to Pb loss than zircon and also because it rarely occurs as xenocrysts in mafic–ultramafic rocks.

Two precise Pb-Pb age determinations on AKLD in this study and the other published U-Pb age are identical within error. Weighted mean ^{207}Pb–^{206}Pb baddeleyite TE-TIMS age of 2215.9 ± 0.3 Ma for sample GD-08 from site D and 2216.6±0.7 Ma for

sample KP-48 are identical with a conventional U-Pb age of 2215.0±2.0 Ma (Srivastava et al. 2011) sampled about 100 km south of GD-08 sites (Fig. 1) on the same dyke are identical within the quoted errors. Consistent and precise Pb-Pb and U-Pb baddeleyite age determinations along the dyke establish AKLD as a single dyke entity running for over 450 km. A weighted mean of the three age determinations on the AKLD gives an age of 2216.0±0.9 Ma which we consider as the best age estimate for this dyke. The three overlapping ages along the entire 450 km length suggest this dyke was emplaced in a very short duration.

The precise Pb-Pb age of 2252.06 ± 0.26 Ma is presented here for N-S trending dyke (IB-90) in the northern part of Cuddapah basin. In addition to this, four other U-Pb ages on N-S dykes in the northern and southern part of Cuddapah basin were recently reported by Demirer (2012) (Figure 4.13). These ages are BNB10-029 (2256±4 Ma), BNB10-031 (2257±4 Ma), BNB10-024 (2252±9 Ma) and BNB10-001B (2255±1 Ma). The Pb-Pb and U-Pb age determined from N-S trending dykes in this study and earlier studies define a new N-S trending dyke swarm at 2255 Ma. A newly recognised 2082 Ma radiating dyke swarm in recent studies (Demirer, 2012 and Kumar et al., 2015) includes two precise dates on N-S dykes from north of Cuddapah basin (Figure 4.13). The newly identified 2080 Ma N-S dykes and ~2255 Ma dyke swarm along with 2215 Ma N-S dyke swarm in the Dharwar craton provide unambiguous evidence that all N-S dykes in this craton are not a part of single dyke swarm.

Present ages combined with recent studies in Dharwar Craton of India have defined to identify six discrete mafic magmatic events (Figure 4.14). This includes (i) the NE-SW to E-W trending 2.6-2.37 Ga Dharwar giant dyke swarm (Halls et al., 2007, French and Heaman 2010, Kumar et al., 2012a) (ii) NNW-SSE to N-S striking 2.25 Ga N-S dyke swarm (Present study, Demirer, 2012) (iii) NNW-SSE to N-S striking 2.21 Ga AKLD swarm (French and Heaman 2010, Kumar et al., 2012b, Demirer, 2012, Srivastava et al., 2014) (iv) WNW-ESE to NW-SE trending ~2.18 Ga Mahabubnagar swarm (French and Heaman 2010, Demirer, 2012) (v) newly identified radiating ~2.08 Ga Devarakonda swarm (Kumar et al., 2015) and (vi) 1.88-1.89 Ga Cuddapah swarm along with mafic sills of Cuddapah basin.

Chapter 5: Principles and Methods of Paleomagnetism

5.1. Introduction:

Magnetism in rocks has emerged as a subject of far reaching study throughout the past fifty years. Magnetism leaves a few hints of unique values in ideal conditions facilitating their measuring and gives informative data in regards to the past. With the development of plate tectonics, the investigation of paleomagnetism accomplished significance in earth science field. Paleomagnetic method is characterized by its speed, simplicity and it is cheaper than other methods. Moreover, it is very useful in studying continental drift, plate tectonics and sea floor spreading. The application of paleomagnetism turned into a significant tool in numerous fields of earth science including paleoclimatology, paleogeography and geotectonic reconstruction. The target of paleomagnetic lab work is to isolate numerous remanence components, and identify the origin of each component. This chapter discusses the fundamental principles of paleomagnetism together with earth magnetic field, magnetic mineralogy, rock magnetism, laboratory techniques along with data analysis and sampling.

5.2. Magnetism in relation to Earth's History:

5.2.1. Earth's magnetic field:

Earth's magnetic field is closely approximated by a dipolar field with a magnetic north near the geographic south pole and magnetic south near the geographic north pole of the Earth. This model adopted for the Earth's magnetic field is that of a Geocentric Axial Dipole (GAD), when averaged over several thousands of years, with the magnetic north pole nearly coincident with the rotation pole (Opdyke and Henry, 1969; McElhinny, 1979; Hijab, 1982). For such a simple model, the geomagnetic and geographic axes coincide, as do the geomagnetic and geographic equators. The intersection of GAD with the earth surface gives the positions of the south and north geomagnetic poles which differ from the real south and north magnetic poles positions (Sharma, 1986). present day Magnetic field of the Earth is slightly inclined (~11½ degree) to a line that joins the north and south geographic poles (Fig. 5.1) (Earth's rotation axis).

Earth's magnetic field has its origin in the convection of the iron rich material of the outer core of the Earth. Generation of the magnetic field can be explained by the dynamo theory. Magnetic field (B) can be described by a vector at any point on the earth surface, which indicates the direction and strength of the field. The field direction is completely defined by Declination (D) and Inclination (I) (Fig. 5.2). Declination is the angle between the horizontal element of magnetic north (B_h) and the geographic north, which ranges from 0 to 360º, and inclination is the vertical angle between magnetic north (B) and the horizontal (B_h), ranging from -90 to 90 º. Inclination is zero at the equator and positive value of inclination indicates that field is pointing downward. The strength of the magnetic field on the earth surface varies between 30,000 nT at the magnetic equator and 60,000 nT near the poles.

The magnetic field vector (B) can be divided in to vertical and horizontal components. The vertical component of the geomagnetic field (B_z) can be given by

$B_z = B \text{ Sin } I$

The horizontal component B_h is given by

$B_h = B \text{ Cos } I$

here I is the inclination and B is the magnitude of geomagnetic field vector.

The geographic north and east components are given by,

$x = B \text{ Cos } I \text{ Cos } D$ and

$y = B \text{ Cos } I \text{ Sin } D$ where 'D' is the declination

Using these relations, declination and inclination can be expressed as

$D = Tan^{-1}\frac{y}{x}$ and $I = Tan^{-1}\frac{z}{B_h}$ where magnitude of $B_h = (x^2 + y^2)^{1/2}$.

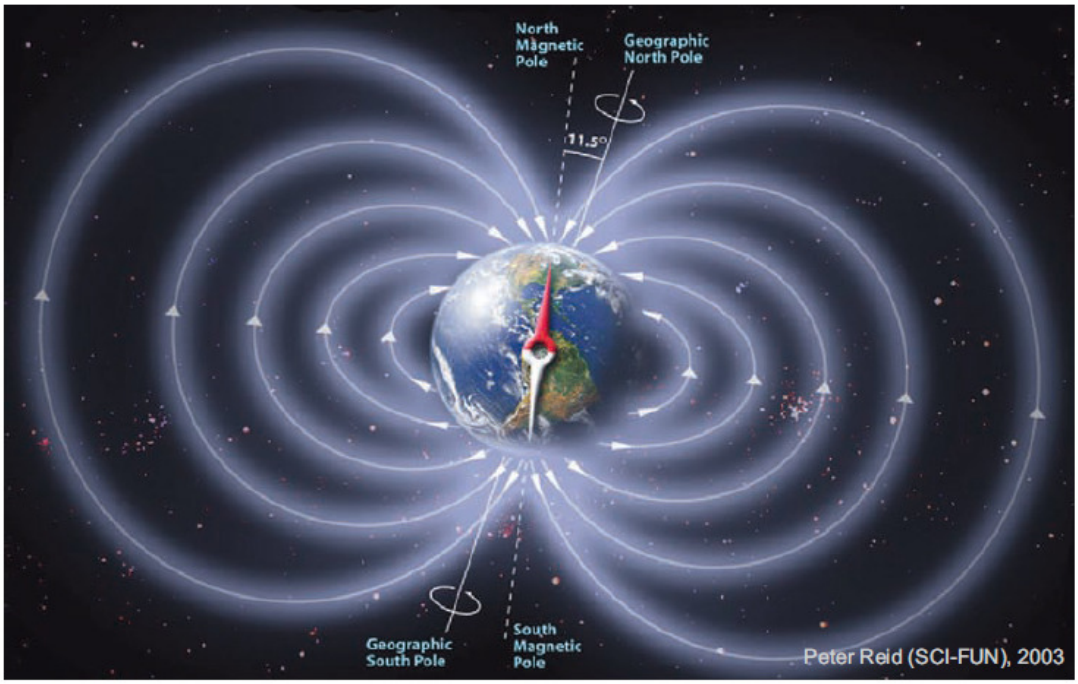

Figure 5.1. *Approximation of the Earth magnetic dipole field tilted 11.5° relative to the axis of rotation of the Earth.*

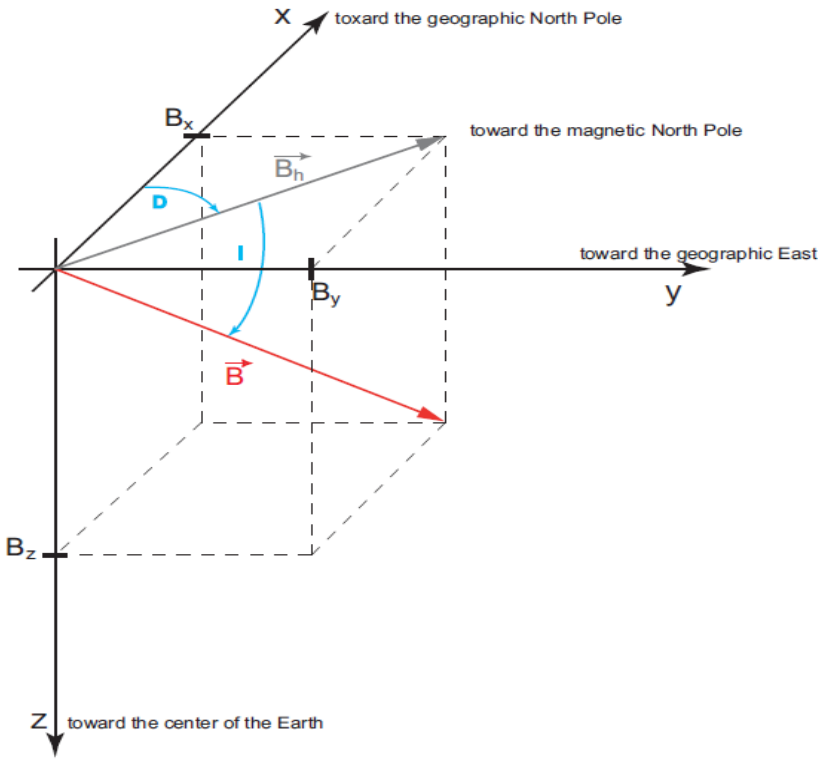

Figure 5.2: *Representation of the components of the magnetic field B. B_x, B_y, B_z are the Cartesian coordinates in the direct frame and B_h is the projection of the field vector in the horizontal plane. D: declination; I: inclination.*

5.2.2. Rock Magnetism:

Every rock contains iron oxide minerals at least in trace amounts. Magnetic moment which is carried by iron oxide mineral is permanent and is known as natural remanent magnetization (NRM). With the effect of geomagnetic field, the NRM is locked in to the rock rapidly after its formation. Magnetite (Fe_3O_4) and Hematite (Fe_2O_3) are the most magnetic terrestrial minerals. However, new magnetic remanence components could also be integrated to the original NRM throughout the rock. The original NRM can also be partially or completely erased. As a rule, the NRM of a rock is a composite of the primary origin, which is imprinted on the rock at or near the time of formation, and any components (secondary) that are subsequently added to that. The primary segment can frequently be segregated from the aggregate NRM by method of stepwise demagnetization until the NRM is totally removed from the specimen.Techniques of demagnetization suggest the main magnetic carrying mineral (Dunlop and Ozdemir, 1997). The component which is most resistant to demagnetization technique is typically treated as primary component. Demagnetization is carried out in a field free space i.e. the samples are protected from the ambient geomagnetic field in the laboratory, to prevent the demagnetized grains from acquiring spurious remanence components with no geological meaning.

5.2.3. Secular Variations:

Geomagnetic information over times of couple of thousand to 1,000,000 years demonstrated that there is a consistent variation within the magnitude and direction of geomagnetic fields. The magnetic fluctuations arising in short time interval varying from few seconds to some years are mainly because of solar effects. If the variations are in long term, then they are known as secular variations. These secular variations are evident in rocks, because rocks have cooled through a long period of time.

The geomagnetic data for the earlier 1,000,000 years confirms that magnetic variations within the north pole had been in a path around with a couple of degrees to the rotational axis. According to geocentric axial dipole (GAD) theory, geomagnetic field is treated to be produced by a single dipole which is aligned along the rotational axis and the secular variations will be averaged out corresponding to this dipole. Paleomagnetism principles are developed based on this concept.

5.2.4. Polarity Reversals:

Several investigations of ancient magnetised rocks show that their Natural Remanent Magnetization (NRM) was oriented opposite to that of the present day magnetic field. Later experiments conducted on reversed NRM directions allowed to suppose that reversed NRM is due to the reversals of geomagnetic field in past geological times. Magnetic 'flip' is a state in which the south pole is transformed in to a north pole and the north pole becomes a south pole. These geomagnetic flips are of three types depending on the duration of the 'flip' time. During reversals the magnetic field strength is nearly zero and increases gradually in opposite direction. Many models or hypothesis are developed to explain the reversals of the magnetic field of the earth. However there is no clear theory which describes how the geomagnetic field might have reversed. Geomagnetic reversals of the polarity are rapid events usually < 5 Ka in duration that occur at random intervals. The magnetic field of the earth has reversed nearly 170 times during the past hundred million years time.

5.3. Laboratory Techniques:

Igneous rocks acquire primary magnetization by thermoremanence process at the time of formation, when they cool through the curie temperatures in the ambient magnetic field of the earth. Even after acquiring the primary magnetization, rocks will be influenced by external magnetic field or temperature. This induces secondary magnetization (e.g. Viscous remanent magnetization (VRM), Chemical remanent magnetization (CRM) and Thermo chemical remanent magnetization (TCRM)) in the rocks. Magnetism remained in the rock by combining two types (primary and secondary magnetization) is treated as natural remanent magnetization (NRM).

Generally secondary components are sufficiently strong enough to cover the primary magnetization, but it is compulsory to remove low stability component (secondary magnetization) to get primary magnetization. Hence, magnetic cleaning (demagnetization) techniques are required to erase secondary magnetization. This demagnetization technique permits to erase secondary NRM in sequential steps by aligning the secondary magnetized particles in random orientation. After each step of demagnetization, remanent magnetization has to be noted for further analysis. Generally high stability component remained in the rock after demagnetization is termed as

characteristic remanent magnetization (ChRM) which is most stable and is identified as the direction which is isolated and the vector decays in a straight line to the origin during stepwise demagnetization. After randomising the secondary overprinted component using either by thermal (TH) or alternating field (AF) demagnetization procedures, ChRM can be identified and isolated.

5.3.1. NRM Measurements:

Measurements of the natural remnant magnetization (NRM) of samples were done using MOLSPIN Spinner magnetometer and JR6 dual speed spinner magnetometer. Initial NRM was first measured for each specimen. It includes inclination (I), declination (D) and magnetic intensity (J) values. In order to understand the nature of the stable magnetic component present in the sample, and the nature of magnetic minerals which carry the remnant magnetization, demagnetizing techniques were applied to the samples.

5.3.2. Demagnetization techniques:

5.3.2.1. Alternating field demagnetization:

Alternating field (AF) treatment relates to the coercivity spectra of the material. In this case specimen is placed in gradually incrementing alternating magnetic field (sinusoidal wave form). This technique is applied to erase NRM of grains with low coercivity than the used peak field of demagnetization (Fig.5.3). All the magnetic mineral grains having lower coersivity than the AF peak value will be re-oriented in the direction of the applied alternating field, just before it decreases to a lower value. Eventually, the grains will be randomized because the sign of the AF is continuously switching between negative and positive and result in a net zero magnetic moment. The AF technique is a fairly quick magnetic cleaning procedure compared with the thermal demagnetization procedure.

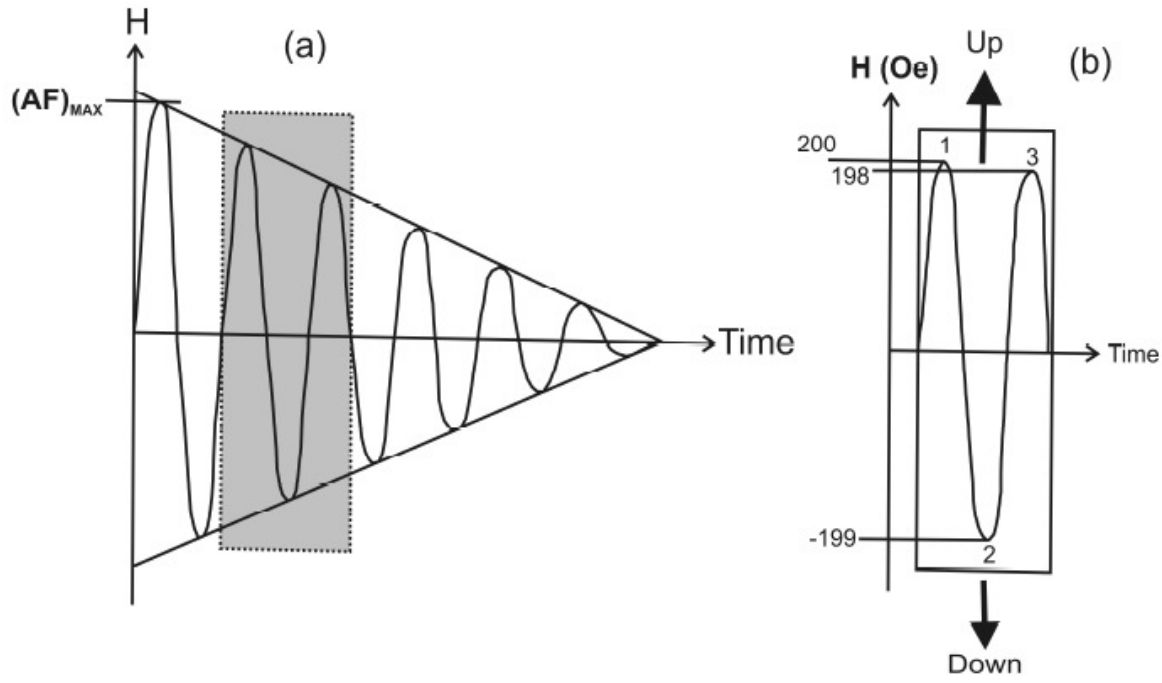

Figure 5.3. *Schematic representation of alternating field demagnetization. Redrawn after Butler, (1992). (a) Generalized waveform of the magnetic field used in alternating field (AF) demagnetization showing magnetic field versus time. (b) Detailed examination of the portion (shaded rectangle) of the AF demagnetization wave form.*

However, some times this technique is not suitable for high coercive minerals such as hematite and goethite. In such case, thermal demagnetization method can be applied.

5.3.2.2. Thermal demagnetization:

Demagnetizing the remanent magnetization of a rock specimen using thermal treatment involves heating-cooling cycles in zero fields at consecutive temperature steps, until the maximum unblocking temperature of the remanence carrying mineral is reached and then cool down to ambient room temperature in zero field. After each step the magnetization is measured. When heating to a particular temperature, grains with low blocking temperatures lose their magnetization and only the grains with high blocking temperatures retain remanent magnetization. Thus, if a specimen is introduced to thermal demagnetization with progressively increasing temperatures, only the grains with high blocking temperatures that remain possesses ChRM and can be measured. Susceptibility at each step can also be monitored to know the alterations of mineralogy.

To retrieve the NRM of a specimen, sometimes both the techniques were combined one after another.

5.4. Demagnetization data display

Data retrieved from progressive demagnetization techniques were presented in both stereographic projection and orthogonal projection.

5.4.1. Stereographic projection

The NRM directions obtained in progressive demagnetization technique are usually presented in equal area projection. Magnetic vectors of declination and inclination were shown on the stereonet of lower hemisphere. Positive inclination (downward) vectors represent solid circles whereas open circles represents negative inclination (upward) vectors.

Considering that the intensities of more than a few vectors cannot be shown on the stereonet, a projection of direction versus intensities also needs to be shown.

5.4.2. Orthogonal projection

The orhogonal projection is also known as the Zijderveld diagram (Zijderveld, 1967; Fig.5.4). The 3-D vectors of intensity and direction of demagnetization were shown separately on both horizontal and vertical planes. Declination is plotted in the horizontal plane whereas inclination is plotted in vertical plane. In both the planes, magnitude of the vector from the origin represents the intensity of demagnetization. The ChRM is confirmed to be isolated when the directions of different vectors are pointing towards the origin.

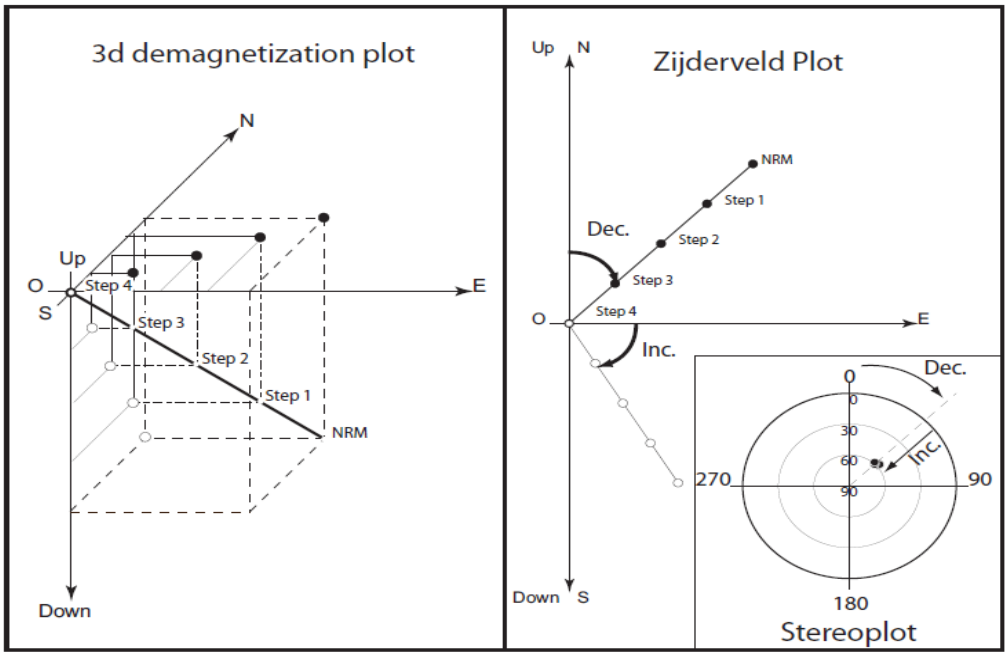

Figure 5.4. *Construction of Zijderveld diagram. (a) Representation in 3D : the evolution of the magnetization vector in one component. (b) Zijderveld diagram corresponding stereographic plot.*

5.5. Principal component analysis:

Various remanence components were isolated using standard principal component analysis method (Kirschvink, 1980). It is a method for determining direction using three dimensional least-squares fit of selected demagnetization steps. The uncertainty of this value can be expressed as maximum angular deviation (MAD). Its value is much larger if the points are not aligned properly. MAD value of < 15° is generally treated as best estimate (Butler, 1992). The points aligned properly towards the origin are considered for ChRM calculation. Although PCA method could give a good approximation, it can be confusing if overprinted secondary component is presented. In such a case, Fisher (1953) distribution should be applied to solve the problem.

Directional analysis of the vector remanence datasets after demagnetization treatment was performed using the Remasoft software. This software allows determining the components of magnetization directions with least square method in 3-D space, as well as its uncertainty. Additionally to numerical analysis of the separated vectors, the software plots the standard Zijderveld plots and a stereoplot in the course of demagnetization steps.

5.6. Calculating pole positions:

Sample magnetization directions (D, I) obtained from the primary Natural Remanent Magnetism (NRM) differs between samples because of errors. The declinations and inclinations of various samples that have evolved at the same time but in different geographic locations will be different. We need to calculate the mean direction and its error to know the dispersion or scatter of individual directions with the mean direction. This represents site mean declination (D_m) and mean inclination (I_m). By the use of known mean direction of the individual site, pole position (Fig. 5.5) can be determined (latitude: λ_p and longitude: ϕ_p; McElhinny, 1973). To know the paleopole position it is compulsory to calculate co-latitude (p) which gives great circle distance. The co-latitude of the sampling site corresponding to the paleopole position can be calculated with the equation,

$$P = Cot^{-1}\left(\frac{1}{2TanI_m}\right) = \pi/2 - Tan^{-1}\left(\frac{1}{2TanI_m}\right)$$

This co-latitude (p) refers to the ancient or apparent magnetic palaeolatitude. This ancient pole position can be converted to present latitude and longitude of ancient pole. If the location of the sampling site is in normal geographic latitude (λ_s) and longitude (ϕ_s) then the latitude (λ_p) and longitude (ϕ_p) of the corresponding pole is given by

$\text{Sin } \lambda_p = \text{Sin } \lambda_s \text{ Cos p} + \text{Cos } \lambda_s \text{ Sin p Cos } D_m$ and

$\phi_p = \phi_s + \beta$ (for $\text{Cos p} > \text{Sin } \lambda_s \text{ Sin } \lambda_p$)

or $\phi_p = \phi_s + (180 - \beta)$ (for $\text{Cos p} < \text{Sin } \lambda_s \text{ Sin } \lambda_p$)

where $\text{Sin } \beta = \text{Sin p Sin } D_m / \text{Cos } \lambda_s$

Latitude is measured between 0 and 90°, positive in northern hemisphere and negative in southern hemisphere, and longitude is measured between 0° and 360°.

The mean site directions (D_m and I_m) connected with the circular confidence limit α95 is converted in to paleopole position with confidence ellipse of semi minor axis "dp" and semi major axis "dm". These "dp" and "dm" can be determined with the following equations,

$dp = \alpha 95\ (1 + 3\ \mathrm{Cos}^2\ p)/2$ and

$dm = \alpha 95\ (\mathrm{Sin}\ p\ /\ \mathrm{Cos}\ I_m)$.

A pole position calculated, for example by spherical trigonometry, from a single observation is known as virtual geomagnetic pole (VGP) corresponds to the location at that particular time. VGPs determined from locations distributed throughout the globe are scattered about the geomagnetic pole at that time.

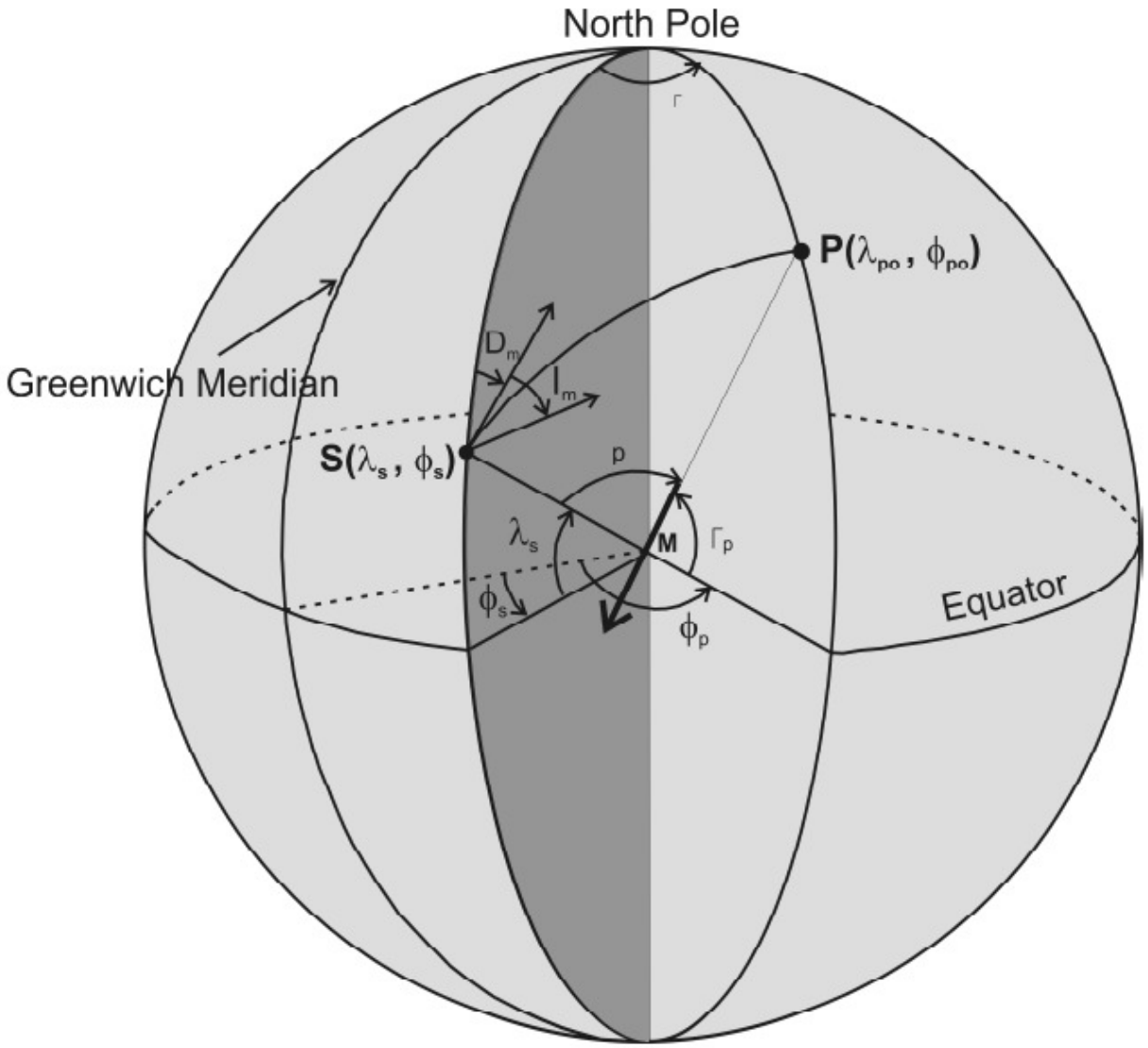

Figure 5.5. *Determination of magnetic pole position from a magnetic field direction, redrawn after Butler, (1992) and Merrill et al., (1996). Site location is at S (λ_s, ϕ_s). M is the geocentric dipole that can account for the observed magnetic field direction.*

5.7. Laboratory set-up and Methodolgy

The Palaeomagnetic Laboratory at the National Geophysical Research Institute, Hyderabad is outfitted with the modern facilities like 'JR6 dual speed spinner magnetometer', Alternating field demagnetiser, MMTD 1 Thermal demagnetiser, MMPM10 Pulse magnetizer and Bartington Susceptibility meter.

5.7.1. JR-6 dual speed spinner magnetometer

The measurements of Natural Remnant Magnetization (NRM) were done to know the direction and intensity of these specimens on a very sensitive instrument, Spinner Magnetometer (JR-6). The range of measuring strength is from 0 to 12500 A/m with an accuracy of ±2.4 μA/m. This instrument is manufactured by Agico Company, Czech Republic (Fig. 5.6). The principle of JR-6 dual speed spinner magnetometer is the generation of voltage through the continuous rotation of magnetic sample inside the coil.Voltage generated in this process is proportional to the magnetic moment of the sample and is further used to correlate with the reference direction.

5.7.2. Alternating Field demagnetiser

The alternating field (AF) demagnetiser can be controlled electronically with a peak field up to 150 mT(Figure 5.7). When alternating current passes through a coil, alternating magnetic field will setup along the axis of the coil. The coil takes up a maximum current of 5 amperes when 220 volts AC is applied. In order to avoid the effects of magnetic field of the earth, coil is covered with double walled mu-metal shield.

The fundamental principle behind this technique is that grains with lower coercive force than the applied field will be randomised.

The demagnetization fields were selected at 2.5, 5, 7.5, 10, 12.5, 15, 17.5, 20, 25, 30, 40, 50, 60, 70, 80, 90 and 100 mT. Few specimens were demagnetized even up to 150 mT.

Figure 5.6. *JR-6 spinner magnetometer.*

Figure 5.7. *Alternating Field demagnetiser (Molspin Ltd; lJK).*

5.7.3. MMTD 1 thermal demagnetiser

The MMTD 1 thermal demagnetiser (Fig. 5.8) enables to heat a sample up to a maximum temperature of 800°C. The temperature in the oven can be controlled by a programme. This oven is covered with mu-metal shield in four layers to nullify the influence of external magnetic fields such as magnetic field due to the earth. With this setup samples are heated to a required temperature and then cooled to room temperature in field free environment. The rise and decrease in temperature are often accomplished in 2 ramps with a hold time of 20 minutes in between. Usually the rate of increase in temperature is chosen to be 50°C per minute below 500°C and 20°C per minute after that. Representative samples from all sites were demagnetised in this process.

Figure 5.8. *The Magnetic Measurements TTM Thermal Demagnetizer.*

5.7.4. MMPM 10 Pulse Magnetizer:

The MMPM10 pulse magnetizer is designed to give a short duration high magnetic field pulse to a sample (Figure 5.9). The amplitude of the pulse is adjustable from 0 T to more than 9 T with 7 ms pulse duration. The magnetic field pulse is generated by discharging a bank of capacitors through a coil. The MMPM10 has two coils, a 3.8 cm coil and a 1.25 cm coil. The maximum field that can be generated in the 3.8 cm coil is 3 T while a field of more than 9 T can be generated in the 1.25 cm coil. The MMPM10 allows us to accurately set the field on either in milli Tesla or Tesla range using a digital display.

Figure 5.9. *MMPM 10 Pulse Magnetizer.*

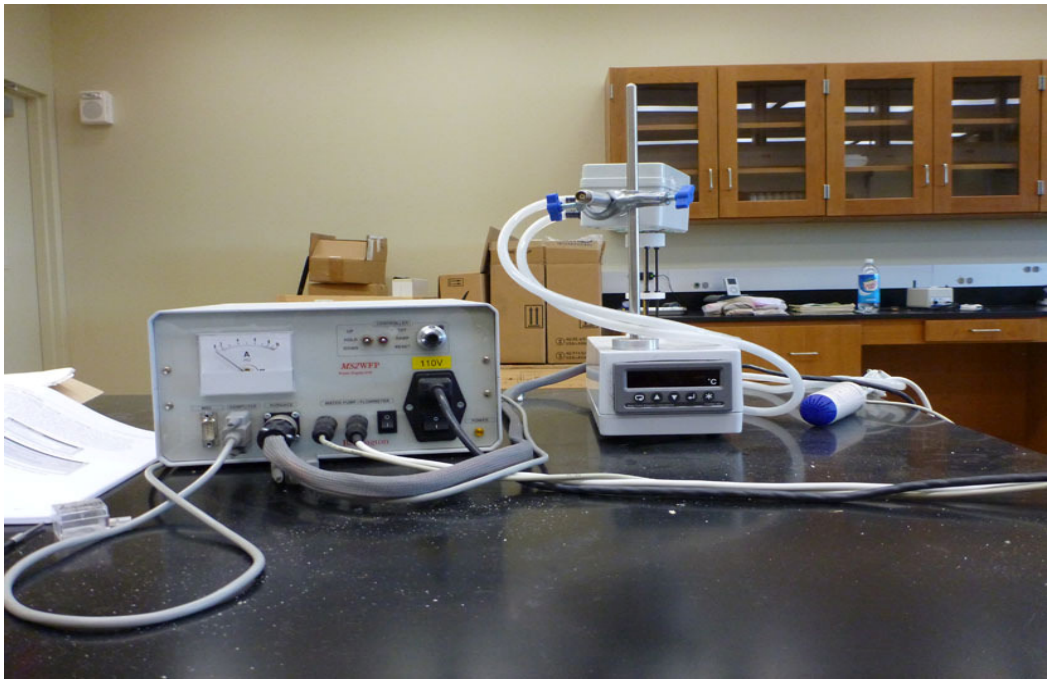

Figure 5.10. *MS2 Bartington Magnetic Susceptibility meter.*

5.7.5. MS2 Bartington Magnetic Susceptibility meter:

The MS2 Bartington Magnetic Susceptibility meter (Figure 5.10) is able to detect minerals and domains in sample that have been cooled below or heated above room temperature because the magnetic behaviour of many minerals and domain states varies with temperature. Three different sequences of susceptibility – temperature measurements are possible: warming from -196°C (temperature of liquid nitrogen) to room temperature (25°C); heating from room temperature to high temperature (up to ~800°C); and cooling from high temperature to room temperature to room temperature (25°C). Three types of thermal effect may be observed. The presence of minerals and domains is detected from the shapes of the temperature vs. susceptibility curves and distinctive transition points.

5.8. Identification of remanence carriers

It is first and foremost to identify the remanence carrier of each component before concluding the origin and paleomagnetic component type (Primary or secondary). The magnetic mineral which carries remanence can be identified with AF and thermal demagnetization techniques, but to confirm that petrographical observations and rock magnetic measurements are needed (Dunlop and Ozdemir, 1997). In this work, both low and high temperature thermomagnetic measurements along with hysteresis properties were carried out.

5.8.1. Thermomagnetic measurements

Thermomagnetic measurement procedure allows assessing the magnetic phases in a rock sample. By studying the mineralogy of magnetic minerals within the samples, one can understand the acquisition of magnetic record in that sample. The basic property of magnetic mineral is to record the ambient magnetic field direction when they were formed through curie temperature. For a given temperature, magnetic mineral can record a maximum magnetization under the influence of applied magnetic field which is termed as saturation magnetization (J_s). If the sample has got its J_s, any increase of the applied field wouldn't reflect in increased magnetization. Below curie temperature (T_c) all the magnetic moments associated with magnetic minerals are partly aligned in within the domains. If the temperature is raised from just below T_c, thermal fluctuations within the

domain progressively destroy the alignment of magnetic moments until it results in zero net magnetic moment at and above T_c.

5.8.2. Hysteresis loop:

A hysteresis loop is defined by changing the magnetization of a sample subjected to a magnetic field of variable intensity. Magnetization of the sample will saturate at a peak magnetic field. This determines the saturation magnetization (J_s). Then decreases the magnetic field until it passes zero and vice versa. This gives a measure of the residual magnetization saturation (J_{rs}). The magnetic field is then reversed and driven to saturation in the opposite direction of the original field. In this process net magnetization of the sample gradually decreases and increases in other direction. The applied magnetic field where the net magnetization of the sample becomes zero is called coercive force (H_c). Logically one should get a saturation magnetization (J_s) and coercive force (H_c) value for wherein the magnetization of the sample (J) passes through zero . The coercivity retentive (H_{cr}) is determined by gradually applying a reverse field after saturation. H_{cr} is the field for which the residual moment becomes zero. H_c , H_{cr} , J_{rs} and J_s parameters are characteristic of the mineral and its state ferromagnetic (or ferrimagnetic) . The shape and the cycle ratio values H_{cr} and $H_c = J_{rs} = J_s$ depend on the microstructure and tell us about the grain size. These values are represented in a diagram of Day (1977).

5.8.3. Isothermal remanent magnetization

The isothermal remanent magnetization (IRM) is a laboratory remanence acquired by a sample (assemblage of ferromagnetic grains) after applying a field continued strong at room temperature. Every magnetic grain in a sample acts as a magnetic dipole with a permanent dipole moment. The minimum field needed to reverse the direction of such dipole is termed as coercive force. If the external field is strong enough to saturate the magnetic minerals within the sample, then the remanence is known as saturation isothermal remanent magnetization (SIRM) which is also same as that of Jrs in hysteresis loop. This saturation is usually achieved for relatively low fields (~300 mT) for the magnetite. In contrast in the presence of hematite, saturation can be reached only beyond 1.5 T. This curve is used to determine threshold saturation and coercive spectra of a sample, and can thus be used for magnetic mineralogy.

Chapter 6: Paleomagnetism Results

6.1. Introduction:

All samples from this study are from the dolerite dykes of the Eastern Dharwar Craton (EDC). The natural remanent magnetization (NRM) measurements of all samples were done using JR6 spinner magnetometer. The AF and thermal demagnetizations carried out on pilot specimens representing all samples demonstrated that every one of them is associated with magnetic overprinted components. At least three specimens per sample were subjected to detailed stepwise alternating field (AF) and/or thermal demagnetization (TD) to a maximum of 150 mT or 600°C in order to separate components based on their coercivity or unblocking temperature. Samples were subjected to progressive AF demagnetization up to a peak field of 150 mT in intervals of 2.5 mT, 5 mT and 10 mT and thermal demagnetizations up a maximum temperature of 600°C in steps of 50°C below 500°C and in 20°C or 25°C steps up to 600°C. After every step of thermal demagnetization, susceptibilities were monitored to identify mineralogical changes during heating. Demagnetizations conducted on all specimens were evidenced to be effective in isolating the sample ChRM. Results of demagnetizations have been examined using zijderveld figures along with intensity decay curves and stereographic projections. More than five collinear points directed towards origin were selected on zijderveld diagrams to calculate principal component analysis (PCA). Acceptance criteria for ChRM directions is maximum angular deviation values should be <10°. Fisher statistics is used to calculate site mean directions. Results from each region are described in general in this chapter with detailed data with individual site mean directions.

6.2. Dykes from different dyke swarms:

2.21-2.22 Ga dyke swarm includes sites on AKLD dyke and two sites adjacent to AKLD nearby Bangalore (considered as dyke ii in Kumar et al., 2012b). 2.25 Ga dyke swarm includes four sites in the north-eastern part of AKLD nearby Mahabubnagar (treated as dyke iii in Kumar et al., 2012b). ~2.18 GaMahabubnagar dyke swarm includes eight sites on E-W trending dyke near Mahabubnagar town, which covers a length of 250 Km. This sampling region is located between 12.767°N to 16.512°N latitude and 76.301°E to 77.71°E longitude.

A total of 79 samples were collected at 17 sites along the strike of AKLD dyke, 11 samples from 2 sites on dyke ii, 21 samples from 4 sites are collected on dyke iii and 50 samples representing eight sites on E-W dyke. A total of 161 samples are representing various dyke swarms in this study. Each of these sites contains a minimum of 5 and a maximum of 9 oriented block samples. All together 544 core specimens were collected after coring and shaping in to required dimensions (2.5 cm diameter and 2.2 cm length). In order to understand the nature of the stable magnetic components in the samples and the nature of the magnetic minerals which carry the remanent magnetization, alternating field and thermal demagnetizations were applied for 330 specimens (at least three specimens per sample) representing 31 sites on three dike swarms. Few specimens were analysed using mixed AF and thermal demagnetization. During the thermal cleaning, the bulk susceptibility was monitored after each step in order to detect mineralogical changes. Minimum of one specimen from all samples were thermally cleaned. In order to identify magnetic carriers, thermomagnetic analyses (susceptibility vs. temperature) were carried out on one sample from each site. Hysteresis characteristics measurements were also performed to identify the domain state of magnetic carrier.

6.2.1. Rock magnetism – magnetic carriers of remanence:

Representative examples of the Curie point analyses are shown in Figure 6.1. These analyses were carried out for one sample from each site except for sites R and S. The samples showed nearly reversibilities of heating and cooling curves, indicating no mineralogical changes during heating. For example GD 3 (site C) and GD 26 (site I) are almost reversible, indicating that these samples are suitable for thermal demagnetization. Most of the samples show only one ferromagnetic phase with Curie points of 550-580°C when plotting the variation of susceptibility with temperature on heating (Fig. 6.2). Susceptibility values in almost all samples showed that gradual increase from room temperature to about 540° to 550°C, by about 5 to 10%, beyond this temperature the values are seen to drop to zero at around 580°C. This behaviour suggests that magnetic grains are either single domain (SD) or pseudosingle domain (PSD) (Dunlop, 1983). Low temperature susceptibility variation was determined by cooling samples in liquid nitrogen to -196°C and recording their susceptibility as the samples warm to room temperature. All samples show a positive anomaly at about -150°C close to Verwey Transition for magnetite (Fig. 6.2).

Conventional IRM study to fields up to a maximum field of 0.5 Tesla has been imparted in step wise by a pulse magnetizer and this process resolves the presence of low coersivity ferromagnets such as titanomagnetite in Fig. 6.2. The specimens were magnetized by progressively increasing fields in steps from 15 to 500 mT, and the intensity of IRM was monitored at each step. As the magnetic field is applied in reverse direction intensity of magnetization reduces to zero, which was continued till IRM saturates in opposite direction. The IRM curves in the present study saturate at low fields (usually in between 150 and200 mT) indicating that titanomagnetite is the main magnetic carrier. The remanence coercivity for all the measured samples was found between 40 and 50 mT revealing the grain size of ChRM carrying mineral type as SD to PSD (Dankers, 1981; Cisowski, 1981; Sharma, 1994). These rock magnetic studies conducted on whole rock samples clearly suggest that the dominant magnetic mineral is single domain (SD) to pseudo single domain (PSD) titanomagnetite. However, careful magnetic experiments on interstitial magnetite grains and on pure plagioclase and pyroxene mineral separates together with electron microscopy studies show the occurrence of elongated <1 micron magnetite inclusions along cleavage planes within the silicate phases pyroxene and plagioclase feldspar (NGRI, IPGP unpublished data). We are inclined to believe that these single domain magnetite grains could be the source of primary remanence in these rocks.

6.2.2. Petrography:

Petrographic studies have been carried out on at least one sample from each site. Samples are medium to coarse grained towards the centre of the dyke and relatively finer towards the margin. Plagioclase, augite, and occasionally hypersthene are the major mineral constituents with minor amounts of magnetite. Modal abundance of magnetite is 4–5%.

Poikilitic texture is very common, though in a few sections porphyritic texture was also observed. All samples are generally fresh, barring minor alteration of plagioclase in a few samples. Degree of alteration or feldspar clouding does not appear to vary along the dyke strike (Fig. 6.3), though the degree of metamorphism in the country rock increases from north to south. However, SEM images (Fig. 6.4) clearly show two types of magnetic minerals. Fine grained needle like single domain (1x5 μm) magnetite located within silicate minerals pyroxene and plagioclase. Though this constitutes a very small modal

percentage of the rock it could be the main carrier of remanent magnetization in this dyke. Medium grained multidomain (~ 50 μm) Ti-poor magnetite occurs more ubiquitously (4 to 5%) as interstitial grains in these samples.

6.3. Results of 2.21-2.22 Ga dyke swarm:

The NRM measurements obtained on all specimens were plotted together in figure 6.5. The orthogonal projections (Zijderveld plots) of alternating field and (or) thermal demagnetizations on one specimen from each site location are presented in figure 6.6. The characteristic magnetization vectors from every site are also plotted in stereographic projection in figure 6.7. The site mean directions of each site are described below and the data representing mean magnetization vectors from all sites are given in table 6.1.

6.3.1. AKLD sites:

Site A:

An aggregate of 7 specimens were examined, every one of them were grouped together and fulfil acceptance criteria and thus taken in to account for the estimation of site mean direction. The seven specimens combined to give site mean direction as: Dm = 243°, Im = -55° (k = 39, α95 = 10°) and therefore the VGP corresponding to this site was calculated as: λ = 30°S; ϕ = 314°E (dp/dm = 10°/14°).

Site B:

Six representative core specimens from five samples show good grouping and yielded consistent direction as: Dm = 245°, Im = -63° (k = 100, α95 = 7°) and the corresponding VGP at: λ = 27°S; ϕ = 304°E (dp/dm = 8°/11°).

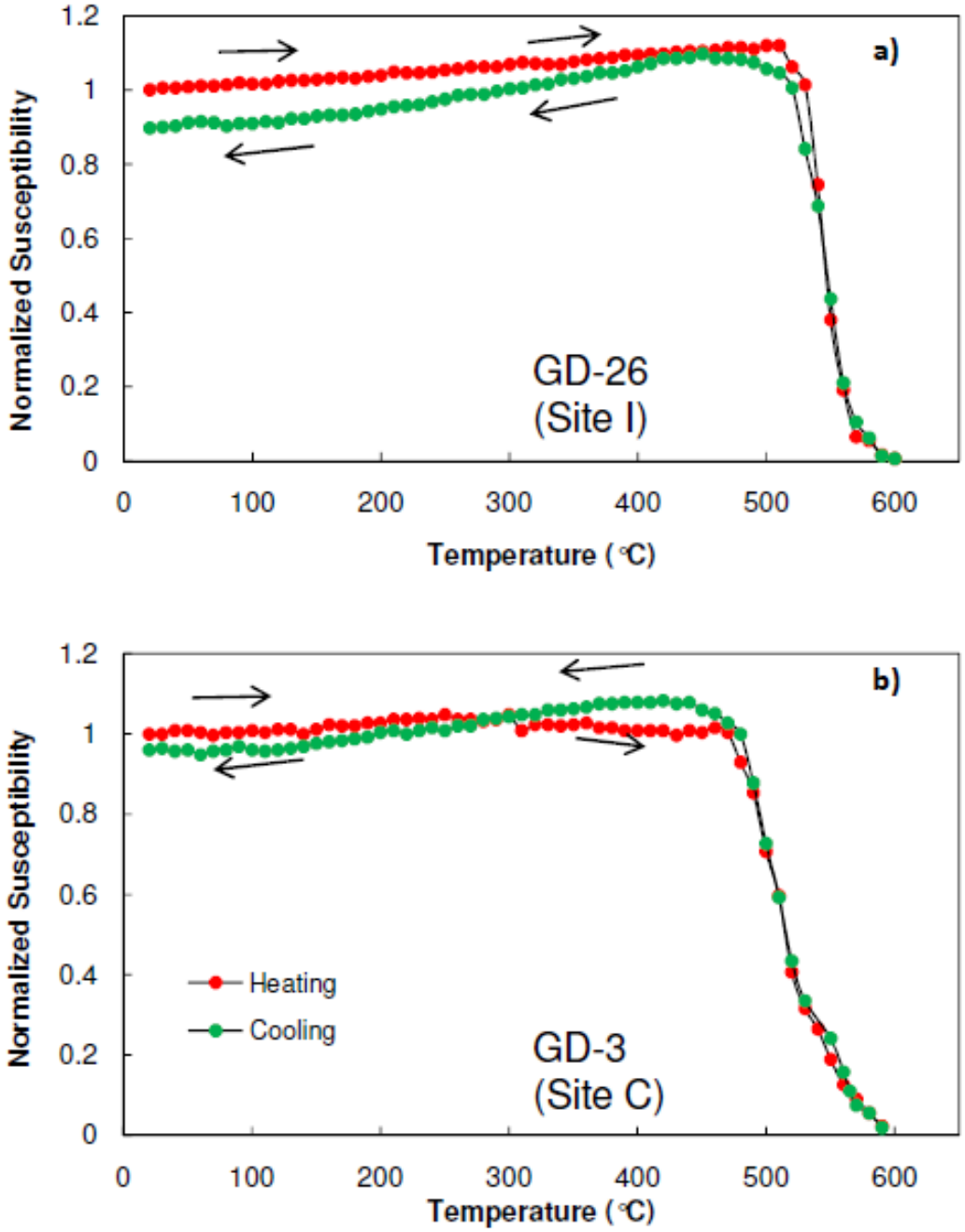

Figure 6.1. *Typical examples of magnetic susceptibility versus temperature dependencies.*

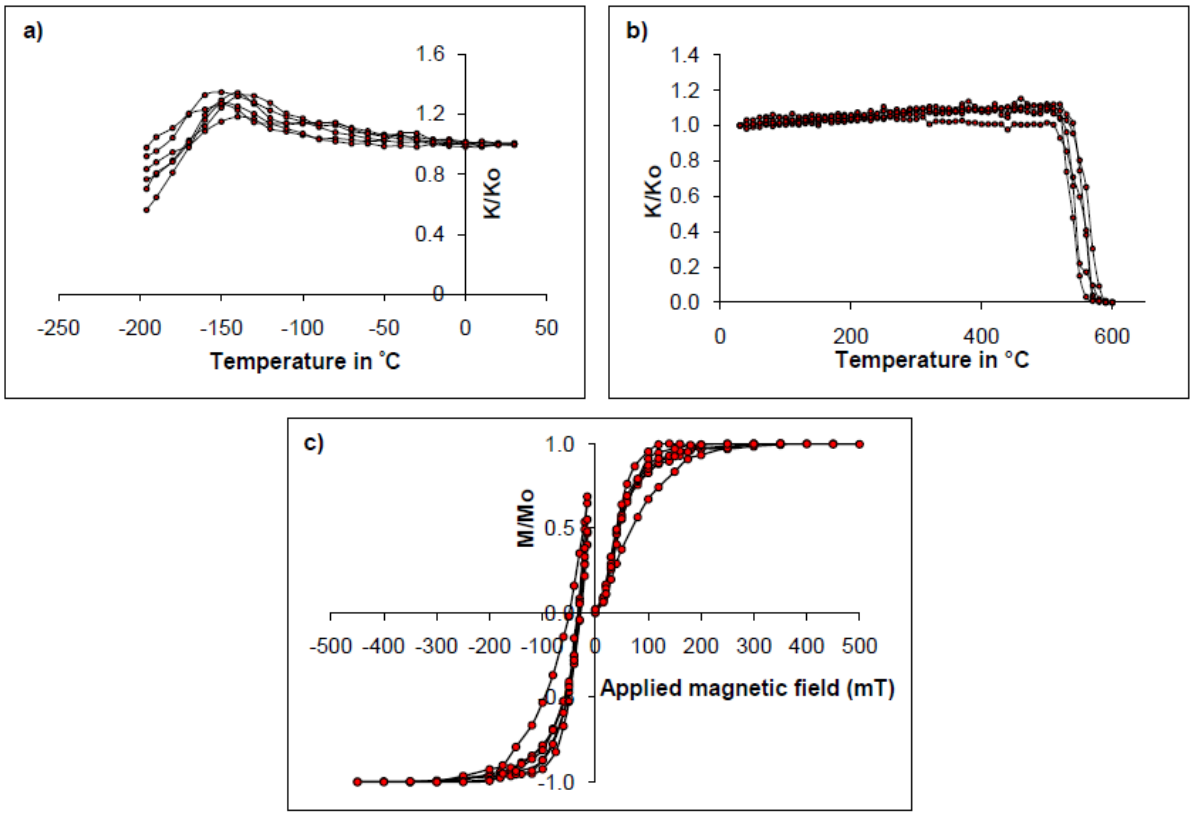

Figure 6.2. ***(a)*** *Variation of magnetic susceptibility from liquid nitrogen temperature (−196°C) to room temperature and* ***(b)*** *room temperature to 600°C for representative samples from different sites.* ***(c)*** *Isothermal remanence acquisition curves (acquired magnetization normalized to saturated values vs. applied field in mT).*

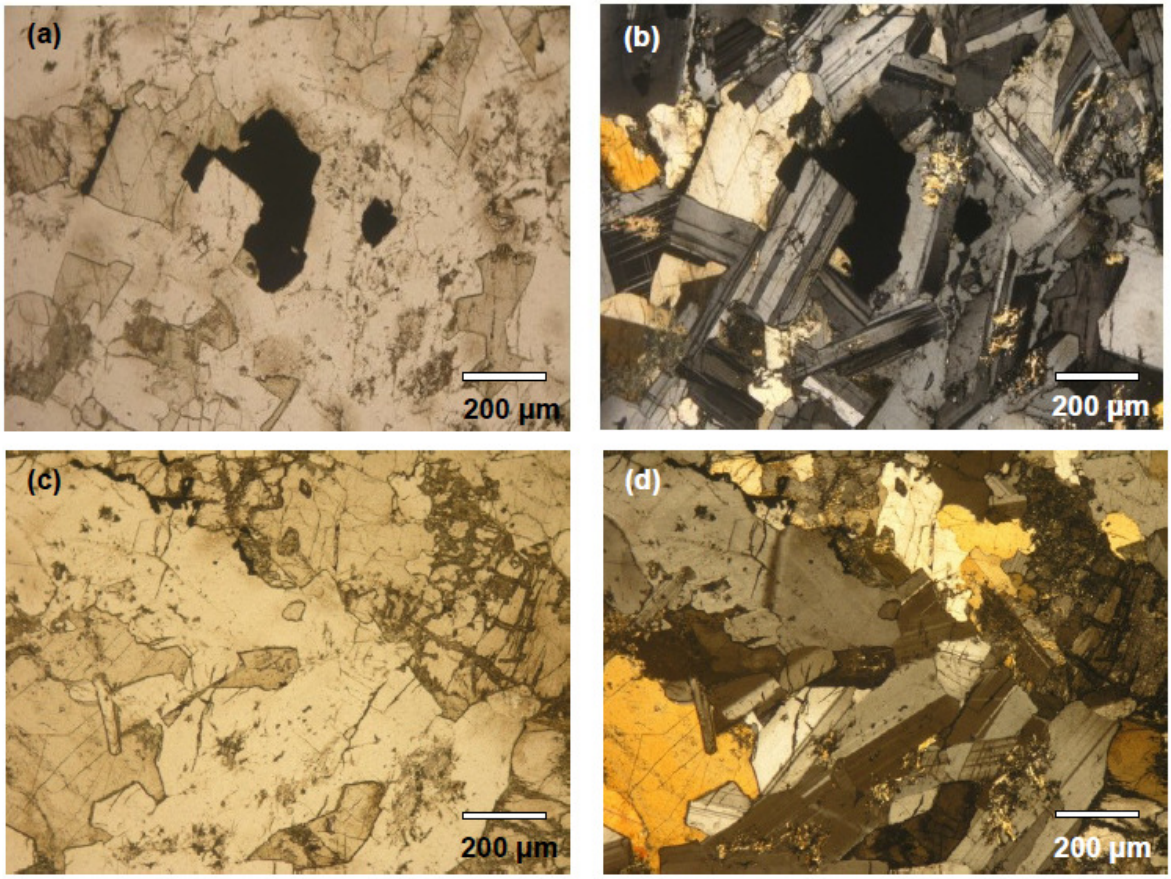

Figure 6.3. *Photomicrographs of AKLD samples. Samples are characterised by minimum alteration. (a) and (b) are from site A (country rock metamorphosed to amphibolites grade), the southernmost site on the AKLD and (c) and (d) from site F (intruded into greenschist facies rocks) from one of the northern sites on it.*

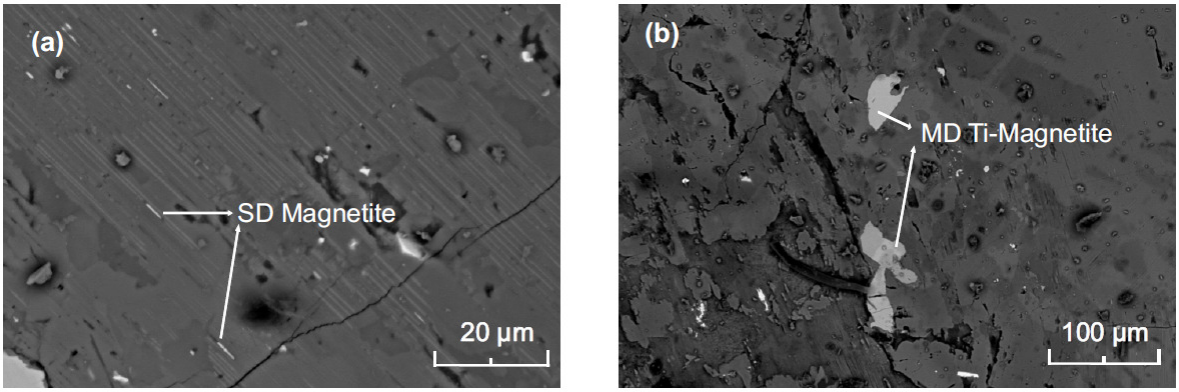

Figure 6.4. *Scanning Electron Microscope (SEM) images showing the types of magnetic minerals.*

Site C:

All the 10 specimens from this site show a good grouping of paleomagnetic vectors yielding a mean site direction as: Dm = 204°, Im = -60° (k = 190, α95 = 4°) and the corresponding VGP at: λ = 56°S; ϕ = 291°E (dp/dm = 4°/5°). Though the mean direction is slightly off from the other directions, but it is overlapping on other mean directions within error.

Site D:

Mean site vectors representing twelve specimens from this site are clustered as a group and hence are considered for calculating mean directions. The mean site direction is summarised as: Dm = 218°, Im = -66° (k = 60, α95 = 6°) and the corresponding VGP is at: λ = 43°S; ϕ = 291°E (dp/dm = 8°/9°).

Site E:

Five specimens out of eight of this site give a good grouping resulting in calculating the mean site direction as: Dm = 220°, Im = -55° (k = 58, α95 = 10°) and the corresponding VGP was found to be: λ = 48°S; ϕ = 310°E (dp/dm = 10°/14°).

Site F:

A total of 11 specimens representing 4 oriented samples were analyzed and 7 of them were showing consistency in directions and are used for calculating site mean direction. The mean site direction is: Dm = 240°, Im = -59° (k = 35, α95 = 10°) and the corresponding VGP was found to be: λ = 32°S; ϕ = 309°E (dp/dm = 11°/15°).

Site G:

All the 15 specimens representing 5 oriented samples were clustered and yield a site mean direction to be, Dm = 231°, Im = -55° (k = 83, α95 = 4°) with the corresponding VGP as: λ = 40°S; ϕ = 312°E (dp/dm = 4°/6°).

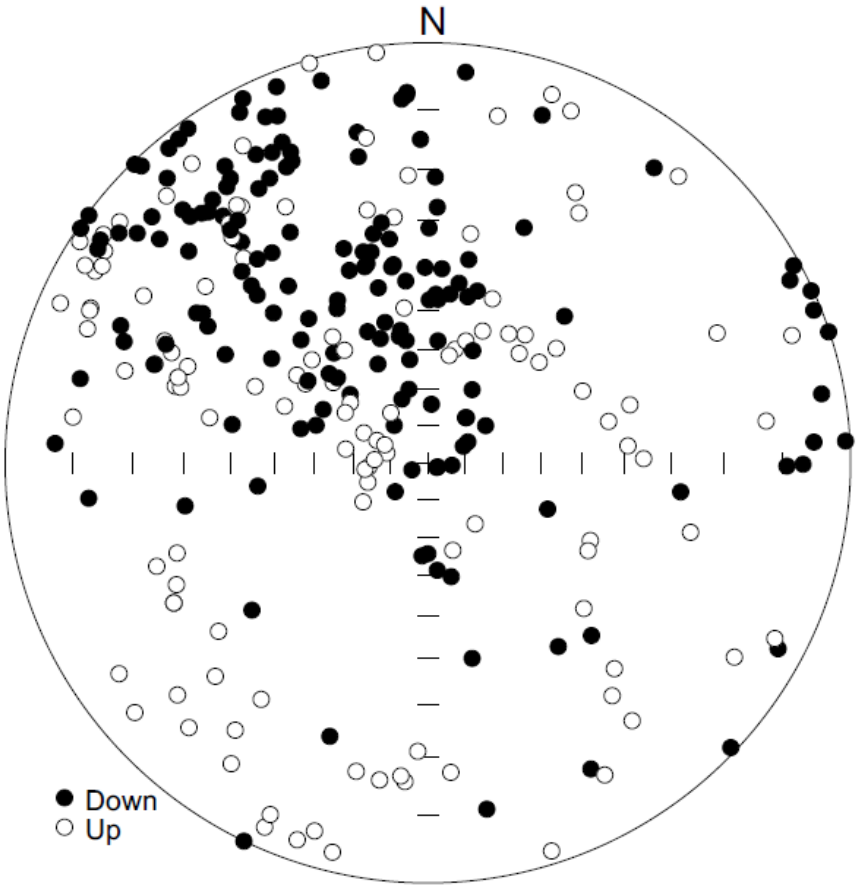

Figure 6.5. *Stereoplot showing the variation of NRM directions.*

Site H:

Nine representative core specimens analyzed were groupedafter plotting ChRM directions on stereonet. The mean site direction of these nine specimens is: Dm = 236°, Im = -63° (k = 80, α95 = 6°) and the corresponding VGP was found to be, λ = 34°S; ϕ = 303°E (dp/dm = 7°/9

Site I:

Though 10 specimens from five samples were examined in this site, only seven of them yielded a less precise but consistent paleomagnetic vector. The site mean direction from this site is, Dm = 215°, Im = -65° (k = 27, α95 = 12°) and the corresponding VGP was found to be: λ = 47°S; ϕ = 291°E (dp/dm = 16°/19°).

Site P:

Seven specimens of seven samples were analysed in this site, but out of them only four specimens yielded a mean paleomagnetic direction as: Dm = 331°, Im = 2° (k = 50, α95 = 13°) and the corresponding VGP was found to be: λ = 58°S; ϕ = 323°E (dp/dm = 7°/13°).Five specimens representing five samples from this site yielded good grouping after the ChRM plotting and the mean site direction was determined as: Dm = 248°, Im = -68° (k = 60, α95 = 10°) and the corresponding VGP was found to be: λ = 26°S; ϕ = 297°E (dp/dm = 14°/17°).

Site Q:

Seven core specimens out of eight from this site yielded consistent paleomagnetic vecor representing Dm = 326°, Im = -5° (k = 64, α95 = 8°) with a corresponding VGP at, λ = 52°S; ϕ = 322°E (dp/dm = 4°/8°).

Site R:

Eleven representative core specimens were analyzed from this site and all of them give a site mean vector as, Dm = 295°, Im = -31° (k = 41, α95 = 7°) and the corresponding VGP was found to be: λ = 18°S; ϕ = 323°E (dp/dm = 5°/9°).

Site S:

All the ten specimens from six samples were closely clustered with consistent paleomagnetic vector and the site mean direction was, Dm = 323°, Im = 6° (k = 148, α95 = 4°) and the corresponding VGP was found to be: λ = 51°S; ϕ = 332°E (dp/dm = 2°/4°).

Site T:

Five specimens representing five samples from this site yielded good grouping after the ChRM plotting and the mean site direction was determined as: Dm = 248°, Im = -68° (k = 60, α95 = 10°) and the corresponding VGP was found to be: λ = 26°S; ϕ = 297°E (dp/dm = 14°/17°).

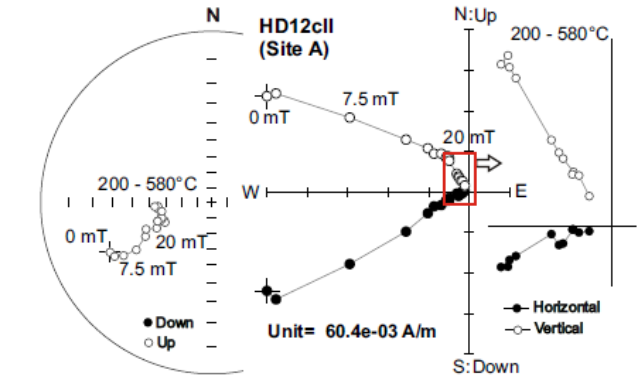
HD12cII
(Site A)
N
N:Up
S:Down
W
E
0 mT
7.5 mT
20 mT
200 - 580°C
Down
Up
Horizontal
Vertical
Unit= 60.4e-03 A/m

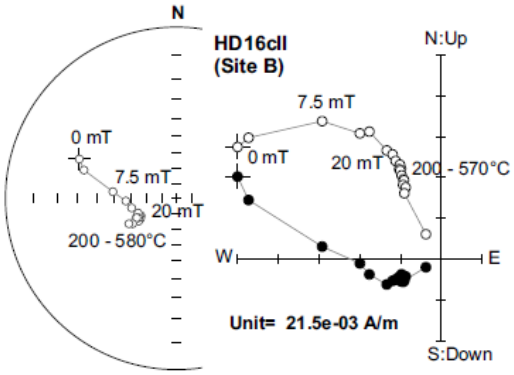
HD16cII
(Site B)
N
N:Up
S:Down
W
E
0 mT
7.5 mT
20 mT
200 - 580°C
200 - 570°C
Unit= 21.5e-03 A/m

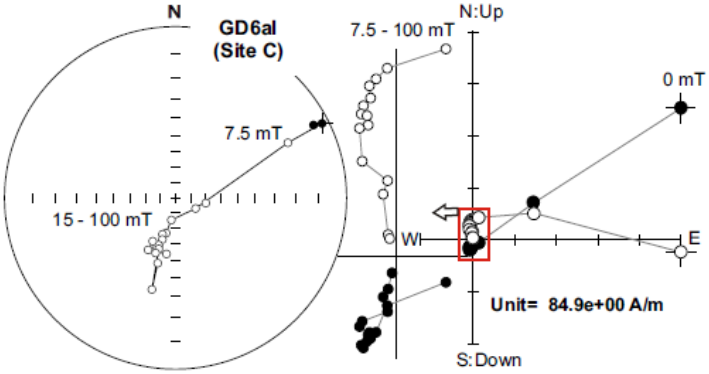
GD6aI
(Site C)
N
N:Up
S:Down
W
E
7.5 mT
7.5 - 100 mT
0 mT
15 - 100 mT
Unit= 84.9e+00 A/m

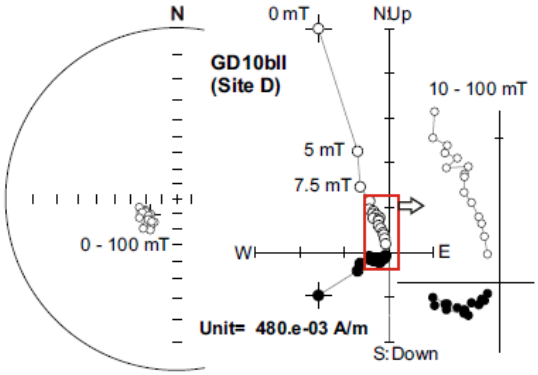
GD10bII
(Site D)
N
N:Up
S:Down
W
E
0 mT
5 mT
7.5 mT
10 - 100 mT
0 - 100 mT
Unit= 480.e-03 A/m

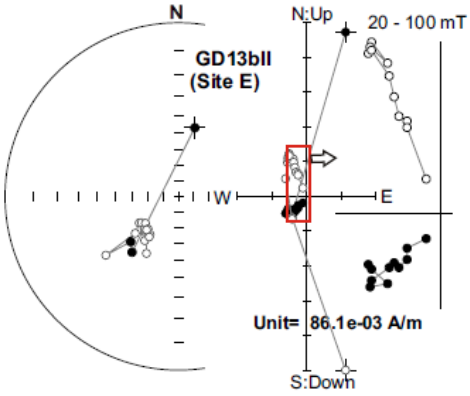
GD13bII
(Site E)
N
N:Up
S:Down
W
E
20 - 100 mT
Unit= 86.1e-03 A/m

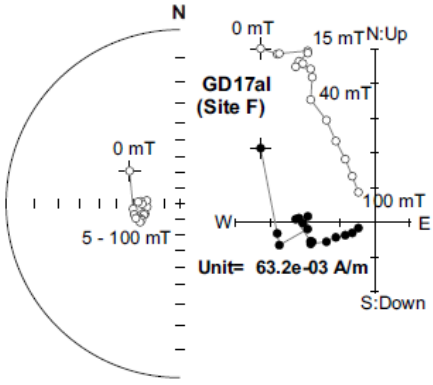
GD17aI
(Site F)
N
N:Up
S:Down
W
E
0 mT
15 mT
40 mT
100 mT
5 - 100 mT
Unit= 63.2e-03 A/m

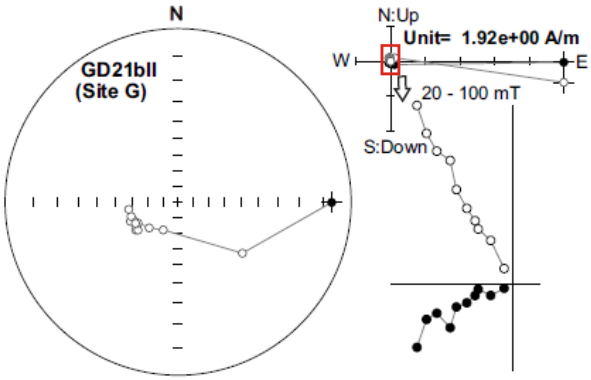
GD21bII
(Site G)
N
N:Up
S:Down
W
E
Unit= 1.92e+00 A/m
20 - 100 mT

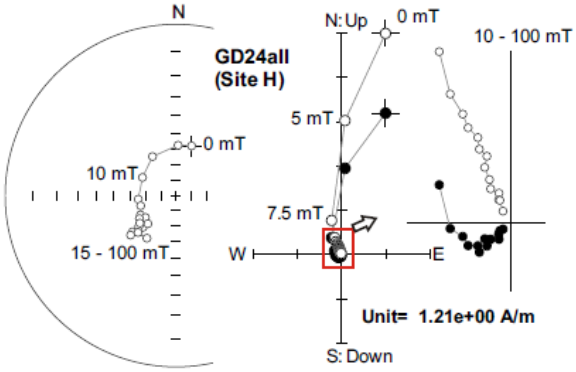
GD24aII
(Site H)
N
N:Up
S: Down
W
E
0 mT
5 mT
10 mT
7.5 mT
10 - 100 mT
15 - 100 mT
Unit= 1.21e+00 A/m

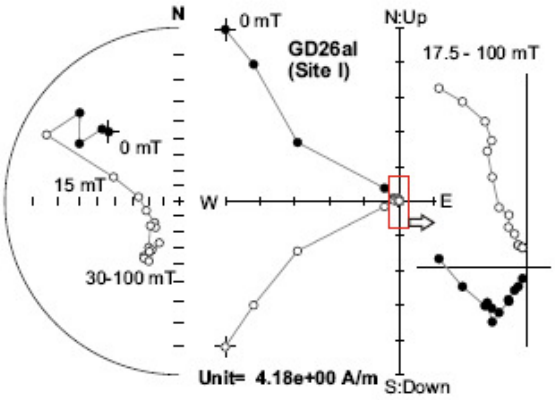
N
0 mT
N:Up
GD26al
(Site I)
17.5 - 100 mT
0 mT
15 mT
W
E
30-100 mT
Unit= 4.18e+00 A/m
S:Down

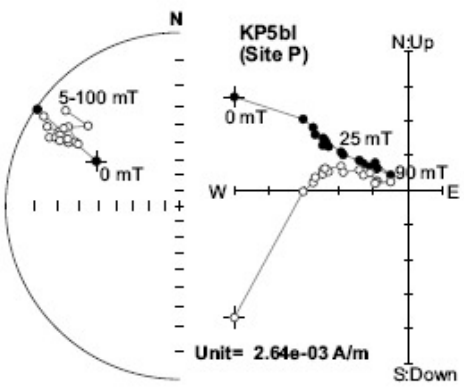
N
KP5bI
(Site P)
N:Up
5-100 mT
0 mT
25 mT
90 mT
W
E
Unit= 2.64e-03 A/m
S:Down

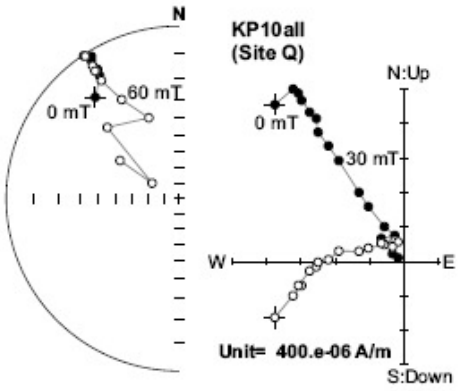
N
KP10all
(Site Q)
N:Up
60 mT
0 mT
0 mT
30 mT
W
E
Unit= 400.e-06 A/m
S:Down

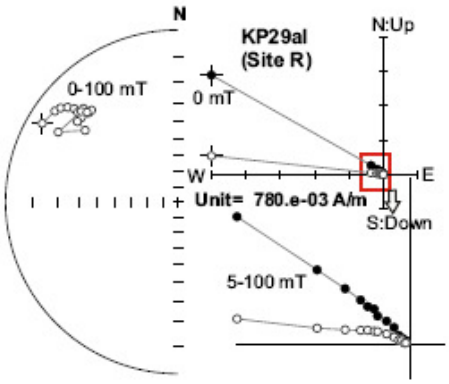
N
KP29al
(Site R)
N:Up
0-100 mT
0 mT
W
E
Unit= 780.e-03 A/m
S:Down
5-100 mT

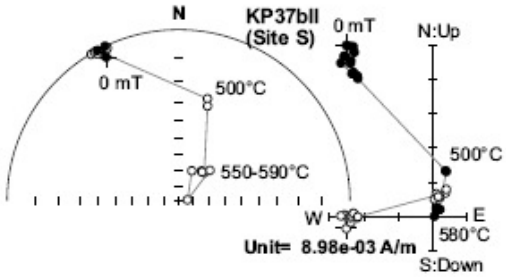
N
KP37bII
(Site S)
0 mT
N:Up
0 mT
500°C
550-590°C
500°C
W
E
580°C
Unit= 8.98e-03 A/m
S:Down

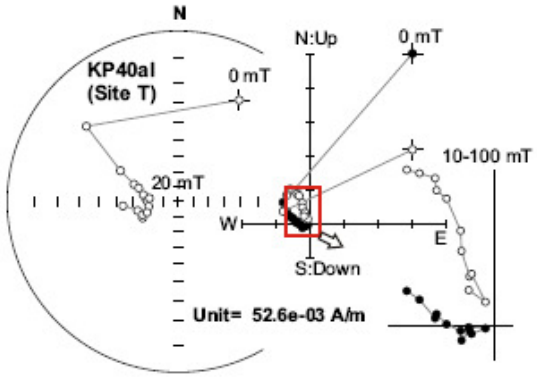
N
KP40al
(Site T)
N:Up
0 mT
0 mT
10-100 mT
20 mT
W
E
S:Down
Unit= 52.6e-03 A/m

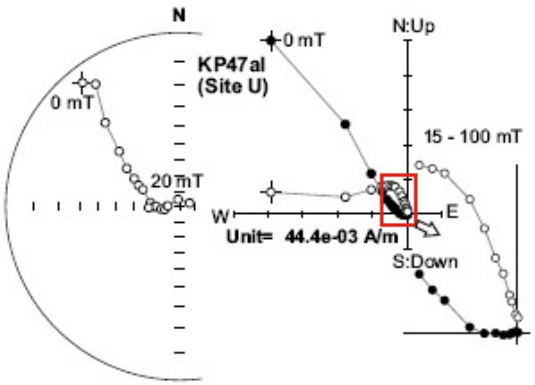
N
KP47al
(Site U)
0 mT
N:Up
0 mT
15 - 100 mT
20 mT
W
E
Unit= 44.4e-03 A/m
S:Down

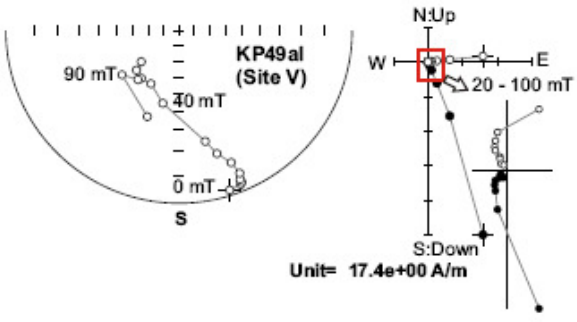
N:Up
KP49al
(Site V)
90 mT
40 mT
0 mT
W
E
20 - 100 mT
S
S:Down
Unit= 17.4e+00 A/m

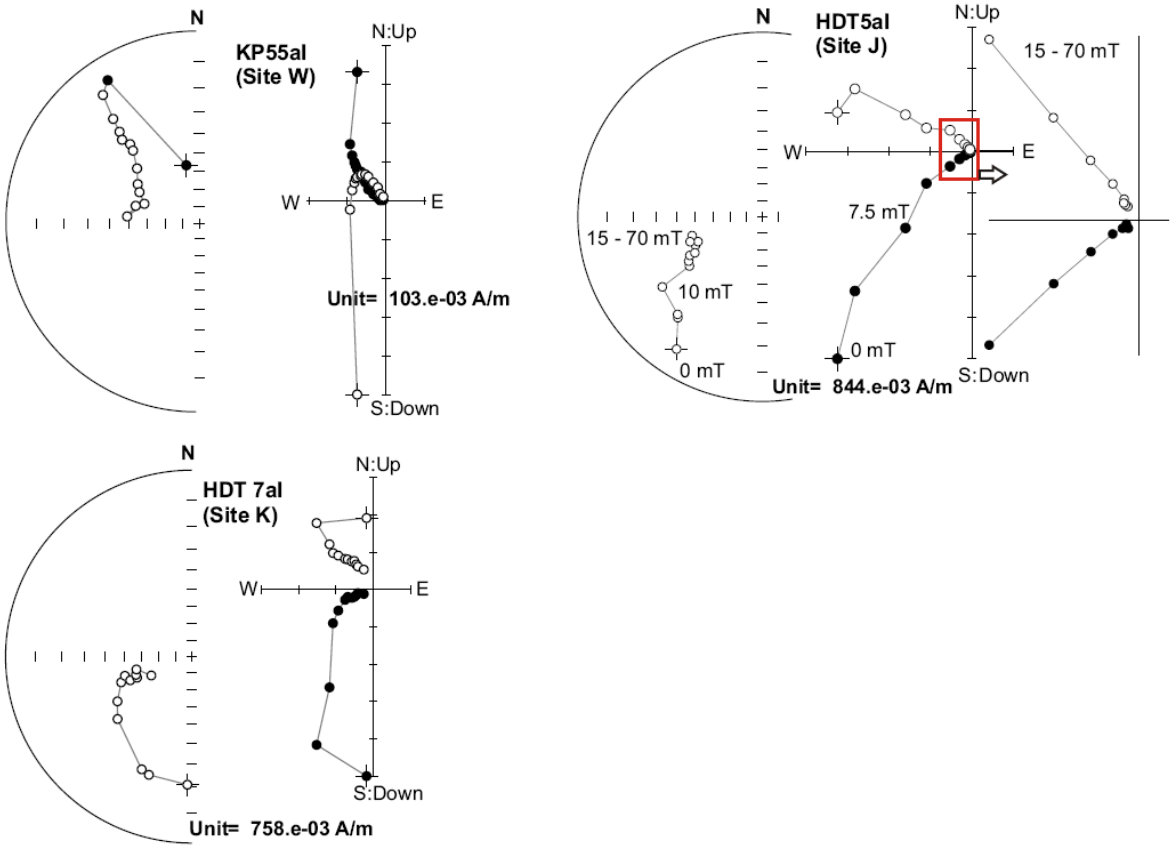

Figure 6.6. *Zijderveld diagram and equal area stereonet pairs showing the behavior of natural remanence to AF and thermal demagnetization for samples representing 2.21-2.22 Ga sites. Thermal measurements are in °C and AF measurements are in millitesla (mT). Open/closed circles in the stereoplots represent upward/downward directed vectors and open/closed circles in the Zijderveld plots represent vertical/horizontal projections. Plotted using Remasoft 3.0 plotting and analysis program (Chadima and Hrouda, 2006).*

Site U:

A total of 9 specimens representing five samples were examined and the primary mean direction was determined as: Dm = 272°, Im = -63° (k = 30, α95 = 10°) and the corresponding VGP was found to be: λ = 10°S; ϕ = 303°E (dp/dm = 12°/15°).

Site V:

Eight specimens out of ten representing six sample give the mean site direction as: Dm = 215°, Im = -53° (k = 14, α95 = 16°) and the corresponding VGP at: λ = 54°S; ϕ = 311°E (dp/dm = 15°/22°). Though the value of 'k' is less and α95 is slightly high, which

is because of scattered data points, site mean direction is in good agreement with the other site mean directions on the same dyke and hence considered for dyke grand mean calculation.

Site W:

Seven specimens from this site were analysed. Six of them were grouped at a point, whereas one specimen is slightly away from the group and was removed from the site mean direction. The mean direction is Dm = 295°, Im = -49° (k = 67, α95 = 8°) and the corresponding VGP was found to be: λ = 13°S; ϕ = 310°E (dp/dm = 7°/11°).

6.3.2. Dyke (ii):

Site J:

Six representative core specimens from six samples shows good grouping and yielded consistent direction as Dm = 238°, Im = -52° (k = 123, α95 = 6°) and the corresponding VGP was found to be: λ = 34°S; ϕ = 317°E (dp/dm = 6°/9°).

Site K:

Five representative specimens from five samples from this site are clustered as a group and the site mean direction is determined as Dm = 253°, Im = -59° (k = 504, α95 = 3°) and the corresponding VGP at: λ = 21°S; ϕ = 309°E (dp/dm = 4°/5°).

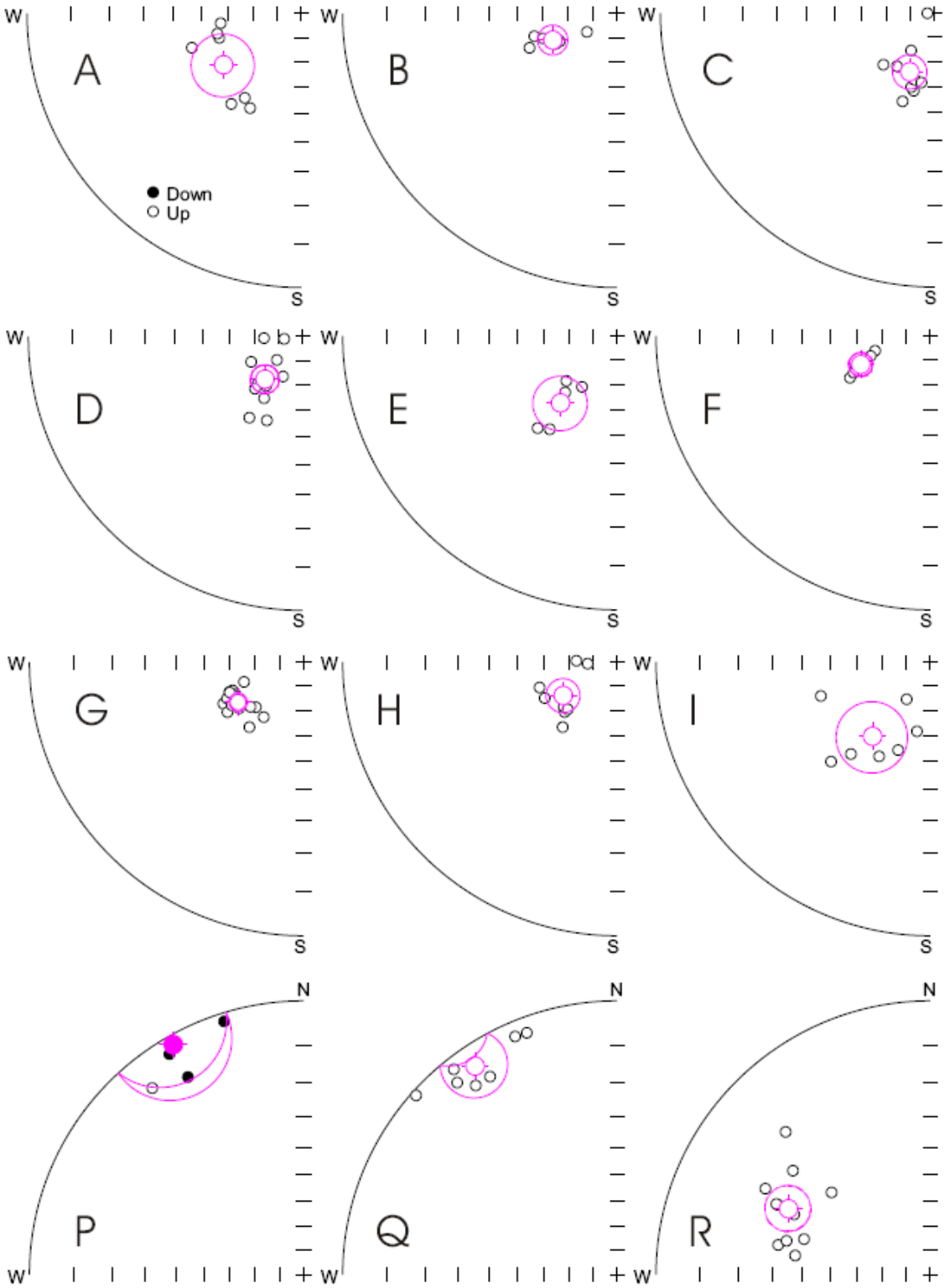
A
B
C
D
E
F
G
H
I
P
Q
R
Down
Up
W
S
N

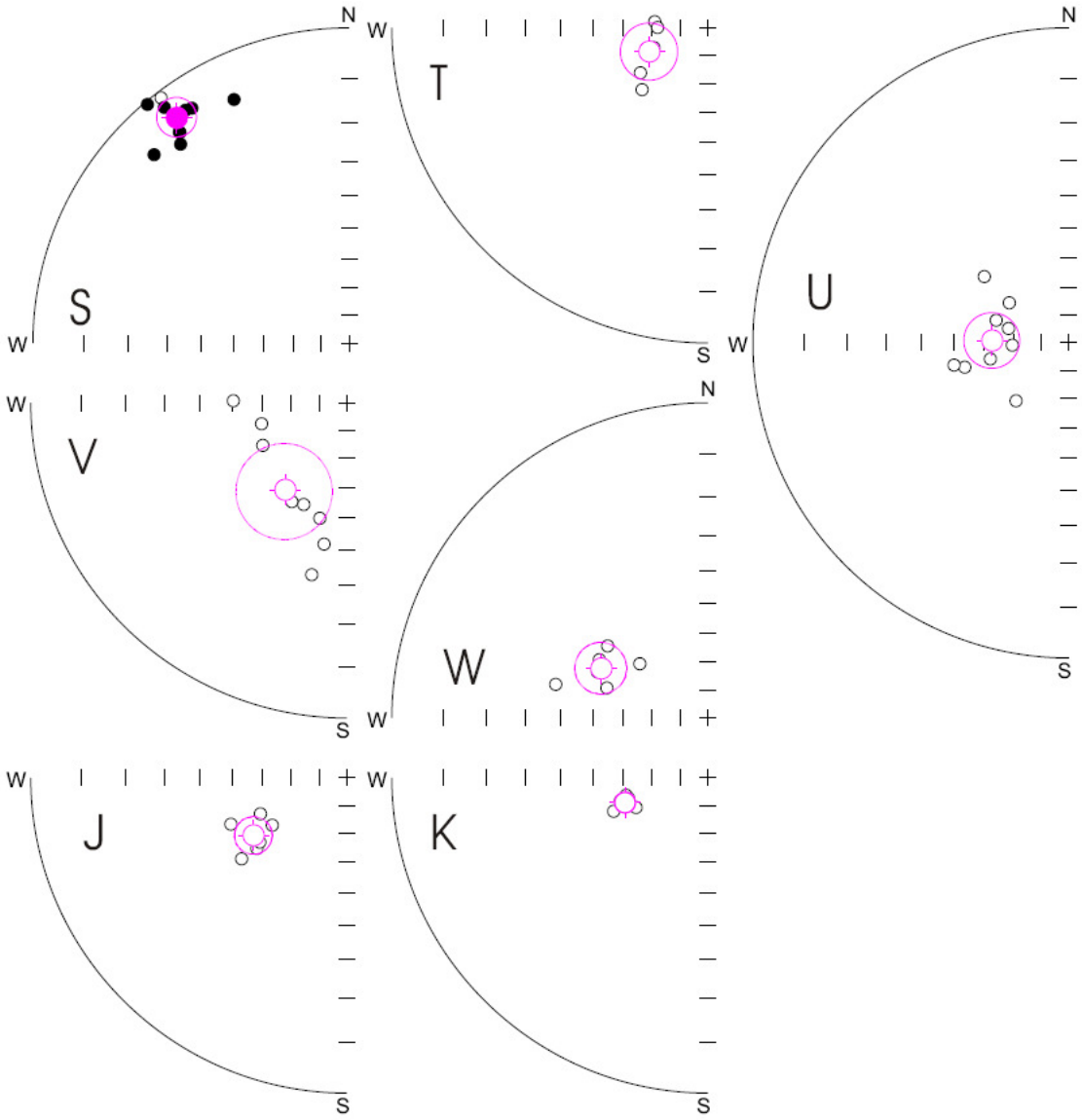

Figure 6.7. *Stereographic projections of the ChRM directions for individual sites from 2.21-2.2 Ga dyke swarm. Pink circles represents site mean direction along with 95% confidence circle.*

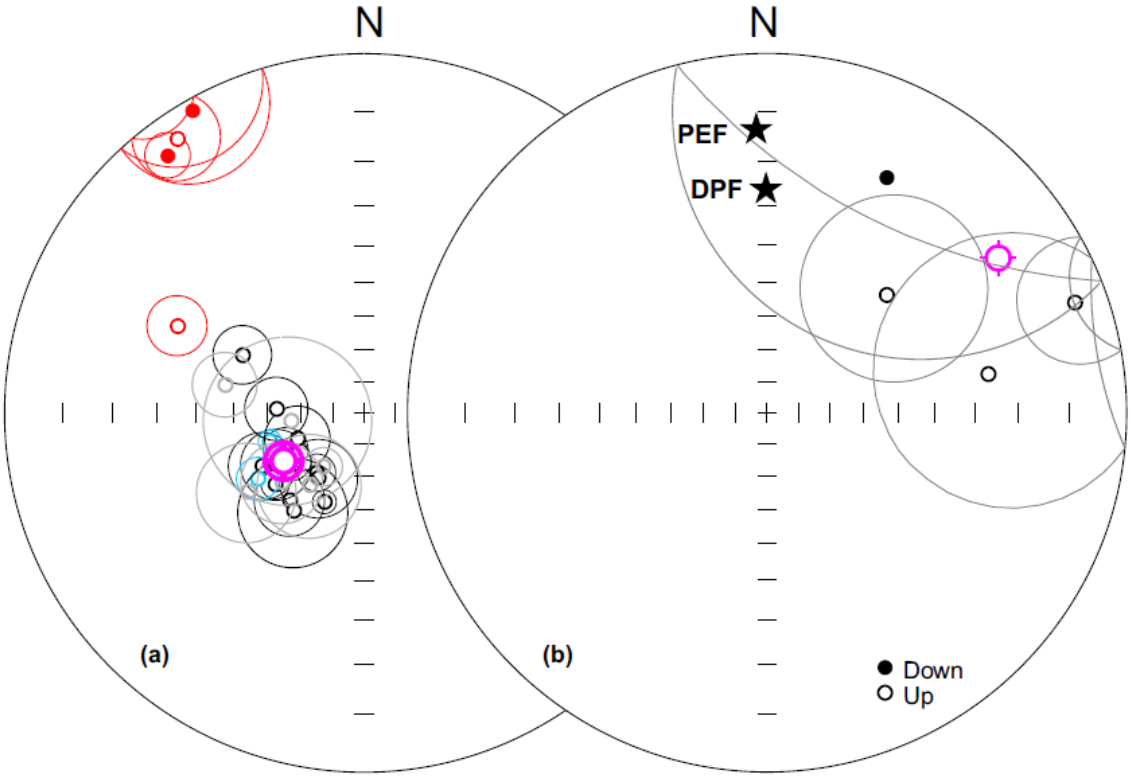

Figure 6.8. *Stereoplots showing paleomagnetic data. (a) Primary site mean directions with ovals of 95% confidence of all the AKLD, dyke ii and published sites in black and grey colours respectively. Baked sites on AKLD are shown in red colour, (b) secondary components are generally scattered in most sites, but a poorly defined component with low coercivity was recovered from sites C, F, G and H. Black stars represent DPF, Dipole field and PEF, Present Earth's field direction based on the 1995 IGRF. Pink circles represent grand means in both figures (a) and (b).*

Table-6.1. Paleomagnetic results on Dharwar dyke swarms.

Site	Lat. (°N)	Long. (°E)	S°	N	D_m	I_m	k	α_{95}	p lat. (°S)	p long. (°E)	A_{95}	Ref
Component '2.21-2.22 Ga'												
A	12.767	77.056	14	7	243	-55	39	10	30	314	12	1
B	12.851	77.069	357	6	245	-63	100	7	27	304	9	1
C	14.216	76.977	1	10	204	-60	190	4	56	291	4	1
D	14.218	76.977	359	12	218	-66	60	6	43	291	8	1
E	14.209	76.977	357	5	220	-55	58	10	48	310	12	1
F	14.204	76.977	358	7	240	-59	35	10	32	309	13	1
G	14.117	76.985	350	15	231	-55	83	4	40	312	5	1
H	14.112	76.993	343	9	236	-63	80	6	34	303	8	1
I	14.778	76.786	335	7	215	-65	27	12	47	291	17	1
J	12.974	77.353	354	6	238	-52	123	6	34	317	7	1
K	12.950	77.378	350	5	253	-59	504	3	21	309	4	1
T	15.662	76.342	350	5	248	-68	60	10	26	297	15	This study
U	15.705	76.331	338	9	272	-63	30	10	10	303	13	This study
V	15.777	76.301	358	8	215	-53	14	16	54	311	18	This study
W	15.773	76.301	350	6	295	-49	67	8	13	310	9	This study
TP	14.387	76.916	350	6	230	-57	33	12	40	310	--	2
P15	14.368	76.907	345	6	38	62	20	16	47	297	--	3
P24	13.537	77.048	345	9	236	-48	15	14	36	321	--	3
17	13.183	77.041	345	4	218	-69	243	6	40	287	--	2
20	13.061	77.037	358	8	282	-47	39	9	4	317	--	2
P6	12.498	77.234	0	5	85	67	10	25	13	299	--	3
Mean (N+R)	**--**	**--**	**--**	**21**	**240**	**-61**	**34**	**6**	**36**	**312**	**7**	
Component '~2.18 Ga'									**(°N)**	**(°E)**		
M20	17.086	78.223	89	5	24	60	42	12	58	114	15	This study
M1	17.076	78.314	102	9	26	58	36	9	59	119	11	This study
M2	17.075	78.319	102	8	10	64	29	11	61	93	15	This study
D21	16.957	79.206	82	13	35	52	28	8	55	137	9	This study
D23	16.958	79.282	98	10	34	62	56	7	51	121	4	This study
S15	16.918	79.433	98	10	30	68	43	8	49	108	11	This study
S14	16.932	79.487	93	10	28	71	26	10	46	102	16	This study
SO	13.488	78.831	135	4	358	73	50	13	45	77	--	2
MD	14.045	78.026	120	9	55	71	51	7	31	111	--	2
64	14.184	78.163	315	4	347	50	45	14	70	45	--	2
568	16.928	77.863	90	6	9	60	76	8	65	94	--	2
571	16.928	77.705	290	10	3	45	171	4	80	93	--	2
P18	14.630	77.790	315	6	51	67	21	15	36	116	--	4
P36	14.800	77.650	315	9	93	77	16	14	12	104	--	4
P61	16.710	79.240	90	5	355	58	8	30	67	69	--	4
Mean	**--**	**--**	**--**	**15**	**20**	**64**	**33**	**7**	**60**	**108**	**10**	

Table 1 contd.

Table 1 contd.

Site	**Lat. (°N)**	**Long. (°E)**	**S°**	**N**	**D_m**	**I_m**	**k**	**α_{95}**	**p lat. (°S)**	**p long. (°E)**	**A_{95}**	**Ref**
Component '2.25 Ga'												
L	16.361	77.721	357	10	261	-70	104	5	19	295	7	1
M	16.287	77.741	4	9	272	-77	111	5	14	284	9	1
N	16.266	77.720	5	7	276	-61	101	6	6	305	8	1
O	16.512	77.717	13	8	283	-72	47	8	10	281	14	1
P34	16.340	78.140	0	6	244	-60	21	15	30	230	--	4
P67	16.450	78.320	0	6	134	65	16	20	15	251	--	4
P65	16.830	79.080	315	3	313	-62	31	22	16	247	--	4
P58	16.820	79.320	0	5	224	-65	41	12	43	240	--	4
35	13.547	78.921	220	8	253	-62	127	5	22	308	--	2
Mean	**--**	**--**	**--**	**9**	**271**	**-69**	**37**	**9**	**16**	**299**	**13**	
Component '1890 Ma'												
KP 10 #	15.301	76.481	90	10	290	-29	61	6	14	326	5	This study
R	15.404	76.487	338	11	295	-31	41	7	18	323	6	This study
NW dyke	14.400	77.700	--	9	320	-34	68	13	39	309	--	5
Cuddapah Traps	14.300	78.200	--	15	299	-6	18	16	27	337	--	6
Mean	**14.851**	**77.217**	**--**	**4**	**301**	**-25**	**22**	**20**	**25**	**325**	**16**	
Other component												
P	15.292	76.529	341	4	331	2	50	13	58	323	10	This study
Q	15.303	76.521	344	7	326	-5	64	8	52	322	6	This study
S	15.456	76.452	337	10	323	6	148	4	51	332	3	This study
I20	17.047	78.723	67	18	38	-35	73	4	38	212	4	This study

Note: Lat. & Long. = latitude and longitude; S^o = is strike of the dyke at the respective sites. N is the number of specimens in each site. D_m is mean declination, $I_{m\ is}$ mean inclination, k is precision parameter, α_{95} and A_{95} are the radius of 95% confidence circle about the mean direction for site and pole respectively and p lat. and p long. are coordinates of paleopole. Angles (D_m, I_m, α_{95} and A_{95}) are in degrees. # = site dated at 1894 Ma (Halls et al., 2007). Ref: 1=Kumar et al., 2012b; 2=Balica et al., 2014; 3=Piispa et al., 2011; 4= Radhakrishna etal., 2013; 5=Kumar and Bhalla, 1983; 6=Clark 1982.

6.4 Results of 2.25 Ga swarm:

The previously reported four U-Pb ages_and present Pb-Pb age confirm the existence and wide distribution of ~2253 Ma dyke swarm in southern and northern parts of the Cuddapah basin. Though dyke (iii) is reported as a part of AKLD swarm (~2215 Ma; Kumar et al., 2012b), based on the ages of N-S dykes in this region, but now these sites are treated as a part of ~2253 Ma dyke swarm based on available precise geochronology on these dykes. Dyke (iii) includes sites L, M, N and O near to Mahabubnagar town.

The orthogonal projections (Zijderveld plots) of alternating field and (or) thermal demagnetizations on one specimen from each site location are presented in figure 6.9. The characteristic magnetization vectors from every site are also plotted in stereographic projection in figure 6.10. The site mean directions of each site are explained below and the data representing mean magnetization vectors from all sites are given in table 6.1.

Site L:

Ten specimens from six samples yielded a consistent paleomagnetic mean direction, Dm = 261°, Im = -70° (k = 104, α95 = 5°) and the corresponding VGP was found to be: λ = 19°S; ϕ = 295°E (dp/dm = 7°/8°).

Site M:

Nine specimens from a total of ten representing five samples yielded a stable characteristic paleomagnetic vector. The site mean direction is found to be Dm = 272°, Im = -77° (k = 111, α95 = 5°) and the corresponding VGP was found to be: λ = 14°S; ϕ = 284°E (dp/dm = 9°/9°).

Site N:

Seven specimens representing four samples from this site gave a characteristic magnetism. The site mean direction is calculated as, Dm = 276°, Im = -61° (k = 101, α95 = 6°) and the corresponding VGP was found to be: λ = 6°S; ϕ = 305°E (dp/dm = 7°/9°).

Site O:

A total of 8 specimens representing five samples were analyzed and the mean direction is found to be Dm = 283°, Im = -72° (k = 47, α95 = 8°) and the corresponding VGP was found to be: λ = 10°S; ϕ = 281°E (dp/dm = 14°/15°).

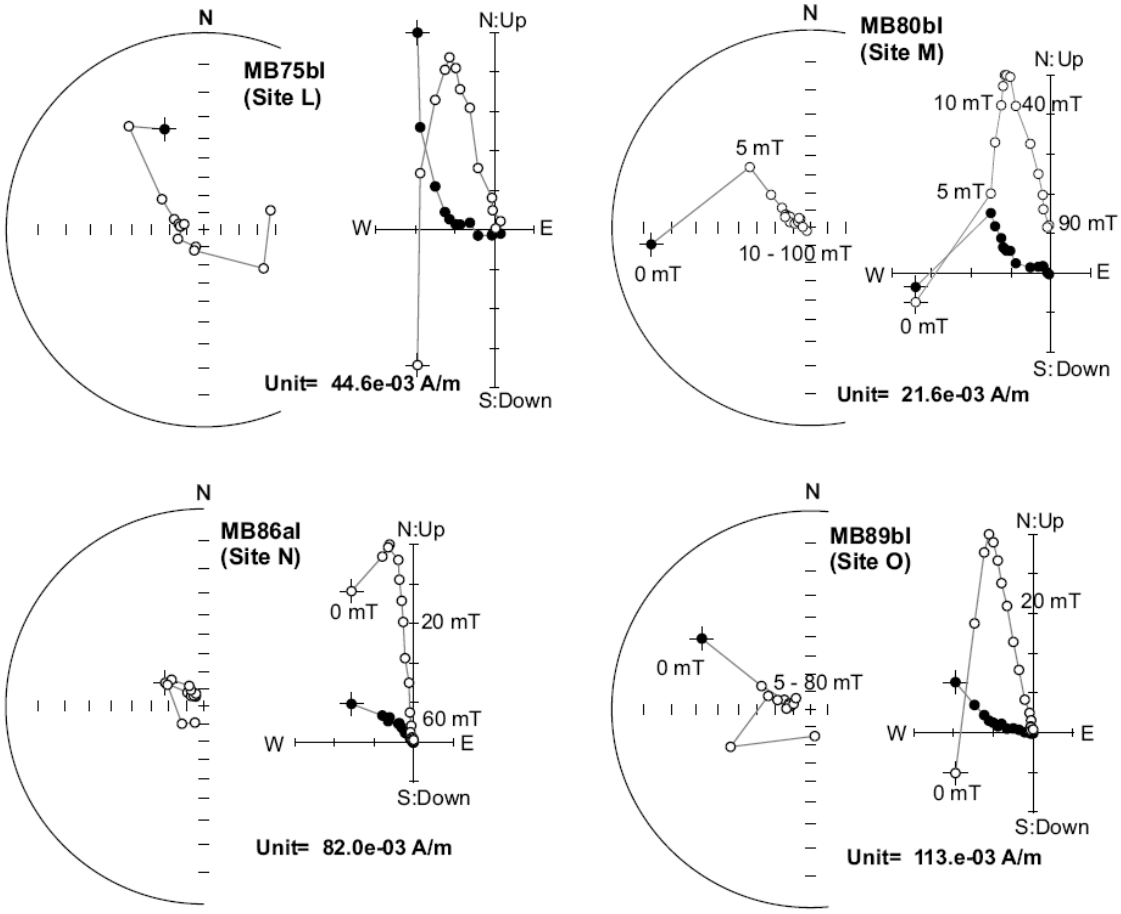

Figure 6.9. *Zijderveld diagram and equal area stereonet pairs showing the behavior of natural remanence to AF and thermal demagnetization for samples representing 2.25 Ga sites. Thermal measurements are in °C and AF measurements are in millitesla (mT). Open/closed circles in the stereoplots represent upward/downward directed vectors and open/closed circles in the Zijderveld plots represent vertical/horizontal projections. Plotted using Remasoft 3.0 plotting and analysis program (Chadima and Hrouda, 2006).*

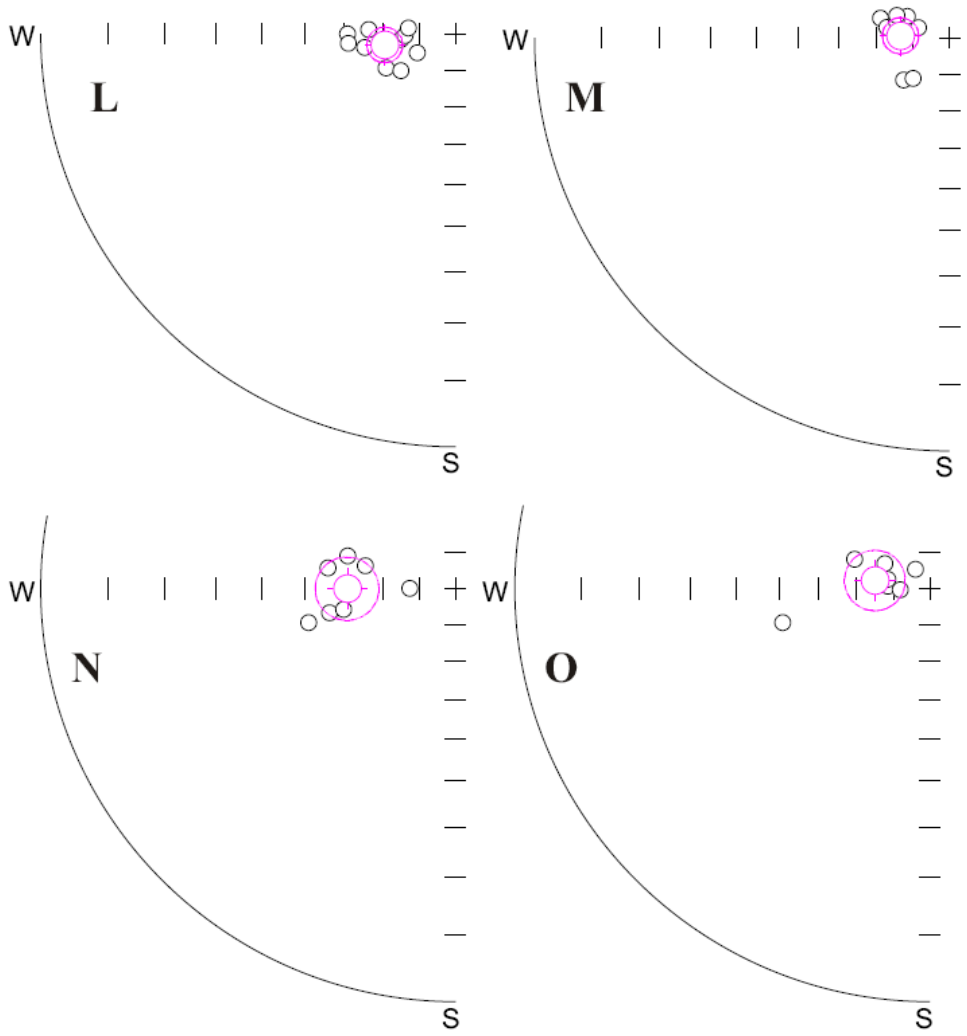

Figure 6.10. *Stereographic projections of the ChRM directions for individual sites from 2.25 Ga dyke swarm. Pink circles represent site mean direction along with 95% confidence circle.*

To better define the extent of other dyke swarms, several other sites were sampled on a slightly younger (~2180 Ma) E-W trending dyke. These sites include M20, M1, M2, D21, D23, S14, S15 and I20.

6.5. Results of E-W dyke (~2.18 Ga swarm):

Eight sites were sampled on a single slightly younger E-W trending dyke of length about 250 Km near Mahabubnagar town. The orthogonal projections (Zijderveld plots) of alternating field and (or) thermal demagnetizations on one specimen from each site location are presented in figure 6.11. The characteristic magnetization vectors from every

site are also plotted in stereographic projection in figure 6.12. The site mean directions of each site are described below and the data representing mean magnetization vectors from all sites are given in table 6.1.

Site M20:

A total of eleven specimens representing five samples yielded a consistent paleomagnetic vector. The site mean direction is determined as Dm = 30°, Im = 61° (k = 36, α95 = 8°) and the corresponding VGP at: λ = 55°N; ϕ = 118°E (dp/dm = 9°/12°).

Site M1:

Ten specimens out of 12 specimens from six samples yielded good grouping. The site mean direction is determined as Dm = 30°, Im = 59° (k = 54, α95 = 7°) and the corresponding VGP at: λ = 55°N; ϕ = 121°E (dp/dm = 10°/14°).

Site M2:

Eight representative specimens from five samples from this site are clustered as a group and the site mean direction is determined as Dm = 10°, Im = 64° (k = 29, α95 = 11°) and the corresponding VGP at: λ = 61°N; ϕ = 93°E (dp/dm = 14°/15°).

Site D21:

Thirteen specimens from this site yielded a mean direction as Dm = 35°, Im = 52° (k = 28, α95 = 8°) and the corresponding VGP at: λ = 55°N; ϕ = 137°E (dp/dm = 10°/17°). Though the directional points are scatter, mean direction is in good agreement with other site mean directions and hence considered for calculating dyke grand mean.

Site D23:

Ten specimens out of eleven representing five sample from this site yielded good grouping after the ChRM plotting and the mean site direction was determined as Dm = 34°, Im = 62° (k = 56, α95 = 7°) and the corresponding VGP at: λ = 51°N; ϕ = 121°E (dp/dm = 7°/10°).

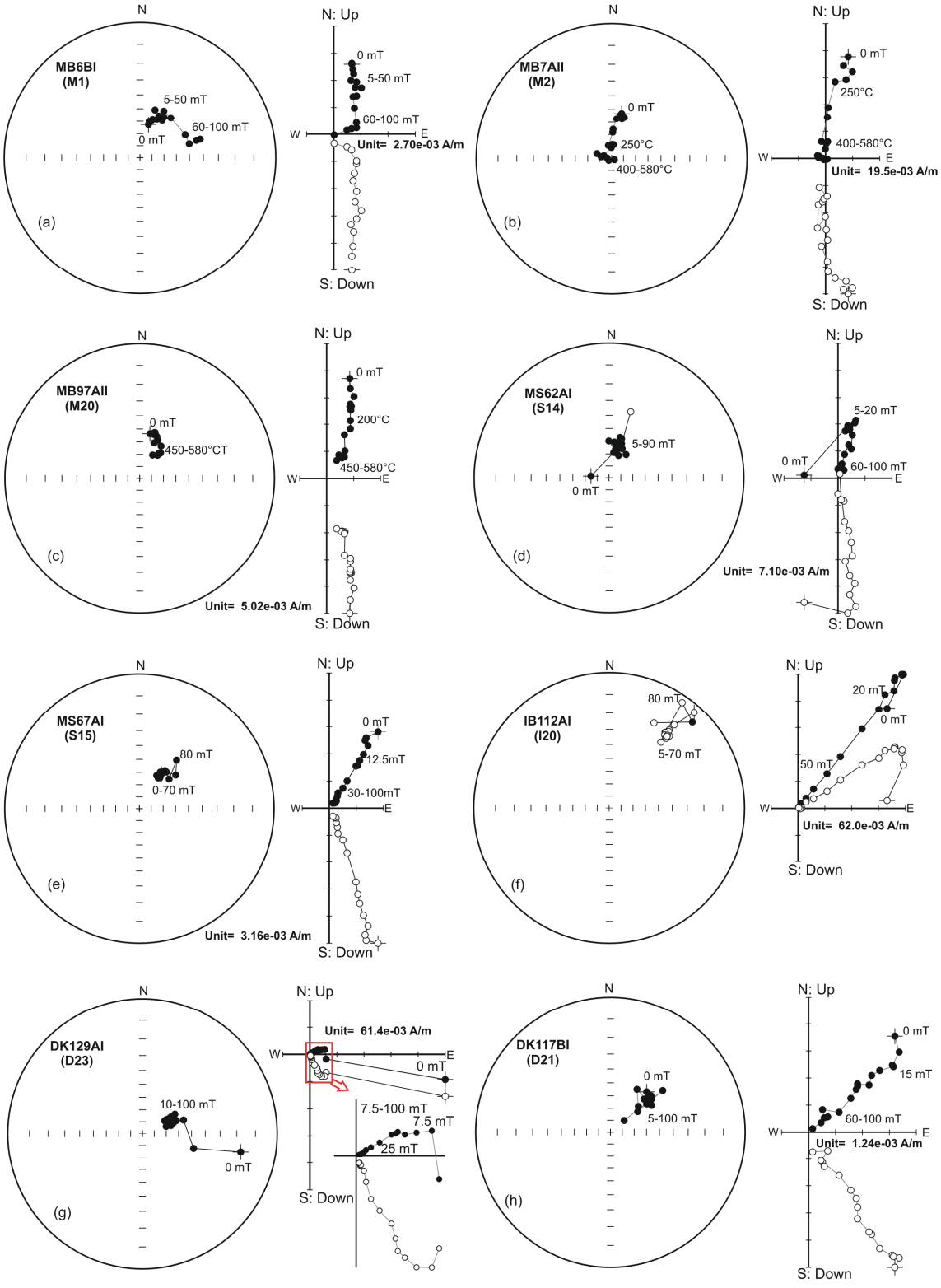

Figure 6.11. *Zijderveld diagram and equal area stereonet pairs showing the behavior of natural remanence to AF and thermal demagnetization for samples representing ~2.18 Ga sites. Thermal measurements are in °C and AF measurements are in millitesla (mT). Open/closed circles in the stereoplots represent upward/downward directed vectors and open/closed circles in the Zijderveld plots represent vertical/horizontal projections.*

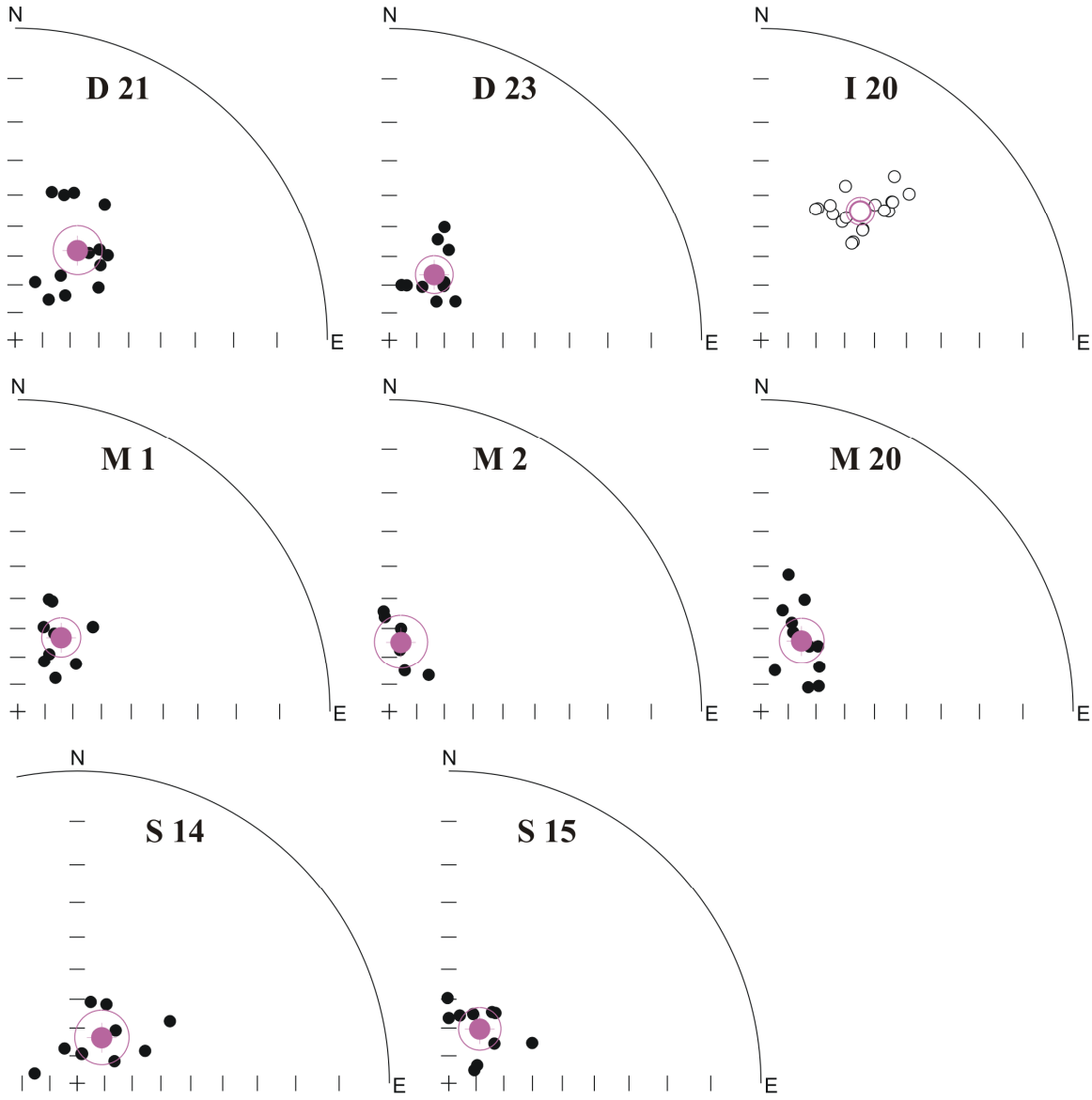

Figure 6.12. *Stereographic projections of the ChRM directions for individual sites from ~2.18 Ga dyke swarm. Pink circles represent site mean direction along with 95% confidence circle.*

Site S14:

Ten specimens representing five samples give a site mean direction as Dm = 28°, Im = 71° (k = 26, α95 = 10°) and the corresponding VGP at: λ = 46°N; ϕ = 102°E (dp/dm = 15°/17°). Though the directional points are scattered, mean direction is in good agreement with other site mean directions and hence condidered for dyke mean calculation.

Site S15:

A total of ten specimens from five samples gave the site mean direction as Dm = 30°, Im = 68° (k = 43, α95 = 8°) and the corresponding VGP at: λ = 49°N; ϕ = 108°E (dp/dm = 10°/12°).

Site I20:

Eighteen specimens representing eight oriented samples from this site yielded a paleomagnetic vector. The site mean direction is determined as Dm = 38°, Im = -35° (k = 73, α95 = 4°) and the corresponding VGP at: λ = 38°S; ϕ = 31°E (dp/dm = 3°/5°).

6.6. Summary of Paleomagnetic results:

6.6.1. 2.21-2.22 Ga dyke swarm:

NRM intensities from the AKLD samples were scattered and range from 1.38 mA/m to 265 A/m. AF and thermal demagnetization results demonstrated that practically all samples carry a minor component of secondary magnetization. This secondary component is characterised by low unblocking temperatures and coercivities. The resultant directions due to overprinting are generally scattered in most sites, but have a poorly defined low coercivity component of north-east declination and moderate negative inclination. This component was recovered from sites C, F, G and H, and was usually removed by AF demagnetization in fields of 5 to 20 mT, or by temperatures of 100°C to 300°C in thermal demagnetization. This direction is similar to the overprinted secondary magnetization recovered from the north-eastern parts (around Hyderabad region) of the older (~2367 Ma) Dharwar giant dyke swarm (Kumar et al., 2012a). The origin of this component is unclear.

The characteristics of demagnetization and direction obtained at low coercivities or low blocking temperatures demonstrate that it is often a secondary viscous remanent magnetization that was presumably produced subsequent to its formation, which is different from present day field. Here again, after having removed a soft component, a segment going through the origin during AF and thermal treatment was recovered between 20 mT and 100 mT (up to 130 mT in few cases) in AF treatment and 400°C and 580°C in thermal demagnetization. The higher coercivity (or higher blocking temperature) component defines a well-defined characteristic magnetization direction, with west to south-westerly declination and moderately steep up inclination (Fig. 6.8). The pole calculated from these directions is close to the direction of 2.37 Ga E-W trending Dharwar giant dyke swarm (Halls et. al., 2007). Hence, we consider this to be the ChRM of the dyke acquired during cooling following dyke emplacement. Isolation of ChRM at higher coercivity and complete unblocking by temperatures below 580°C suggests that the main carrier of magnetization is low-Ti titanomagnetite.

Among seventeen sites on this dyke, four sites (P, Q, R and S) recorded within site grouping with a mean declination and inclination of 321°/-6°, with a pole position of 7°S/234°E. These sites were collected near the contacts of younger E-W dykes, and record a direction that is identical to the ChRM of the younger ~1890 Ma dykes in this region. These sites provide a positive baked contact test to demonstrate the primary nature of the dominant magnetization for sites on AKLD i.e. A through I and the sites T through W.

These unbaked site directions demonstrate good within site and between site groupings. A mean direction from the unbaked thirteen sites on a single dyke has a declination of 237° and inclination of -62° (k = 33, $\alpha 95$ = 7°) and a corresponding virtual geomagnetic pole at latitude 34°S and longitude 305°E (dp = 9°, dm = 11°).

Apart from these sites on AKLD, Piispa et al., 2011 and Belica et al., 2014 reported similar directions on five more sites (sites P6, P15, P24 and TP, 17 and 20 respectively) on AKLD along with a single but significant reverse magnetic direction (Table 6.1). The reverse direction is approximately antipodal to that of normal directions

Dyke (ii) includes only two sites J and K, which are located east of AKLD and near to Bangalore. Paleomagnetic results from these sites show good within site grouping

and are very similar to those obtained from the AKLD. A site mean direction calculated from two sites on this dike gives a declination of 245° and inclination of –56° with a VGP at lat 28°S., long 313°E.

Combining data from all 21 sites including normal and reverse directions (this study and published sites) are all similar within errors despite dissimilar orientation between dykes towards the northern end of the swarm, with a grand mean of Dm = 240° and Im = -61°, corresponding to a paleopole at lat. 36°S; long. 312°E (A95=7°). To prove the primary nature of the remanence direction obtained here, along with the baked site several observations suggest that rocks in the study region have not been heated above their blocking temperature (~450-550°C), after the emplacement of these dykes. Observations supporting this view include: (i) very high coercivities and unblocking temperatures of the grains preserving the characteristic remanence, (ii) consistency of paleomagnetic data between sites despite being separated by up to 450 km, (iii) absence of metamorphic events after ~2500 Ma as evidenced by the consistency of titanite and zircon ages in the country rocks (both yielding ~2500 Ma ages) around Hutti, Kolar and Ramagiri (summarised by Anand and Balakrishnan, 2010) despite the marked difference in the blocking temperatures of titanite (600-650^{o}C) and zircon (~900^{o}C) Cherniak, (1993) and also by several ~ 2.45 Ga biotite-whole rock Rb-Sr two point isochron ages (biotite has a much lower closure temperature of ~350^{o} C) for granites and gneisses in the region. One of these biotite age determinations (2489±35 Ma) is less than 15 km from sites A and B (Krishna, 2007) and (iv) preservation of primary remanence in the older 2367 Ma dominant dyke swarm in this region, as inferred from a positive baked contact test (Halls et al., 2007; Kumar and Bhalla, 1983). Thus we are inferring that the nature of magnetization recorded by AKLD and the other N-S dykes in this swarm is primary acquired at the time of dyke emplacement.

Except for the 2367 Ma dyke swarm, the steep negative inclination magnetization direction of these dykes is not found in any other Paleoproterozoic dyke swarms in the Dharwar craton. However, a similar paleomagnetic direction as this has been reported from charnokites (Neoarchean) near Vandallore (Mondal et al., 2009) within the southern granulite province located about 30 km southwest of Chennai and more than 300 km south east of our sampling sites. This direction was interpreted as acquired at the time of uplift cooling of the charnokite rocks.

To use the paleomagnetic data obtained from 2215 Ma dyke swarm in this study for paleocontinental reconstructions, it is mandatory to ascertain if the calculated Virtual Geomagnetic Pole (VGP) has averaged out Secular Variation (SV). The calculated VGP scatter value (Cox, 1970) for the fifteen sites studied on this dyke swarm is 16.8° +2.5°/-5.1° and is similar to the observed VGP angular dispersion value of about 16° (Johnson et al., 2008 and McElhinny and McFadden, 1997) at the same latitude (Dharwar N-S dyke swarm paleolatitude of 45°S), during the last 0-5 Ma period suggesting that SV was adequately averaged out.

6.6.2. 2.25 Ga dyke swarm:

NRM intensities from these dyke samples were fairly uniform. Paleomagnetic results from these sites show good within site as well as between site groupings and are similar to those obtained from the AKLD. A mean direction from four sites on these dykes has a declination of 273° and inclination of -72° (k = 98, α95 = 9°) and a corresponding virtual geomagnetic pole at latitude 12°S and longitude 292°E (dp = 14°, dm = 16°).

Apart from these four sites, Radhakrishna et al., 2013 has also reported similar directions in four sites on four different dykes. Similar direction is also observed on one more NNE-SSW dyke (site 35) in the southern part of Cuddapah basin (Belica et al., 2014). Integrating all previously reported and present data from nine sites on different N-S dykes yields a mean magnetic direction at 16°S and 299°E (A95=13°; Fig.6.13a).

6.6.3. ~2.18 Ga dyke swarm:

Except site I20, almost all the samples belonging to this E-W dyke have shown good groupings within site as well as between sites after removal of secondary component of viscous origin. Sites on this dyke have given reverse polarity directions with positive inclination, whereas slightly older 2215 Ma dyke swarm yielded normal polarity with negative inclination. Stable ChRM directions were recovered between 20-100 mT and/or 300-580°C

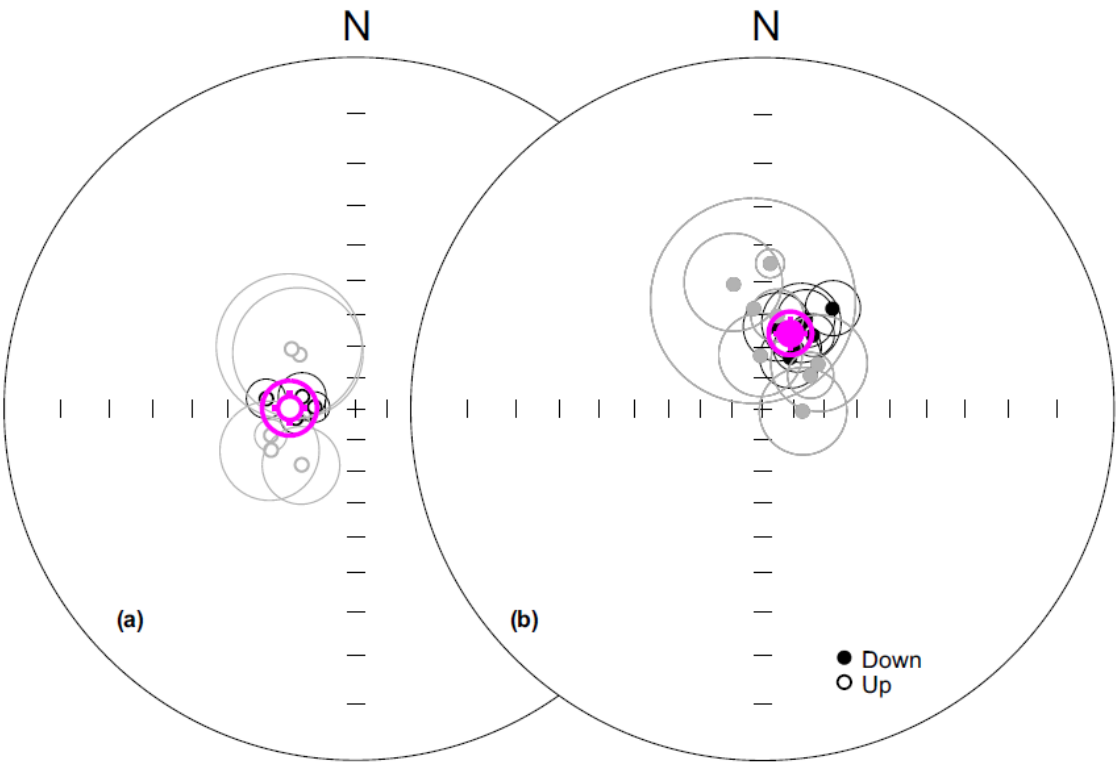

Figure 6.13. *Stereoplots showing paleomagnetic data. (a) Primary site mean directions with ovals of 95% confidence of 2.25 Ga swarm and published sites in black and grey colours respectively, (b) Primary site mean directions with ovals of 95% confidence of ~2.18 Ga swarm and published sites in black and grey colours respectively. Pink circles represent grand means in both figures (a) and (b).*

Table-6.2. Palaeomagnetic data used for Reconstruction.

Age (Ma)	S_{lat} (°N)	S_{long} (°E)	P_{lat} (°N)	P_{long} (°E)	dp	dm	Formation	Authors
2231±2	64.5	-110.3	-51	310	6	8	Malley dykes (Slave)	Buchan et al. (2012)
~2190	62.5	-99	-1	122	6	10	Tulemalu (Rae)	Fahrig et al. (1984)
2210±10	14.5	77	-32	302	8	10	AKLDykes (Dharwar)	This study
2216+8/-4	48.4	-79	15	104	4	7	Senneterre (Superior)	Buchan et al. (1993)

S_{lat} and **S_{long}** are Site Latitude (°N) and Site Longitude (°E) respectively. **P_{lat}** and **P_{long}** are Pole latitude (°N) and Pole longitude (°E) of the Virtual Geomagnetic Poles; **dp**, **dm** are the semi-axes of the oval of 95% confidence ellipse in degrees for the VGP.

Table-6.3. Euler poles used for reconstruction.

Age (Ma)	Fit	λ (°N)	Φ (°E)	ω (degree)
Dharwar to Superior:				
2210±10	Fit"S"	43.4	355.8	151.6
2210±10	Fit"N"	-26.9	193.5	27.6
Slave to Superior:				
2231±2	Fit"S"	-27.4	180.2	45.3
Rae to Superior:				
~2190	Fit"S"	-61.1	32.2	26.9

λ and Φ are the latitude and longitude of Euler poles respectively. ω is the Euler angle used for rotation. Euler angle (ω) is positive for counter-clockwise rotation and negative for clockwise rotation.

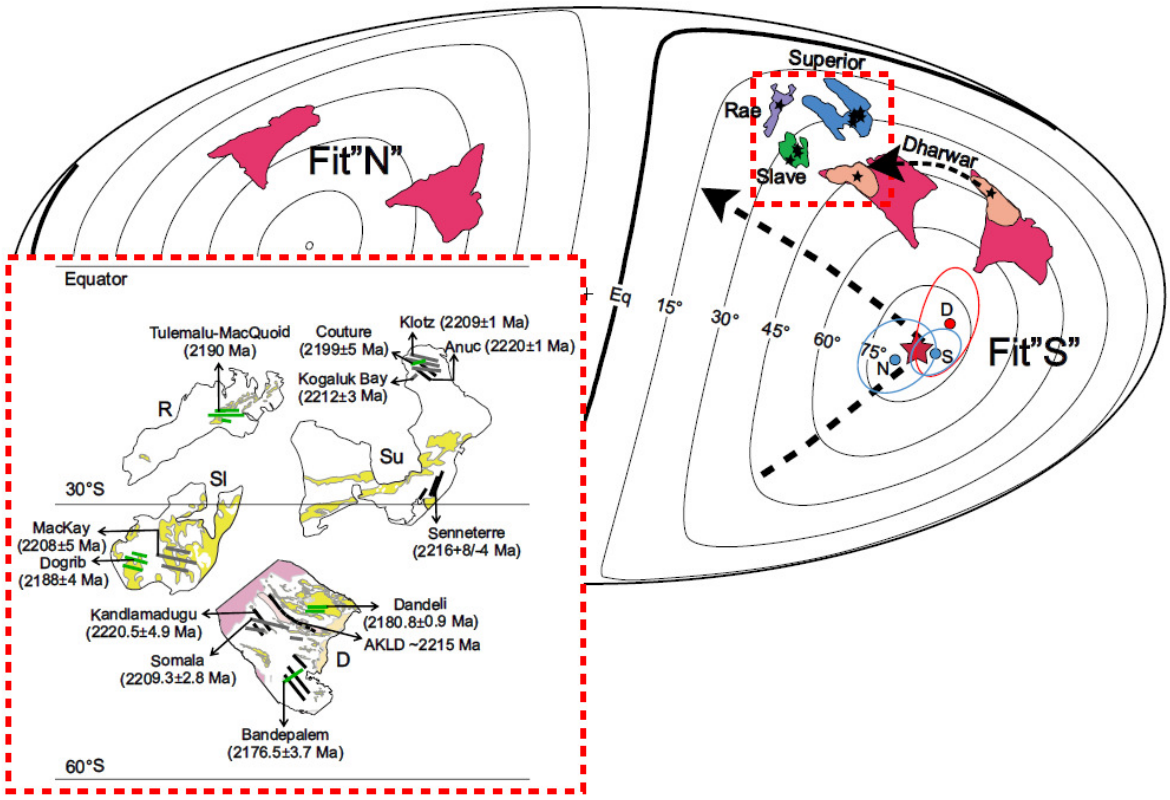

Figure 6.14. *Mollweide projection showing paleopositions of the North American cratons Superior (in blue), Slave (green), Rae (purple), and the Dharwar craton (in brown) at ~2215 Ma. This reconstruction was done with respect to Superior craton. Assuming that the field was a geocentric axial dipole, Earth's rotation axis for this reconstruction is based on the proximity of the 2215 Ma poles from Superior craton and is shown as a red star. Blue dots represent Senneterre (S), Nipissing (N; Stupavsky and Symons, 1981) and Dharwar (D) VGPs (Table 6.3). Dashed line represents the Apparent Polar Wandering Path (APWP) for the Superior craton (after Buchan et al., 2007). Thick black line in the figure represents the paleo-equator (Eq.) and thin lines are the latitude grids, spaced at 15°. Black stars: Paleomagnetic sampling sites. Figure also illustrates several alternate positions for India when rotated along its paleolatitude, both in the southern and northern hemispheres due hemispheric ambiguity. This reconstruction was done using "PaleoMac" computer program (Cogne, 2003). Inset is an enlarged view of the reconstructed cratons at ~2215 Ma to display dyke swarm orientation (shown in Galls projection using Torsvik and Smethurst, 1999, plotting program). Coeval ~2215 Ma dyke swarms are represented as gray and black thick lines and the marginally younger (~2190 Ma) swarms are shown as green lines. Outlines of Neoarchean sequences are also shown within the cratons in light green for comparison of their regional structural grain.*

Seven of the paleomagnetic sites collected on this dyke are stably magnetized in a northeasterly direction with a steep positive inclination (Table 6.1; Fig.6.13b). Evenly distributed seven sites on E-W trending dyke gives a mean direction of D=27°, I=62° (k=118, α95=6°) and a VGP at lat 12°S, long 292°E (d*p* = 14°, d*m* = 16°).

Similar reverse magnetic directions were also reported on eight other sites by Radhakrishna etal., 2013 and Belica et al., 2014 in this region. This reverse magnetic directions include five sites (sites 64, P18, P36, MD and SO) on N-W trending dykes near southwest corner of Cuddapah basin and three sites (sites 568, 571 and P61) on E-W dyke near Mahabubnagar town in this region. Integrating all these results (this study and published sites) within-site mean values of all fifteen sites yielded a overall mean paleomagnetic pole at 60°N and 108°E (A95=10°). Though site I20 is also collected on the same dyke, paleomagnetic directions are overprinted by northeast intermediate upward direction.

6.7. Global incidence of the 2215 Ma Event:

Mafic magmatism at 2210±20 Ma (only U-Pb ages are considered here) has a wide distribution and occurs in several continental regions including North America, Greenland, Europe, Africa, Australia and India. The impact of this event was most prolific in North America which includes Klotz (2209±1 Ma; Buchan et al., 1998), Senneterre dykes (2216+8/-4 Ma; Buchan et al., 1998), Nipissing sills (2217±4 Ma; Noble and Lightfoot, 1992), and a few smaller dyke swarms including Anuc (2220±1 Ma), Kogaluk bay (2212±3 Ma) and Couture (2199±5 Ma) all within the Superior province (Maurice et al., 2009). The Malley (2231±2 Ma; Buchan et al., 2012), MacKay (2208±5 Ma; LeCheminant et al., 1996), Blachford Lake Intrusion (2186±10 Ma; Wanless et al., 1979) and Dogrib dykes (2188±4 Ma; LeCheminant et al., 1997) in the Slave province and the Tulemalu- MacQuoid dyke swarm (2190 Ma; LeCheminant et al., 1997) in the Rae province are roughly the same age. Coeval events reported from the Greenland shield are the BN-1 (Isukasia) dykes (2214±10 Ma; Nutman et al., 1995), in the Fennoscandian shield, the Koli event which includes the Pera Pohja (2200 Ma; Perttunen, 1991), Lapland (2220±11 Ma; Tyrvainen, 1983) and Kuusamo intrusives (2206±9 Ma; Silvennoinen, 1991) and coeval volcanism at Cheela Springs (2209±15 Ma; Martin et al., 1998) from the Hamersly province, NW Australia. Kandlamadugu, Somala (French and Heaman,

2010) and 2215 Ma dyke swarm from the Dharwar craton when added to this long list, indicate wide spread contemporaneous mafic magmatism at ~2215 Ma that may be linked to enhanced mantle plume activity, resulting in the breakup of Archean supercontinents during this time (LeCheminant et al., 1997; Buchan et al., 1998).

6.8. Paleoreconstruction:

Though the ~2215 Ma event has a worldwide distribution as summarised above, reliable paleomagnetic data together with precise age determinations ('key poles', Buchan et al., 2000) are limited to only a few cratons. These include the Senneterre dykes of the Superior, Malley dykes from the Slave and the Tulemalu dykes from Rae cratons, besides the 2215 Ma dyke swarm from the Dharwar. Our paleoreconstructions are therefore limited to only these cratons (Table 6.2).

When plotted (Fig. 6.14, using PaleoMac plotting program of Cogné 2003) in their ancient latitudes and azimuthal orientations as originally reported (Table 6.2), Dharwar at ~2215 Ma is located at intermediate latitudes (45°) in the southern hemisphere, Superior and Rae cratons also plot in the same hemisphere but at shallower latitudes of 27° and 20° respectively. The Slave craton plots in the northern hemisphere at about 31° latitude.

There could be several possibilities of assembling these cratons, however, our approach was to plot Dharwar, Slave and Rae with respect to the Superior craton, as it has a fairly well defined Paleoproterozoic Apparent Polar Wander Path (APWP, Buchan et al., 2007). After plotting Slave in the southern hemisphere by reversing its polarity (since magnetic field could reverse), Dharwar, Slave and Rae were rotated about their respective Euler poles (Euler pole coordinates and the degree of rotation are given in Table 6.3) resulting in a reconstruction that is illustrated in Figure 6.14 (using PaleoMac, Cogné 2003).In this configuration (enlarged in Fig. 6.14), which is in sharp contrast with that proposed recently by French and Heaman (2010), the Somala and Dandeli dykes from the Dharwar, Dogrib and Mackay dykes from the Slave, Tulemalu-MacQuoid from the Rae and Klotz dykes from the Superior craton are all approximately (within 30°) parallel to each other. The AKLD and Kandlamadugu appear to be parallel to the Anuc and perpendicular to the Senneterre dyke swarms in the Superior craton. Though all these swarms were emplaced within a short time span, a critical evaluation of not only the

swarm geometry but also their geochemical characteristics is essential for establishing inter swarm correlation across cratons to infer their tectonic setting.

Regarding the ancestry of the four cratons in this assembly, based on the degree of geological similarity, Superior was inferred to be part of the Superia supercraton, but that of the Rae craton was unknown (Bleeker, 2003; Mueller et al., 2005). Dharwar and Slave cratons were believed to be the progeny of the Supercraton Sclavia (that existed between 2.6 and 2.2 Ga; Bleeker, 2003) as they were characterised by strikingly similar Archean histories with several corelatable features, including coeval large scale granite emplacement (granite bloom) at ca. 2.60–2.58 Ga, which marked the end of cratonization in these granite–greenstone terrains. In our reconstruction at ~2.21 Ga, though Dharwar, Slave, Superior and Rae are shown to be juxtaposed, with common mafic dyke events at ~ 2.21 and 2.18 Ga (French and Heaman, 2010), the conspicuous absence of the 2.367 Ga Dharwar giant dyke swarm (Kumar et al., 2012a) in the other three cratons and with their Neoarchean structural grain being nearly perpendicular to each other, suggests this assembly may not be valid during the Paleoproterozoic-Neoarchean times. In which case, neither Superia nor Sclavia could have been an ancestral supercraton for the Dharwar. The only other craton known to be located at steep latitudes (~50°S) during the Paleoproterozoic time is the Yilgarn, as inferred from the ~2400 Ma Widgiemooltha dyke swarm paleomagnetic data (Evans, 1968; Smirnov and Evans, 2006; Nemchin and Pidgeon, 1998, Doehler and Heaman 1998). Based on this evidence a common supercraton ancestry for both Dharwar and Yilgarn cratons was proposed (Halls et al., 2007). The inferred Archean supercraton 'Ur' could be a likely candidate (Rogers and Santosh, 2003).

6.9. Apparent polar wander path

The available Paleoproterozoic paleomagnetic data for the Dharwar craton reported by recent studies were recalculated to obtain Virtual Geomagnetic pole (VGP) positions corresponding to normal polarity (Table 6.4). The VGPs obtained from precisely dated rocks for the Paleoproterozoic period form six clusters (i.e. 2.36-2.37 Ga, 2.25 Ga, 2.21-2.22 Ga, ~2.18 Ga, ~2.08 Ga and ~1.89 Ga). Based on the above well defined clusters of pole positions, an updated APWP for Dharwar craton during Paleoproterozoic time is reconstructed (Figure 6.15).

Paleomagnetic results from this study help refine the APWP for the Dharwar craton during the Paleoproterozoic from about 2.37 Ga to ~1.88 Ga. To test the supercontinent hypothesis, lengths and shapes of APWPs are compared with other continents using the pairs of well dated paleomagnetic poles and coeval magmatic events. Except Superior and Kaapaval cratons, APWP of any other craton is not matching with the Dharwar craton in shape. But on comparing the length/drift rates and latitudinal positions of two cratons, they are distinctly different. APWP of Dharwar craton suggests that relatively rapid drift occurred between 2215 Ma and 2180 Ma time period at which change in magnetic polarity is observed.

Table 6.4: Paleomagnetic data of the dykes reported from Dharwar craton used to reconstruct an updated APWP for Paleoproterozoic period.

Rock unit	**Age in Ma**	**Dec**	**Inc**	**Pole Lat.** (°N)	**Pole Long.** (°E)	**Ref**
Giant radiating dyke swarm (2.36-2.37 Ga)	2365±1.5	99	-79.4	14	56	Halls et al., 2007, Kumar et al., 2012a
2.25 Ga dyke swarm	2253.2±1.4	271	-69	16	119	Present study
AKLD swarm (2.21-2.22 Ga)	2215.9±0.3	240	-61	36	132	Kumar et al., 2012b & Present study
~2.18 Ga Mahabubnagar dyke swarm	ca. 2180	20	64	60	108	Present study
~2.08 Ga radiating dyke swarm	2081.8±1.1	51	1	38	180	Kumar et al., 2015
~1.88 Ga swarm	1885.4±3.1	129.1	4.2	37	336	French et al., 2008, Belica et al., 2014

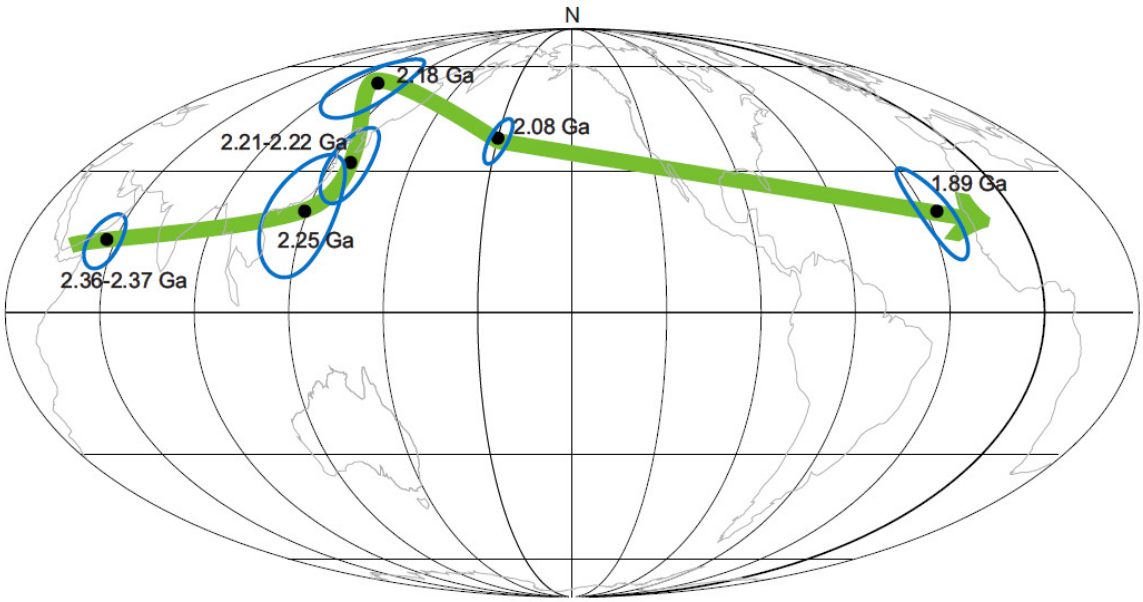

Figure 6.15. *Refined Apparent polar wander path (APWP) drawn for Paleoproterozoic period for Dharwar craton. Details of reference poles are given in table 6.4.*

6.10. Summary:

Rock magnetic studies from this study reveal that the remanent magnetization in these dykes is of primary origin and carried by a single domain (SD) magnetite located within silicate minerals pyroxene and plagioclase. The overall mean paleomagnetic directions obtained for different dyke swarms is as follows. (a) 2.21-2.22 Ga AKLD swarm yielded a paleomagnetic pole position at Plat=36°S, Plong=312°E (A_{95}=8°) (b) ~2.18 Ga dyke swarm yielded a mean pole at 60°N and 108°E (A_{95}=10°) (c) 2.25 Ga N-S dyke swarm yields a mean magnetic direction at 16°S and 299°E (A95=14°).

The paleopoles obtained from precisely dated rocks/formations for Paleoproterozoic period form six clusters. Paleopoles of these clusters include 14°N/56°E, 2.36-2.37 Ga; 16°N/119°E, 2.25 Ga; 36°N/132°E, 2.21-2.22 Ga; 60°N/108°E, ~2.18 Ga; 38°N/180°E, ~2.08 Ga; 37°N/336°E, ~1.89 Ga. Based on the well defined clusters of pole positions, APWP for Dharwar craton during Paleoproterozoic time is refined. The APWP for the Dharwar craton, India for the Paleoproterozoic period resembles the segment of APWP obtained for the superior craton and Kaapaval craton.

Paleoproterozoic pole from the Dharwar at 2.21-2.22 Ga has coeval poles from the Slave, Superior and Rae provinces and allows a Paleoproterozoic reconstruction of these cratons. Our reconstruction at ~2215 Ma shows that all these cratons could have been located within about 30° of each other, with Slave and Dharwar being remarkably closer (<10°). However, lack of reliable Neoarchean paleomagnetic data from the Dharwar inhibits tracing its ancestry to either of the Neoarchean Supercratons: Sclavia or Superia.

Chapter 7: Conclusions

7.1. Introduction:

The present work on Dharwar dolerite dykes constitutes a comprehensive integrated multidisciplinary study encompassing geochronology, paleomagnetism and petrology. The study is significant, as no other comparable data are available on the Paleoproterozoic magmatic suites in Indian shield. The study helped in drawing the following conclusions.

1. Procedure presented in this study completely avoids the need for sample dissolution and isotope dilution required for conventional U-Pb dating technique and hence the requirement of an ultra-clean laboratory. The main limitation to precision is fractionation uncertainty, which is estimated to be about ± 0.05% at 2 sigma.

2. Geochronological results using this method demonstrate that TE-TIMS on baddeleyite can easily furnish $^{207}Pb/^{206}Pb$ ages (~ 0.1%) that are as accurate and precise as can be achieved by conventional methods.

3. Though all N-S dykes of Eastern Dharwar craton appear to be part of a single dyke swarm in google satellite images, the baddeleyite Pb-Pb geochronological study of N-S dykes yielded 2 distinct ages i.e. 2253.2 ± 1.4 Ma and 2215.9 ± 0.3 Ma. In addition to this, 2081.8 ± 0.7 Ma and 2081.1 ± 0.7 Ma are also found for N-S dykes which are a part of radiating dyke swarm skirting the Cuddapah basin (Kumar et al., 2015). The three different age groups on N-S dykes established in this study along with recently published work, refutes the popular assumption that all N-S dykes of Dharwar craton are a part of single dyke swarm event.

4. The present geochronological study together with the earlier reported geochronological information indicates at least three different episodes of magmatism occurred between 2.36 Ga and 2.1 Ga causing intrusion of dykes of different generations in the Dharwar craton.

5. Present ages combined with recent studies in Dharwar Craton of India identify six discrete mafic magmatic events. These include (i) the NE-SW to E-W trending 2.6-2.37 Ga Dharwar giant dyke swarm (ii) N-S to NNW-SSE trending 2.25 Ga N-S dyke swarm (iii) N-S to NNW-SSE trending 2.21 Ga AKLD swarm (iv) NW-SE to WNW-ESE trending ~2.18 Ga Mahabubnagar swarm (v) newly identified radiating ~2.08 Ga Devarakonda swarm and (vi) 1.88-1.89 Ga Cuddapah swarm along with mafic sills of Cuddapah basin.

6. The paleomagnetic data of Dharwar dykes are complex because of overprinting. However, detailed stepwise alternating field (AF) and thermal demagnetizations have successfully delineated the primary characteristic remanent magnetism of studied dykes. Most samples revealed two or three natural remanent magnetization components. For majority of the dikes, the characteristic remanent magnetization (ChRM) was isolated within a narrow temperature range above 550^{o}C, or in the high-coercivity part of AF demagnetization spectra. The mean ChRM directions were found to be different for each of the studied swarms. Three new well dated poles from Dharwar craton include (a) a 2.25 Ga paleomagnetic pole of P_{lat} = 16°S and P_{long} = 299°E (A_{95}=14°); (b) a 2.21-2.22 Ga pole of P_{lat} = 36°S and P_{long} = 312°E (A_{95}=8°) and (c) a ~2.18 Ga pole of P_{lat} = 60°N and P_{long} = 108°E (A_{95}=10°).

7. Occurrence of the ~2215 Ma event in the Dharwar and in at least six other cratons suggests it has a truly global distribution, which could indicate large scale mantle perturbation and re-organization of the mantle convection regime during this time, which could have resulted in the breakup of Archean supercratons.

8. Of the several possible Paleoreconstructions at ~2215 Ma, one shows that the four cratons Dharwar, Slave, Superior and Rae could have been juxtaposed at intermediate to shallow latitudes (20 to 45°) at this time. However, lack of reliable Neoarchean paleomagnetic data from the Dharwar inhibits tracing its ancestry to either of the Neoarchean Supercratons: Sclavia or Superia.

9. Based on the above well defined clusters of pole positions, an updated APWP for Dharwar craton during Paleoproterozoic time is reconstructed. APWP of Dharwar

craton suggesting that relatively rapid drift occurred in the interval between 2215 Ma and 2180 Ma at which change in magnetic polarity is observed.

10. The APWP for the Dharwar craton, India for the period of 2.36 Ga – 1.88 Ga resembles the segment of APWP (2.44 Ga – 1.88 Ga) obtained for the Superior craton (North America) and Kaapaval craton (South Africa) indicating that Dharwar craton, Superior craton and Kaapaval craton might have maintained the same relative positions during Paleoproterozoic period.

References

Allen, P. A., Homewood, P., Williams, G. D., 1986. Foreland basins: an introduction. In: Foreland Basins (eds: Allen, P. A. and Homewood, P.). Spec. Publ. Ass. Sedimental. 8, 3-12.

Anand, R., Balakrishnan, S., 2010. Pb, Sr and Nd isotope systematics of metavolcanic rocks of the Hutti greenstone belt, Eastern Dharwar craton: constraints on age, duration of volcanism and evolution of mantle sources during Late Archean. Journal of Asian Earth Sciences 39, 1–11.

Baer, G., 1995. Fracture propagation and magma flow in segmented dykes: field evidences and fabric analyses, Makhtesh Ramon, Israel, in Physics and Chemistry of Dykes, pp. 125–140, edited by G. Baer and A. Heimann, Balkema, Rotterdam, Neth.

Balakrishnan, S., Hanson, G.N., Rajamani, V., 1990. Pb and Nd isotope constrains on the origin of high-Mg and tholeiitic amphibolites, kolar schist belt, South India. Contrib. Mineral. Petrol. 107, 279–292.

Balakrishnan, S., Rajamani, V., Hanson, G.N. 1999. U-Pb ages for zircon and titanite from the Ramagiri area, Southern India: evidence for accretionary origin of the eastern Dharwar craton during the late Archean. J. Geol. 107, 69–86.

Bayanova, T.B., 2006. Baddeleyite: A promising geochronometer for alkaline and basic magmatism. Petrologiya 14, 203-216.

Belica, M.E., Piispa, E.J., Meer, J.E., Pesonen, L.J., Plado, J., Pandit, M.K., Kamenov, G.D., Celestino, M., 2014. Paleoproterozoic mafic dyke swarms from the Dharwar Craton; paleomagnetic poles for India from 2.37 to 1.88 Ga and rethinking the Columbia supercontinent. Precamb. Res. 244, 100-122.

Bhandari, A., Pant, N.C., Bhowmik, S.K., Goswami, S., 2010. ~1.6 Ga ultrahightem-perature granulite metamorphism in the Central Indian Tectonic Zone: insightsfrom metamorphic reaction history, geothermobarometry and monazite chem-ical ages. Geological J. 45, 1–19.

Bhaskar Rao, Y.J., Pantulu, G.V.C., Damodara Reddy, V., Gopalan, V., 1995. Time ofearly sedimentation and volcanismin the Proterozoic Cuddapah Basin, SouthIndia: evidence from the Rb–Sr age of Pulivendla mafic sill. In: Devaraju, T.C.(Ed.), Mafic Dyke Swarms of Peninsular India, Mem. Geol. Soc. India, no. 33, pp.329–338.

Bhattacharyya, T., Pal, D. K., Mandal, C., Velayutham, M., 2000. Organic carbon stock in Indian soils and their geographical distribution. Current Science, 79(5), 655-660.

Bleeker, W., 2003. The late Archean record: a puzzle in ca. 35 pieces. Lithos 71, 99-134.

Bryan, S. E., Ernst, R. E., 2008. Revised definition of Large Igneous Provinces (LIPs). Earth Sci. Rev., 86, 175-202.

Buchan, K.L., Goutier, J., Hamilton, M.A., Ernst, R.E., Matthews, W., 2007. Paleomagnetism, U-Pb geochronology and geochemistry of Lac Esprit and other dyke

swarms, James Bay area, Quebec, and implications for palaeoproterozoic deformation of the superior province. Canada. Can. J. Earth Sci. 44(5), 643-664.

Buchan, K.L., LeCheminant, A.N., Breemen, O., 2012. Malley diabase dykes of the slave craton, Canadian Shield: U-Pb age, paleomagnetism, and implications for continental reconstructions in the early Paleoproterozoic. Can. J., Earth Sci. 49, 435-454.

Buchan, K.L., Mertanen, S., Park, R.G., Pesonen, L.J., Elming, S.A., Abrahamsen, N., Bylund, G., 2000. Comparing the drift of Laurentia and Baltica in the Proterozoic: the importance of key Palaeomagnetic poles. Tectonophys. 319, 167-198.

Buchan, K.L., Mortensen, J.K., Card, K.D., Percival, J.A., 1998. Palaeomagnetism and U-Pb geochronology of diabase dyke swarms of Minto block, Superior Province, Quebec, Canada. Can. J. Earth Sci. 35, 1054-1069.

Butler, R.F., 1992. Paleomagnetism: Magnetic Domains to Geologic Terranes. Blackwell Scientific, Boston, p. 319.

Cameron, A.E., Smith, D.E., Walker, R.L., 1969. Mass spectrometry of nanogram size samples of lead. Analytical Chemistry. 41, 525-526.

Chadima, M., Hrouda, F., 2006. Remasoft 3.0 user-friendly data browser and analyzer. Travaux Geophys. XXVII, 20-21.

Chadwick, B., Vasudev, V.N., Hegde, G.V., 1997. The Dharwar craton, southern India, and its Late Archean plate tectonic setting: current interpretations and controversies. Ind. Acad. Sci. (Earth and Planet. Sci.) Proc. 106 (4), 1-10.

Chadwick, B., Vasudev, V.N., Hegde, G.V., 2000. The Dharwar craton, southern India, interpreted as the result of late Archean oblique convergence. Precamb. Res. 99, 91–111.

Chadwick, B., Vasudev, V.N., Krishna Rao, B., Hegde, G.V., 1992. The Dharwar Supergroup: basin development and implications for late Archean tectonic setting in western Karnataka, Southern India. In: Glover, J.E., Ho, S.E. (Eds.), The Archean: Terrains, Processes and Metallogeny. Univ. West. Aus. Publ. 22,.3-15.

Chapman, H.J., Roddick, J.C., 1994. Kinetics of Pb release during the zircon evaporation technique. Earth and Planetary Science Letters. 121, 601-611.

Chardon, D., Jayananda, M., 2008. Three-dimensional field perspective on deformation, flow, and growth of the lower continental crust (Dharwar Craton, India). Tectonics 27, TC1014. http://dx.doi.org/10.1029/2007TC002120.

Chardon, D., Jayananda, M., Chetty, T.R.K., Peucat, J.J., 2008. Precambrian continental strain and shear zone patterns: the South Indian case. J. Geophys. Res. 113, B08402.

Cherniak, D.J., 1993. Lead diffusion in the titanite and preliminary effects of radiation damage on Pb transport. Chem. Geol. 110, 177-194.

Cherniak, D.J., Watson E. B., 2003. Diffusion in Zircon. in: Hanchar, J. M., Hoskin P.W.O.,Zircon (Eds.), Reviews in Mineralogy and Geochemistry. 53, 113-143.

Chukhonin, A.P., 1978. A mass spectrometric study of the forms taken by lead in zircon. Geochemistry International. 15, 186-189.

Cisowski, S., 1981. Interacting vs. non-interacting single domain behavior in natural and synthetic samples. Phys. Earth Planet. Int. 26, 56–62.

Clark, D.A., 1982. Preliminary paleomagnetic results from the Cuddapah traps of Andhra Pradesh. In: Monograph-2, on Evolution of the intracratonic Cuddapah Basin. HPG, Hyde, India, pp. 47–51.

Cogne, J.P., 2003. Paleo Mac: A Macintosh™ application for treating paleomagnetic data and making plate reconstructions. Geochem. Geophys. Geosystems 4, 1007, doi:10.1029/2001GC000227.

Cox, A.V., 1970. Latitude dependence of the angular dispersion of the geomagnetic field. Geophys. J.R. Astron. Soc., 20: 253-269.

Dankers, P., 1981. Relationship between medium destructive field and remanent coercive forces for dispersed natural magnetite. Geophys. J. Roy. Astron. Soc. 64, 447–461.

Davis, D.W., 2008. Sub-million-year age resolution of Precambrian igneous events by thermal extraction -thermal ionization mass spectrometer Pb dating of zircon: Application to crystallization of the Sudbury impact melt sheet. Geology. 36, 383-386.

Day, R., 1977. TRM and its variation with grain size, J. Geomagn. Geoelectr., 29, 233–265.

Demirer, K., (Dissertations in Geology at Lund University, Master's thesis) 2012.U–Pb Baddeleyite Ages from Mafic Dyke Swarms in Dharwar Craton, India –Links to an Ancient Supercontinent, 308 pp.

Doehler, J.S., Heaman, L.M., 1998. 2.41 Ga baddeleyite ages for two gabbroic dykes from the Widgiemooltha swarm, western Australia: a Yilgarn-Lewisian connection?, Geol. Soc. America Abstracts with Programs, 30(7), A291-292.

Doucelance, R., Manhes, G., 2001. Re-evaluation of precise lead isotope measurements by thermal ionization mass spectrometry: Comparison with determinations by plasma source mass spectrometry. Chemical Geology. 176, 361–377.

Dunlop, D.J., 1983. Determination of domain structure in igneous rocks by alternating field and other methods. Earth and Planetary Interiors 26, 1–26.

Dunlop, D.J, Ozdemir, O., 1997. Rock Magnetism. Cambridge University Press, p. 576.

Drury, S.A., 1984. A Proterozoic intra-cratonic basin, dykeswarms and thermal evolution in South Indian. Geol. Soc. India Jour. 25, 437-449.

Drury, S.A., Holt, R.W., 1980. The tectonic framework of the South Indian craton: a reconnaissance involving LANDSAT imagery. Tectonophys., 65, 1-15.

Ernst, R.E., Srivastava, R.K., 2008. India's place in the Proterozoic world constraints from the Large Igneous Province (L.I.P) record In: Indian Dyke Geochemistry Geophysics and Geochronology, Srivastava, R.K., Sivaji, C., Chalapathi Rao, N.V. (eds). Narosa Publishing House Pvt Ltd: New Delhi; 413–445.

Evans, M.E., 1968. Magnetization of dikes: a study of the paleomagnetism of theWidgiemooltha dike suite, Western Australia. J. Geophys. Res. 73, 32361-33270.

Fisher, R.A., 1953. Dispersion on a sphere. Proc. Roy. Soc. London, Ser. A, 217, 295–305.

French, J.E., 2007. U–Pb Dating of Paleoproterozoic mafic dyke swarms of the South Indian shield: implications for paleocontinental reconstructions and identifying ancient mantle plume events. Ph.D. Thesis. University of Alberta, Edmonton, Alberta, 373 pp.

French, J.E., Heaman, L.M., 2010. U-Pb dating of Paleoproterozoic mafic dyke swarms of the south Indian Shield: Implications for paleocontinental reconstructions and identifying ancient mantle plume events. Precamb. Res.183, 416-441.

French, J.E., Heaman, L.M., Chacko, T., Rivard, B., 2004. Global mafic magmatism andcontinental breakup at 2.2 Ga: evidence from the Dharwar craton, India. Geol.Soc Am. Abstracts Program 36 (5), 340.

French, J.E., Heaman, L.M., Chacko, T., Srivastava, R.K., 2008. 1891-1883 a southernBastar craton-Cuddapah mafic igneous events, India: a newly recognized largeigneous province. Precambrian Res. 160, 308–322.

Friend, C.R.L., Nutman, A.P., 1991. SHRIMP U–Pb Geochronology of the Closepet Granite and Peninsular Gneiss, Karnataka, South India. Journal of the Geological Society of India 38, 357–368.

Gallagher, K., Hawkesworth, C.J., 1992. Dehydration melting and generation of continental flood basalt. Nature, 358: 57-59.

Gentry, R.V., Sworski, T.J., Mckown H.S., Smith D.H., Eby, R.E., Christie, W.H., 1982. Differential lead retention in zircons: Implications for nuclear waste containment. Science. 216, 296-298.

Gerstenberger, H., Haase, G., 1997. A highly effective emitter substance for mass spectrometric Pb isotope ratio determinations. Chemical Geology. 136, 309-312.

Goldberg, A.S., 2010. Dyke swarms as indicators of major extensional events in the 1.9–1.2 Ga Columbia supercontinent. Journal of Geodynamics 50, 176–190.

Grew, E.S., Manton, W.I., 1984. Age of allanite from Kabbaldurga Quarry, Karnataka. J. Geol. Soc. India, 25, 193--195.

Gupta, S., Rai, S.S., Prakasam, K.S., Srinagesh, D., Bansal, B.K., Chadha, R.K., Priestly, K., Gaur, V.K., 2003. The nature of the crust in the southern India: implications for Precambrian crustal evolution. Geophys. Res. Lett. 30 (8), 1419 (doi:10.1029/2002GL016770).

Habfast, K., 1998. Fractionation correction and multiple collectors in thermal ionization isotope ratio mass spectrometry. International Journal of Mass Spectrometry. 176, 133–148. doi: 10.1016/S1387–3806(98)14030–7.

Halls, H.C., 1982. The importance and potential of mafic dyke swarms in studies ofgeodynamic process. Geosci. Canada 9, 145–154.

Halls, H.C., Kumar, A., Srinivasan, R., Hamilton, M.A., 2007. Paleomagnetism and U–Pb geochronology of easterly trending dykes in the Dharwar craton, India: feldspar clouding, radiating dyke swarms and the position of India at 2.37 Ga. Precamb. Res. 155, 47–68.

Harris, N.B.W., Jayaram, S., 1982. Metamorphism of cordierite gneisses from the Bangalore region of the Indian Archaean. Lithos 15, 89– 98.

Heaman, L.M., 2009. The application of U-Pb geochronology to mafic, ultramafic and alkaline rocks: An evaluation of three mineral standards. Chemical Geology. 261, 43-52.

Heaman, L.M., LeCheminant, A.N., 1993. Paragenesis and U-Pb systematics of baddeleyite (ZrO2). Chemical Geology. 110, 95-126.

Heaman, L.M., LeCheminant, A.N., 2000. Anomalous U-Pb systematics in mantle-derived baddeleyite xenocrysts from Ile Bizard: evidence for high temperature radon diffusion?. Chemical Geology. 172, 77-93.

Heaman, L.M., Tarney, J., 1989. U-Pb baddeleyite ages for the Scourie dyke swarm, Scotland: evidence for two distinct intrusion events. Nature. 340, 705-708.

Hijab, B.R., 1982. Paleomagnetic studies of Jurrasic sediments. University of Newcastle upon Tyne.

Hou, G., Santosh, M., Qian, X., Lister, G.S., Li, J., 2008. Configuration of the Late Paleoproterozoic supercontinent Columbia: insights from radiating mafic dykeswarms. Gondwana Research 14, 395–409.

Huyskens, M.H., Iizuka, T., Amelin, Y., 2012. Evaluation of colloidal silica gels for lead isotopic measurements using thermal ionisation mass spectrometry. Journal of Analytical Atomic Spectrometry. 27, 1439-1446.

Jaffey, A.H., Flynn, K.F., Glendenin, L.E., Bentley, W.C., Essling, A.M., 1971. Precision measurements of half lives and specific activities of ^{235}U and ^{238}U. Physical Review. 4, 1889-1906.

Jayananda, M., Chardon, D., Peucat, J.J., Capdevila, R., 2006. 2.61 Ga potassic granites and crustal reworking in the western Dharwar craton, southern India: tectonic, geochronologic and geochemical constraints. Precambrian Research 150, 1–26.

Jayananda, M., Mahabaleshwar, B., 1991. Relationship between shear zones and igneous activity: the Closepet granite of southern india. Ind. Acad. Sci. (Earth and Planet. Sci.) Proc. 100, 31-36.

Jayananda, M., Martin, H., Peucat, J.-J., Mahabaleswar, B., 1995. Late Archean crust–mantle interactions: geochemistry of LREE-enriched mantle derived magmas. Example of the Closepet batholith, southern India. Contributions to Mineralogy and Petrology 119, 314–329.

Jayananda, M., Moyen, J.F., Martin, H., Peucat, J.-J., Auvray, B., Mahabaleswar, B., 2000. Late Archean (2500–2520 Ma) juvenile magmatism in the Eastern Dharwar craton, southern India: constraints from geochronology, Nd–Sr isotopes and whole rock geochemistry. Precambrian Research 99, 225–254.

Johnson, C.L., Constable, C.G., Tauxe, L., Barendregt, R., Brown, L.L., Coe, R.S., Layer, P., Mejia, V., Opdyke, N.D., Singer, B.S., Staudigel, H., Stone, D.B., 2008. Recent investigations of the 0-5 Ma geomagnetic field recorded by lava flows. Geochem. Geophys. Geosystems 9, doi: 10.1029/2007GC001696.

Kazmi, S.M.K., Kumar, C.G., 1991. Regional geochemical surveys in Kadiri schists belt, Anantapur and Chittoor districts, A.P. Records of Geological Survey of India 124 (Pt 5), 30–31.

Kirschvink, J.L., 1980. The least-squares line and plane and the analysis of palaeomagnetic data. Geophys. J. Roy. Astronom. Soc., 62, 699–718.

Kober, B., 1986. Whole-grain evaporation for $^{207}Pb/^{206}Pb$ age investigations on single zircons using a double-filament thermal ion source. Contributions to Mineralogy and Petrology. 93, 482-490.

Kober, B., 1987. Single-grain evaporation combined with Pb+ emitter bedding for $^{207}Pb/^{206}Pb$ age investigations using thermal ion mass spectrometry, and implications to zirconology. Contributions to Mineralogy and Petrology. 96, 63-71.

Kosztolanyi, C., 1965. Nouvelle methode d'analyse isotopique des zircons a l'etat naturel apres attaque directe sur le filament. Compt. Rend. Acad. Sci. 261, 5849-5851.

Kovacheva, M., 1980. Summarized results of the archaeomagnetic investigation of the geomagnetic field variation for the last 8000 yr in south-eastern Europe. Geophys. J.R. Astron. Soc., 61, 57–64.

Krishna, K.V.S.S., 2007. Rb-Sr age and tectonic significance of major Proterozoic shear zones in the Dharwar Craton. PhD thesis. Osmania University, Hyderabad, 213p.

Kumar, A., Bhalla, M.S., 1983. Paleomagnetics and igneous activity of the area adjoining the southwestern margin of the Cuddapah basin, India. Geophys. J. Royal Astron. Soc., 73, 27-37.

Kumar, A., Bhaskar Rao, Y.J., Padma Kumari, Dayal, A.M., Gopalan, K., 1988. Late Cretaceous mafic dykes in the Dharwar craton. Proc. Indian Acad. Sci. (Earth Planet. Sci.) 97, 107-114.

Kumar, A., Heaman, L.M., Manikyamba, C., 2007. Mesoproterozoic kimberlites in South India: a possible link to 1 Ga global magmatism. Precambrian Research 154, 192–204.

Kumar, A., Pande, K., Venkatesan, T.R., Bhaskar Rao, Y.J., 2001. The Karnataka Late Cretaceous dykes as products of the Marion hotspot at the Madagascar-India break up event: evidence from ^{40}Ar-^{39}Ar geochronology and geochemistry. Geophys. Res. Lett. 28, 2715-2718.

Kumar, A., Nagaraju, E., Besse, J., Bhasker Rao, Y.J., 2012b. New age, geochemical and paleomagnetic data on a 2.21 Ga dyke swarm from south India: Constraints on Paleoproterozoic reconstruction. Precam. Res. 220, 123-138.

Kumar, A., Nagaraju, E., Srinivasa Sarma, D., Davis, D.W., 2014. Precise Pb baddeleyite geochronology by the thermal extraction-thermal ionization mass spectrometry method. Chem. Geol. 372, 72-79.

Kumar, A., Hamilton, M.A., Halls, H., 2012a. A Paleoproterozoic giant radiating dyke swarm in the Dharwar Craton, southern India. Geochem. Geophys. Geosyst., 13, doi: 10. 1029/2011GC003926.

Kumar, A., Parashuramulu, V., Nagaraju, E., 2015. A 2082 Ma radiating dyke swarm in the Eastern Dharwar Craton, southern India and its implications to Cuddapah basin formation. Precam. Res. 266, 490-505.

LeCheminant, A.N., Buchan, K.L., Breemen, O., Heaman, L.M., 1997. Palaeoproterozoic continental break-up and reassembly: Evidence from 2.19 Ga diabase dyke swarms in the Slave and Western Churchill Provinces, Canada. Geol. Assoc. Can./ Mineral. Assoc. Can., Abstract Volume 22, p. A86.

LeCheminant, A.N., Heaman, L.M., van Breemen, O., Ernst, R.E., Baragar, W.R.A., Buchan, K.L., 1996. Mafic magmatism, mantle roots and kimberlites in the slave craton. In: Searching for diamonds in Canada, (LeCheminant, A.N., Richardson, D.G., Dilabio, R.N.W. and Richardson, K.A. eds.) Geol. Surv. Can., Open File 3228, 161-168.

Li, Q.L., Li, X.H., Liu, Y., Tang, G.Q., Yang, J.H., Zhu, W.G., 2010. Precise U-Pb and Pb-Pb dating of Phanerozoic baddeleyite by SIMS with oxygen flooding technique. Journal of Analytical Atomic Spectrometry. 25, 1107-1113.

Li, X. H., Su, L., Chung, S. L., Li, Z. X., Liu, Y., Song, B., Liu, D. Y., 2005. Formation of the Jinchuan ultramafic intrusion and the world's third largest Ni-Cu sulfide deposit: Associated with the 825 Ma south China mantle plume?. Geochemistry Geophysics and Geosystems. 6, Q11004, doi:10.1029/ 2005GC001006.

Lowrie, W., 1990. Identification of ferromagnetic minerals in a rock by coercivity and unblocking temperature properties. Geophys. Res. Lett., 17, 159–162.

Lowrie, W., Fuller, M., 1971. On the alternating field demagnetization characteristics of multidomain thermoremanent magnetization in magnetite, J. Geophys. Res., 76, 6339–6349.

Ludwig, K.R., 2003. User's manual for Isoplot 3.00 a geochronological toolkit for Excel: Berkeley Geochronological Center Special Publication 4, 71 p.

Manikyamba, C., Kerrich, R., Khanna, Tarun C., Satyanarayanan, M., Keshav Krishna, A., 2009. Enriched and depleted arc basalts, with Mg-andesites and adakites: a potential paired arc–back-arc of the 2.6 Ga Hutti greenstone terrane, India. Geochimica et Cosmochimica Acta 73, 1711–1736.

Manikyamba, C., Kerrich, R., Naqvi, S.M.,RamMohan, M., 2004. Geochemical systematic of tholeiitic basalts from the 2.7 Ga Ramagiri–Hungund greenstone belts, Dhawar craton. Precambrian Research 134, 21–39.

Martin, D,M., Li, Z.X., Nemchin, A.A., Powell, C.M., 1998. A pre-2.2 Ga age for hematite ores of the Hamersley Province, Australia. Econ. Geol. 93, 1084-1090.

Mattinson, J.M., 2005. Zircon U-Pb chemical abrasion ("CA-TIMS") method: Combined annealing and multi-step partial dissolution analysis for improved precision and accuracy of zircon ages. Chemical Geology. 220, 47-66.

Maurice, C., David, J., O'Neil, J., Francis, D., 2009. Age and tectonic implications of Plaeoproterozoic mafic dyke swarms for the origin of 2.2 Ga enric enriched lithosphere beneath the Ungava Peninsula, Canada. Precamb. Res. 174, 163-180.

McElhinny, M.W, 1973. Palaeomagnetism and Plate Tectonics. Cambridge Univ. Press, London, p. 368.

McElhinny, M.W., 1979. Rock magnetism, Palaeomagnetism and plate tectonics. Cambridge University Press, New York.

McElhinny, M.W., McFadden, P.L., 1997. Palaeosecular variation over the past 5 Myr based on a new generalized database. Geophys. J. Int. 131, 240-252.

Meert, J.G., Pandit, M.K., Pradhan, V.R., Banks, J.C., Sirianni, R., Stroud, M., Newstead,B., Gifford, J., 2010. The Precambrian tectonic evolution of India: A 3.0 billionyear odyssey. J. Asian Earth Sci. 39, 483–515.

Merrill, R.T., McElhinny, M.W., McFadden, P.L., 1996. The magnetic field of the Earth. Paleomagnetism, the core, and the deep mantle. Academic Press, Int. Geophysics Series **63**, 527p.

Molyneux, L., 1971. A complete result magnetometer for measuring the remanent magnetization of rocks. Geophysical Journal of the Royal Astronomical Society, 24, 1–5.

Mondal, S, Piper, J.D.A., Hunt, L., Bandyopadhyay, G., Basu Mallik, S., 2009. Palaeomagnetic and rock magnetic study of charnockites from Tamil Nadu, India, and the 'Ur' protocontinent in Early Palaeoproterozoic times. J. Asian Earth Sci. 34, 493–506.

Moyen, J.F., Nedelec, A., Martin, H., Jayananda, M., 2003. Syntectonic granite emplacement at different structural levels: the Closepet granite, South India. J. Struct. Geol. 25, 611-631.

Mueller, W.U., Corcoran, P.L., Pickett, C., 2005. Mesoarchean continental break-up: Evolution and inferences from the >2.8 Ga Slave craton-cover succession, Canada. J. Geol. 113, 23-45.

Mukhopadhyay, D., 2001. The Archaean nucleus of Singhbhum: the present state of knowledge. Gondwana Res., 4, 307–318.

Murthy, Y.G.K., Babu Rao, V., Guptasarma, D., Rao, J.M., Rao, M.N., Bhattacharji, S., 1987. Tectonic, petrochemical and geophysical studies of mafic dyke swarms around the Proterozoic Cuddapah Basin, south India. In: Halls, H.C., Fahrig, W. (Eds.), Mafic Dyke Swarms, Geology Association of Canada Special Paper, vol. 34, pp. 303–316.

Naganjaneyulu, K., Santosh, M., 2010. The Central India Tectonic Zone: a geophys-ical perspective on continental amalgamation along a Mesoproterozoic suture.Gondwana Res. 18 (4), 547–564.

Naha, K., Srinivasan, R., Naqvi, S.M., 1986. Structural unity in the Early Precambrian Dharwar tectonic province, Peninsular India. Q. J. Geol., Min, Metall. Soc. India, 58, 218-243.

Naqvi, S.M., 2005. Geology and Evolution of the Indian Plate. Capital Publishing Company, New Delhi, 450p.

Naqvi, S.M., Divakar Rao, V., Narain, H., 1974. The protocontinental growth of the Indian Shield and the antiquity of its rift valleys. Precamb. Res. 1, 345–398.

Naqvi, S.M., Manikyamba, C., Gnaneshwar, R.T., Subba Rao, D.V., Ram Mohan, M., Srinivasa Sarma, D., 2002. Geochemical and isotopic constraints of late Archaean fossil plume for the evolution of the volcanic rocks of the Sandur Greenstone belt. Journal of the Geological Society of India 60, 27–56.

Naqvi, S.M., Rogers, J.J.W., 1987. Precambrian Geology of India. Oxford University Press Inc. 223 pp.

Narayanaswami, S., 1970. Tectonic setting and manifestation of the upper mantle in the Precambrian rocks of South India. Proceedings of Second Symposium on Upper Mantle Project, Hyderabad, pp. 377–403.

Nemchin, A.A., Pidgeon, R.T., 1998. Precise conventional and SHRIMP baddeleyite age for the Binneringie dyke near Narrogin, Western Australia. Australian J. Earth Sci. 45, 673-675.

Niihara, T., Kaiden, H., Misawa, K., Sekine, T., Mikouchi, T., 2012. U–Pb isotopic systematics of shock-loaded and annealed baddeleyite: Implications for crystallization ages of Martian meteorite shergottites. Earth and Planetary Science Letters. 341-344, 195-210.

Noble, S.R., Lightfoot, P.C., 1992. U-Pb baddeleyite ages of the Kerns and Triangle Mountain intrusions, Nipissing Diabase, Ontario. Can. J. Earth Sci. 29, 1424-1429.

Nutman, A.P., Chadwick, B., Ramakrishnan, M., Vishwanatha, M.N., 1992. SHRIMP U-Pb ages of detrital zircon on Sargur supracrustal rocks in western Karnataka, southern India. J. Geol. Soc. India, 39, 367–374.

Nutman, A.P., Hagiya, H., Maruyama, S., 1995. SHRIMP U-Pb single zircon geochronology of a Proterozoic mafic dyke, Isukasia, Southern West Greenland. Geol. Soc. Denmark Bull. 42, 17-22.

Opdyke, N.D., Henry, K.W., 1969. A test of the dipole hypothesis. Earth Planet. Sci. Lett. 6, 139–151.

Pandey, B.K., Gupta, J.N., Sarma, K.J., Sastry, C.A., 1997. Sm–Nd, Pb–Pb and Rb–Srgeochronology and petrogenesis of the mafic dyke swarm of Mahbubnagar,south India: implications for Paleoproterozoic crustal evolution of the easternDharwar craton. Precambrian Res. 84, 181–196.

Perttunen, V., 1991. Kemin, Karungin, Simon ja Runkauksen kartta-alueiden kalliopera. Kallioperakarttojen Selitykset, lehdet 4411, 4412, 4413. Suomen geologinen kartta 1:100000. Summary. Pre-Quaternary rocks of the Kemi, Karunki, Simo and Runkaus map-sheet areas. Geol. Surv. Finland. 80p.

Peucat, J.J., Bouhallier, H., Fanning, C.M., Jayananda, M., 1995. Age of Holenarsipur schist belt, relationships with the surrounding gneisses (Karnataka, south India). Journal of Geology 103, 701–710.

Peucat, J.J., Mahabaleswar, B., Jayananda, M., 1993. Age of younger tonalitic magmatism and granulitic metamorphism in the South Indian transition zone (Krishnagiri area): comparison with older Peninsular gneisses from the Gorur-Hassan area. J. Met. Geol. 11, 879–888.

Piispa, E.J., Smirnov, A.V., Pesonen, L.J., Lingadevaru, M., Ananthamurthy, K.S., Devaraju, T.C., 2011. An Integrated study of Proterozoic Dykes, Dharwar Craton, Southern India. In: Dyke swarms: Keys for Geodynamic Interpretation. Springer-Verlag, Berlin/Heidelberg, pp.33-45.

Pradhan, V.R., Meert, J.G., Pandit, M.K., Kamenov, G., Gregory, L.C., Malone, S.J., 2010. India's changing place in global Proterozoic reconstructions: Newgeochronologic constraints on key paleomagnetic poles from the Dharwar andAravalli/Bundelkhand cratons. Journal of Geodynamics, 50, 224–242.

Raase, P., Raith, M., Ackermand, D., Lal, R.K., 1986. Progressive metamorphism of mafic rocks from greenschist to granulite facies in the Dharwar craton of South India. Journal of Geology 94, 261–282.

Radhakrishna, B.P., Naqvi, S.M., 1986. Precambrian continental crust of India and its evolution. Journal of Geology 94, 145–166.

Radhakrishna, T., Dallmeyer, R.D., Joseph, M., 1994. Paleomagnetism and $^{36}Ar/^{40}Ar$ vs. $^{39}Ar/^{40}Ar$ isotope correlation ages of dyke swarms in central Kerala, India: Tectonic implications. Earth Planet. Sci. Lett. 121, 213-226.

Radhakrishna, T., Krishnendu, N., Balasubramonian, G., 2013. Palaeoproterozoic Indian shield in the global continental assembly: evidence from the palaeomagnetism of mafic dyke swarms. Earth-Sci. Rev. 126, 370–389.

Ramakrishnan, M., 1990. Crustal development in southern Bastar central Indian craton. Geological Survey of India Special Publication, 28, pp. 44–66.

Ramakrishnan, M., Vaidyanadhan, R., 2008. Geology of India. Geological Society of India, vol. 1. Bangalore, 556 pp.

Ramakrishnan, M., Vaidyanadhan, R., 2010. Geology of India. Geol Soc India, Bangalore, pp 994.

Rao, V.P., Pupper, J.H., 1996. Geochemistry and petrogenesis and tectonic setting of Proterozoic mafic dykes swarms, East Dharwar Craton, India. Jour. Geol. Soc. India 47: 165-174.

Reddy, P.R., Rajendra Prasad, B., Vijaya Rao, V., Sain, K., Prasada Rao. P., Khare, P., Reddy, M.S., 2003. Deep seismic reflection and refraction/wide-angle reflection studies along Kuppam-Pilani geotransect in the southern granulite terrain of India. In: Ramakrishnan, M. (Eds.), Tectonics of southern Granulite Terrain: Kuppam-Pilani Geotransect, Memoir vol. 50, Geological Society of India, Bangalore, pp.79-106.

Reischmann, T., 1995. Precise U/Pb age determination with baddeleyite (ZrO2), a case study from the Phalaborwa igneous complex, South Africa. South African Journal of Geology. 98, 1-4.

Rioux, M., Bowring, S., Dudas, F., Hanson, R., 2010. Characterizing the U-Pb systematics of baddeleyite through chemical abrasion: application of multi-step digestion methods to baddeleyite geochronology. Contributions to Mineralogy and Petrology. 160, 777-801.

Rogers, J.J.W., 1986. The Dharwar craton and the assembly of peninsular India. J.Geol. 94, 129–144.

Rogers, J.J., Santosh, M., 2002. Configuration of Columbia, a Mesoproterozoic super-continent. Gondwana Res. 5, 5–22.

Rogers, J.J., Santosh, M., 2003. Supercontinents in Earth History. Gond. Res. 6, 357-368.

Rollinson, H.R., Windley, B.F., Ramakrishnan, M., 1981. Contrasting high and intermediate pressures of metamorphism in the Archaean Sargur Schists of southern India. Contributions to Mineralogy and Petrology 76, 420–429.

Rubin, A. M., 1995. Propagation of magma-field cracks, Annu. Rev. Earth Planet. Sci., 23, 287–336.

Schoene, B., Crowley, J.L., Condon, D.J., Schmitz, M.D., Bowring, S.A., 2006. Reassessing the uranim decay constants for geochronology using ID-TIMS U-Pb data. Geochemica et Cosmochimica Acta 70, 426-445.

Sharma, P.V., 1986. Geophysical Methods in Geology. Elsevier, Amsterdam, p. 432.

Sharma, P.V., 1994. Late Palaeocene geomagnetic polarity transition in the vestmanna core of the lower basalt sequence on the Faeroc islands. In: Subbarao, K.V. (Ed.), Magnetism: Rocks to Superconductors Mem. Geol. Soc. India, No. 10 (supplement).

Sharma, R.S., 2009. Cratons and Fold Belts of India, Lecture Notes in Earth Sciences 127, p41, DOI 10.1007/978-3-642-01459-8_2

Silvennoinen, A., 1991. Kuusamon ja Rukatunturin karttaalueiden kalliopera. Kallioperakarttojen selitykset, lehdet 4524+4542 ja 4613: Suomen geologinen kartta 1:100000. Pre-Quaternary rocks of the kuusamo and Rukatunturi map-sheet areas. Geol. Surv. Finland. 63p.

Smeeth, W.F., 1915. Geological Map of Mysore. Department of Mines and Geology, Mysore.

Smirnov, A.V., Evans, D.A.D., 2006. Paleomagnetism of the ~2.4 Ga Widgiemooltha dike swarm (Western Australia): Preliminary results: Eos (Transactions, A.G.U), v.87, no. 36, abstract no. GP23A-01.

Söderlund, U., Johansson, L., 2002. A simple way to extract baddeleyite (ZrO2). Geochemisty Geophysics Geosystems. 3, 1-7.

Srinivasan, K.N., 1990. Geology of the Veligallu and Gadwal schist belts. Records of Geological Survey of India (Pt 5), 123.

Srinivasan, Krishnappa, 1991. Geology of Peddavuru and Jonnagiri schists belts, A.P. Records of Geological Survey of India 124 (Pt 5), 261–263.

Srikantia, S.V., 1995. Geology of the Hutti–Maski greenstone belt. In: Curtis, L.C., Radhakrishna, B.P. (Eds.), Hutti Gold Mine into the 21st Century. Geological Society of India, pp. 8–27.

Srivastava, R.K., Ahmad, T., 2009. Precambrian mafic magmatism in the Indian shield – part II. J Geol Soc India 73(1), 1–152.

Srivastava, R.K., Hamilton, M.A., Jayananda, M., 2011. A 2.21 Ga Large Igneous Province in the Dharwar Craton, India. International Symposium: Large Igneous Provinces of Asia; Mantle Plumes and Metallogeny. Abstract Volume, Irkutsk, Russia.

Srivastava, R.K., Jayananda, M., Gautam, G.C., Samal, A.K., 2014. Geochemical studies and petrogenesis of ~2.21-2.22 Ga Kunigal mafic dyke swarm (trending N-S to NNW-SSE) from eastern Dharwar craton, India: implications for Paleoproterozoic large igeous provinces and supercraton superia. Miner. Petrol. 108, 695-711.

Stacey, J. S., Kramers, J. D., 1975. Approximation of terrestrial lead isotope evolution by two-stage model, Earth and Planetary Science Letters. 26, 207-221.

Stupavsky, M., Symons, D.T.A., 1981. Extent of Grenvillian remanence components in rocks of southern province. Canadian Journal of Earth Sciences 19, 698–708.

Swami Nath, J., Ramakrishnan, M., 1981. Early Precambrian supracrustals of Southern Karnataka. Geological Survey of India; Memoirs 112, 363.

Sunin, L.V., Malyshev, V.I., 1983. The thermoisochron method of determining Pb–Pb ages. Geochem. Int. 20, 34–45.

Swami Nath, J. and Ramakrishnan, M. (1990). Early Precambrian supracrustals of southern Karnataka. A present classification and correlation. Geol. Soc. India Mem., vol. **19**, pp. 145–163.

Torsvik, T.H., Smethurst, M.A., 1999. Plate tectonic modelling; virtual reality with GMAP. In: Butler, J.C. (Ed.), Computers and Geosciences, 25, 395–402.

Tyrvainen, A. 1983. Sodankylan ja Sattasen Kartta-alueiden kallioperakarttojen selitykset, lehdet 3713 ja 3714: Suomen geologinen kartta 1:100000. Pre-Quaternary rocks of the Sodankyla and Sattanen map-sheet areas. Geol. Surv. Finland. 59p.

Viswanatha, M.N., Ramakrishnan, M., 1981. Bababudan belt: In: J. Swaminanath, M. Ramakrishnan (Eds.), Early Precambrian supracurstals of southern Karnataka. Geological Survey of India Memoir 112, 91-114.

Wanless, R.K., Stevens, R.D., Lachance, G.R., DcLabio, R.N., 1979. Age determinations and geological studies, K-Ar isotopic ages. report 14. Geol. Sur. Can. Pap. 79-2.

Wingate, M.T.D., Campbell, I.H., Compston, W., Gibson, M., 1998. Ion microprobe U-Pb ages for Neoproterozoic basaltic magmatism in south-central Australia and implications for the breakup of Rodinia. Precambrian Research. 87, 135-159.

Wingate, M.T.D., Compston, W., 2000. Crystal orientation effects during ion microprobe U–Pb analysis of baddeleyite. Chemical Geology. 168, 75-97.

Zijderveld, J.D.A., 1967. A.C. demagnetization of rocks: analysis of results. In: D.W. Collinson, K.M. Creer, S.K. Runcorn (Eds.), Methods in Paleomagnetism, Elsevier, Amsterdam, 254–286.

Zindler.. A., Hart, S., 1986. Chemical geodynamics. Ann. Rev. Earth Planet. Sci., 14,493-571.

Zykov, S.I., Stupnikova, N.I., 1957. Isotopic analysis of lead not requiring any preliminary chemical preparation of the mineral. Geochemistry International. 5, 506-510.

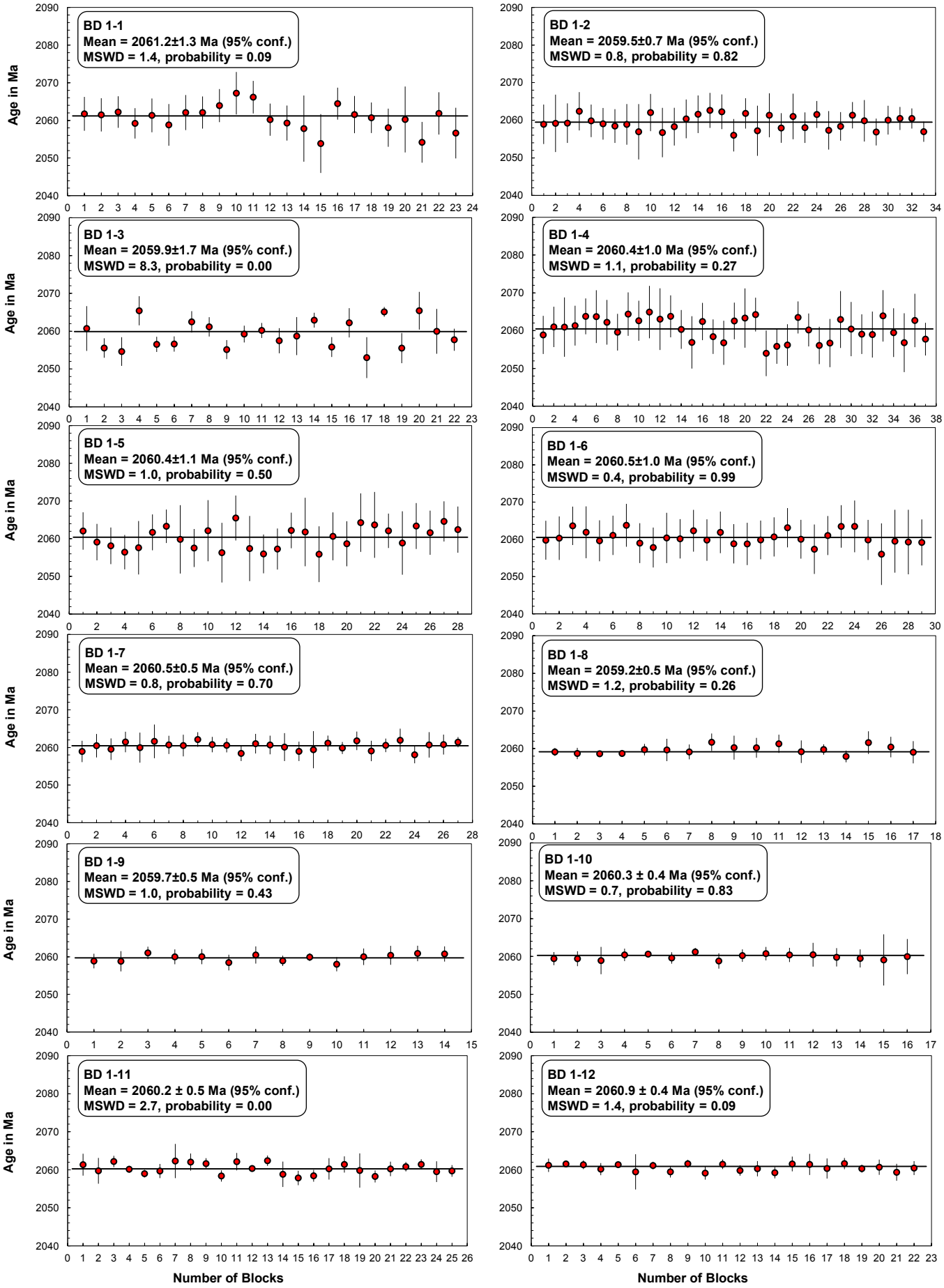
BD 1-1
Mean = 2061.2±1.3 Ma (95% conf.)
MSWD = 1.4, probability = 0.09
BD 1-2
Mean = 2059.5±0.7 Ma (95% conf.)
MSWD = 0.8, probability = 0.82
BD 1-3
Mean = 2059.9±1.7 Ma (95% conf.)
MSWD = 8.3, probability = 0.00
BD 1-4
Mean = 2060.4±1.0 Ma (95% conf.)
MSWD = 1.1, probability = 0.27
BD 1-5
Mean = 2060.4±1.1 Ma (95% conf.)
MSWD = 1.0, probability = 0.50
BD 1-6
Mean = 2060.5±1.0 Ma (95% conf.)
MSWD = 0.4, probability = 0.99
BD 1-7
Mean = 2060.5±0.5 Ma (95% conf.)
MSWD = 0.8, probability = 0.70
BD 1-8
Mean = 2059.2±0.5 Ma (95% conf.)
MSWD = 1.2, probability = 0.26
BD 1-9
Mean = 2059.7±0.5 Ma (95% conf.)
MSWD = 1.0, probability = 0.43
BD 1-10
Mean = 2060.3 ± 0.4 Ma (95% conf.)
MSWD = 0.7, probability = 0.83
BD 1-11
Mean = 2060.2 ± 0.5 Ma (95% conf.)
MSWD = 2.7, probability = 0.00
BD 1-12
Mean = 2060.9 ± 0.4 Ma (95% conf.)
MSWD = 1.4, probability = 0.09
Age in Ma
Number of Blocks

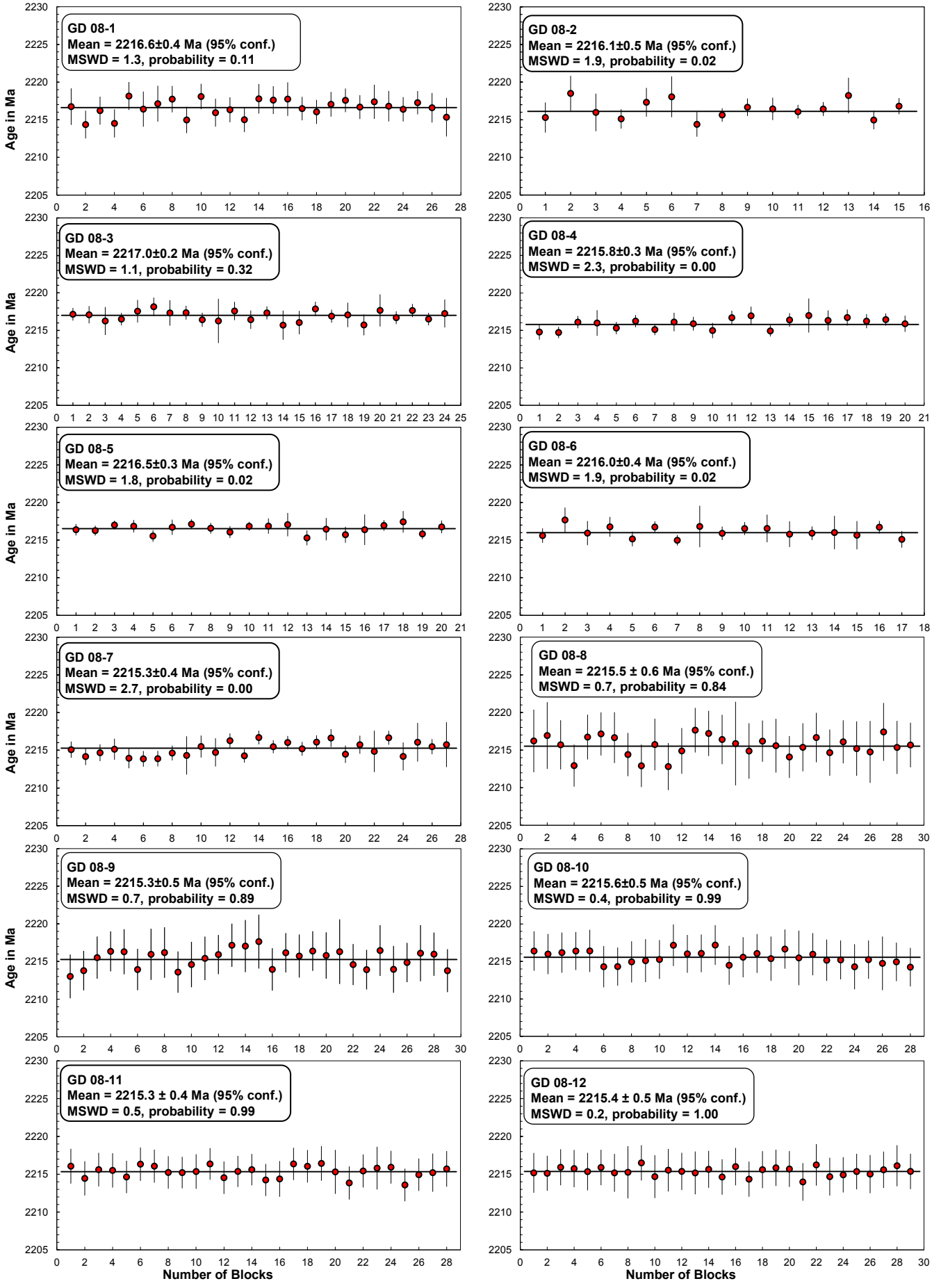
GD 08-1
Mean = 2216.6±0.4 Ma (95% conf.)
MSWD = 1.3, probability = 0.11
GD 08-2
Mean = 2216.1±0.5 Ma (95% conf.)
MSWD = 1.9, probability = 0.02
GD 08-3
Mean = 2217.0±0.2 Ma (95% conf.)
MSWD = 1.1, probability = 0.32
GD 08-4
Mean = 2215.8±0.3 Ma (95% conf.)
MSWD = 2.3, probability = 0.00
GD 08-5
Mean = 2216.5±0.3 Ma (95% conf.)
MSWD = 1.8, probability = 0.02
GD 08-6
Mean = 2216.0±0.4 Ma (95% conf.)
MSWD = 1.9, probability = 0.02
GD 08-7
Mean = 2215.3±0.4 Ma (95% conf.)
MSWD = 2.7, probability = 0.00
GD 08-8
Mean = 2215.5 ± 0.6 Ma (95% conf.)
MSWD = 0.7, probability = 0.84
GD 08-9
Mean = 2215.3±0.5 Ma (95% conf.)
MSWD = 0.7, probability = 0.89
GD 08-10
Mean = 2215.6±0.5 Ma (95% conf.)
MSWD = 0.4, probability = 0.99
GD 08-11
Mean = 2215.3 ± 0.4 Ma (95% conf.)
MSWD = 0.5, probability = 0.99
GD 08-12
Mean = 2215.4 ± 0.5 Ma (95% conf.)
MSWD = 0.2, probability = 1.00
Age in Ma
Number of Blocks

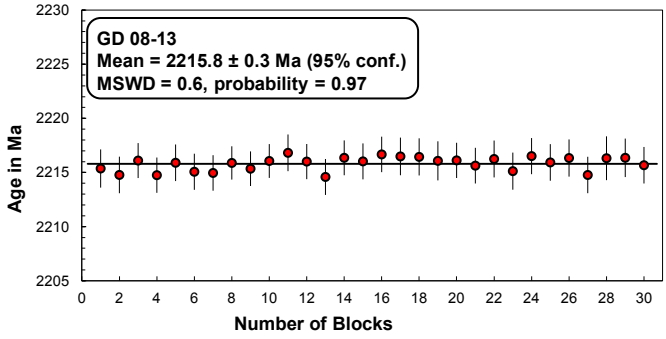
GD 08-13
Mean = 2215.8 ± 0.3 Ma (95% conf.)
MSWD = 0.6, probability = 0.97
Age in Ma
Number of Blocks

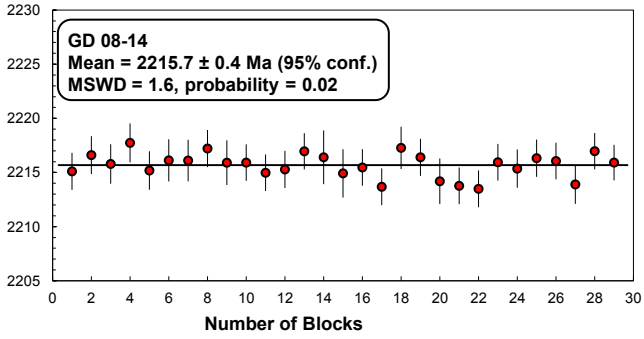
GD 08-14
Mean = 2215.7 ± 0.4 Ma (95% conf.)
MSWD = 1.6, probability = 0.02
Number of Blocks